UNIVERSITY OF OKLAHOMA

GRADUATE COLLEGE

DETECTION, DISTRIBUTIONS, AND BIOGEOCHEMICAL IMPLICATIONS OF FOSSIL ARSENOLIPIDS IN MARINE AND LACUSTRINE SEDIMENTS

A DISSERTATION

SUBMITTED TO THE GRADUATE FACULTY

in partial fulfillment of the requirements for the

Degree of

DOCTOR OF PHILOSOPHY

By

CHENXI XU

Norman, Oklahoma

2026

DETECTION, DISTRIBUTIONS, AND BIOGEOCHEMICAL IMPLICATIONS OF FOSSIL ARSENOLIPIDS IN MARINE AND LACUSTRINE SEDIMENTS

A DISSERTATION APPROVED FOR THE

SCHOOL OF GEOSCIENCES

BY THE COMMITTEE CONSISTING OF

Dr. Xiao-Lei Liu, Chair

Dr. Michael H. Engel

Dr. Caitlin Hodges

Dr. Xingru Wu

ACKNOWLEDGEMENTS

I am deeply grateful to my advisor, Dr. Xiao-Lei Liu, for his sustained guidance, scientific mentorship, and boundless patience throughout the development of this dissertation. Dr. Liu is the kind of mentor who genuinely cares about his students as people — checking in on life outside the lab, organizing gatherings during holidays, and creating a group culture that felt warm and welcoming from the very beginning. After joining his research group, he invested an enormous amount of time in building up my laboratory skills, and his patience through that process never wavered. I am equally grateful to him for welcoming me into his group during a difficult transition in my doctoral journey and for introducing me to the world of biogeochemistry — a field I have come to love in no small part because of his guidance and the way he nurtures curiosity in everyone around him.

My doctoral path did not begin the way I expected. I began my PhD under the mentorship of Dr. John D. Pigott, who was not only my advisor but one of the most formative figures in my life. He was endlessly generous — not only in guiding my research, but in helping me navigate life in the United States, understand its culture, and feel at home in a place that was entirely new to me. His care extended well beyond academics, and his warmth made a lasting impression that I will carry with me always. His sudden passing was a profound loss, and I think of him often. I am grateful to Dr. John Antonio, Dr. Matthew Pranter, and Dr. Heather Bedle, who stepped in during that period of uncertainty with steadiness and kindness. Their support helped me find my footing again, and I would not have made it through that chapter of my graduate career without them.

I also extend my sincere thanks to the members of my doctoral committee. Dr. Michael H. Engel's contributions to my development as a researcher stretch back to my earlier doctoral years

— his hands-on help with laboratory analyses and his thoughtful feedback during my progress reports shaped my early thinking in ways that continued to inform this work, even where his data does not appear directly in these pages. Dr. Xingru Wu, as my outside committee member, brought a broader perspective that pushed me to think beyond the boundaries of my immediate field, and his suggestions were instrumental in sharpening the final form of this dissertation. I am also grateful to Dr. Caitlin Hodges for joining my committee during a difficult period of transition — her willingness to step in and provide stability when I needed it most meant more than she may know. This dissertation would not have been possible without them.

I thank Olawale O. Alo, Wenshuo Zhao, Junpeng Fu, and Derek Parks for their friendship and everything that came with it — lending a hand in the lab when things got complicated, talking through problems that felt unsolvable, and then turning around and being the same people I could grab a meal with, laugh with, and call genuine friends. The lab was a better place because of all of them, and so was my time here.

I also thank the administrative staff of the School of Geosciences, especially Rebecca Fay, for her patience, helpfulness, and willingness to answer my many questions over the years. I am equally grateful to Gail Holloway, whose coordination and mentorship during my time as a teaching assistant gave me opportunities to grow as an educator in ways that extended well beyond the classroom.

I am also grateful to Eric Blaszczyk for giving me the opportunity to work in industry during my doctoral studies. The experience allowed me to apply what I had learned in graduate school to real-world geological problems while gaining insight into the energy industry. Working alongside talented professionals broadened my perspective, challenged me to think differently, and

helped me grow both professionally and personally. The lessons I learned during this time will continue to influence my career long after the completion of this dissertation.

I thank the Ocean Drilling Program (ODP) for providing core samples from Legs 201 and 207 (Sites 1227 and 1259C), which were essential to the analyses presented in this dissertation. I also thank the USGS EDMap Program and NASA Exobiology Program for the financial support during my PhD program.

To my mother, Heng Chen—despite the distance between us, your strength, encouragement, and unwavering belief in me have always been a source of comfort and motivation. Knowing that you were cheering me on from afar gave me more courage than you will ever know. To my father, your memory has remained a constant presence throughout this journey. Though you were not here to witness its completion, your influence has shaped the person I became and the perseverance that carried me through difficult moments. I think of you often, and I wish I could share this achievement with you.

To my girlfriend, Ziwei Zhang, thank you for your love, patience, and steadfast support throughout these years. Your encouragement sustained me through challenges both academic and personal, and your presence brought balance and happiness to a demanding chapter of my life. Thank you for celebrating the successes, helping me through the setbacks, and reminding me to keep moving forward when the path seemed uncertain. I could not have done this without you.

ABSTRACT

Arsenolipids are a class of arsenic-containing lipids that occur widely in modern aquatic environments and are produced by phylogenetically diverse microorganisms through a conserved arsenic-methylation pathway. Their potential as molecular biomarkers in the geological record, however, has been limited by analytical, distributional, and interpretive uncertainties. This dissertation establishes fossil arsenolipids—including both arsenic-containing hydrocarbons (AsHCs, bearing an $O{=}As(CH_3)_2–$ head group) and thioxoarsenolipids—as a class of element-specific molecular fossils, systematically characterizing their analytical detection, sedimentary distribution, and stratigraphic variability.

Chapter 2 establishes an analytical framework for fossil arsenolipid detection that combines silica-gel solid-phase extraction (SPE), normal-phase liquid chromatography (NPLC), and dual-energy collision-induced dissociation (CID) mass spectrometry. The framework recovers arsenolipid signals from matrices ranging from algal biomass to ancient sedimentary rocks for which conventional reversed-phase methods do not yield arsenolipid detection.

Chapter 3 demonstrates the broad distribution and long-term preservation of arsenolipids through a survey of fourteen samples comprising eight modern aquatic settings (spanning algal biomass, coastal and lacustrine sites) and six fossil sedimentary samples spanning the Quaternary to the mid- to late Cenomanian (~94–100 Ma). At least one arsenolipid class was detected in every sample, but the two classes differed in range: AsHCs were recovered from twelve of the fourteen samples and thioxoarsenolipids from thirteen, across organic-rich shales, lacustrine deposits, and carbonate-rich pelagic chalks. AsHCs were detected in fossil sediments as old as the Late Cretaceous (~90 Ma), whereas thioxoarsenolipids persisted into the older OAE2 black-shale interval (~94–100 Ma); together these extend the preservation record across at least ~100 Myr of

sedimentary burial and indicate that the two classes differ in long-term preservation. The pelagic chalk recovery further extends the lithological range beyond the high-TOC anoxic settings of classical biomarker work.

Chapter 4 presents the first stratigraphically resolved record of two arsenolipid compound classes across thirteen samples from the Holocene Black Sea sapropel sequence (GGC18, 11.7–0.6 ka). The two compound classes follow contrasting stratigraphic patterns involving distinct biogeochemical controls (producer-side for AsHCs and sulfide-mediated formation for thioxoarsenolipids), but both trace to the same upstream environmental transition (the development of photic-zone euxinia). The ratio of AsHCs to thioxoarsenolipids (the AsHC/thioxoarsenolipid ratio) integrates both responses into a composite metric whose approximately eleven-fold response across the Unit III/II boundary supports its use as an indicator of major regime transitions in sedimentary archives.

Together, these results characterize the analytical detection, distribution, and time-resolved environmental response of arsenolipids and support their further development as a paleoenvironmental tool.

TABLE OF CONTENTS

LIST OF FIGURES

LIST OF TABLES

Chapter 1 General Introduction

1.1 Motivation: Arsenolipids as a New Paleoenvironmental Tool

The reconstruction of past environmental conditions in sedimentary archives relies on the identification of molecular fossils—organic compounds preserved in sediments whose distributions and abundances carry information about the biological producers and physical-chemical conditions of the depositional environment. The molecular-fossil framework that paleoenvironmental geochemistry has developed over the past five decades draws primarily on hydrocarbon biomarkers (hopanes, steranes), pigment-derived biomarkers (porphyrins, chlorin derivatives), and isotopic signatures of bulk and compound-specific organic carbon. Each of these classes carries information about a specific subset of producer communities or depositional processes, and their combined application has enabled the reconstruction of marine and lacustrine environmental change at unprecedented resolution.

Arsenolipids—organic molecules containing covalently bound arsenic atoms—occupy a distinct position in this framework. Unlike hydrocarbon and pigment-based biomarkers, which derive primarily from membrane biochemistry and photosynthetic activity, arsenolipid biosynthesis depends on a distinct upstream pathway of arsenate uptake, reduction, and methylation. Because this pathway is carried out by a broad range of producers—eukaryotic algae, cyanobacteria, and heterotrophic bacteria—arsenolipids carry information about a producer dimension that is complementary to that captured by classical biomarkers (Xue et al., 2014; Glabonjat et al., 2018; Heal et al., 2022). Their chemical structures—saturated alkyl chains, fatty acid analogs, sugar-bearing phosphatidyl variants, and sulfur-substituted thioxoarsenolipids—offer a structural diversity comparable to that of established lipid biomarkers.

The application of arsenolipids as fossil molecular biomarkers, however, has been constrained by three interconnected uncertainties. The first is analytical: arsenolipids occur at trace levels in sediments and are difficult to detect against the lipid-matrix background of typical sedimentary extracts. The second is distributional: although arsenohydrocarbons (AsHCs) have been documented in modern biological matrices (primarily fish, algae, and surface-water particulates), their occurrence in modern sediments has been examined at only a few sites, and—more importantly—AsHCs in particular had not been reported in geological sedimentary archives over significant geological time prior to this work (Glabonjat et al., 2019a; Heal et al., 2022; Xue et al., 2022), whereas sedimentary thioxoarsenolipids were first reported only recently (Liu, 2023). The third is interpretive: the producer organisms of arsenolipids in natural environments remain incompletely characterized, and the formation pathways of structurally distinct arsenolipid sub-classes—including sulfur-containing arsenolipids that have only recently been reported—are not yet mechanistically resolved. Together, these uncertainties have limited the application of arsenolipids in paleoenvironmental reconstruction.

This dissertation addresses these three uncertainties through three complementary investigations: development of an analytical framework for fossil arsenolipid detection, a survey of arsenolipid occurrence and preservation across modern and ancient sedimentary archives, and a stratigraphically resolved case study of arsenolipid response to documented environmental transitions in the Holocene Black Sea sapropel sequence. The work presented here sits at the intersection of organic geochemistry, biogeochemistry, and analytical mass spectrometry, and aims to extend the molecular-fossil toolkit to a class of biomolecules whose information content has been largely unexplored in the deep-time record. Sections 1.2 and 1.3 introduce the

geochemical and biological background needed to interpret arsenolipid distributions in marine sedimentary records; Section 1.4 frames the three central questions.

The principal contributions of this dissertation are: (i) the development of a single-instrument NPLC–dual-energy CID analytical framework for fossil arsenolipid detection in geological samples, demonstrated on matrices ranging from modern algal biomass to Cretaceous black shale; (ii) the first reports of fossil AsHCs from sedimentary archives spanning nearly 100 million years of geological time; and (iii) the first stratigraphically resolved record of arsenolipid response to documented redox transitions in a Holocene marine sequence, integrating two distinct compound classes (AsHCs and the thioxoarsenolipids) into a coupled paleoenvironmental record.

1.2 Arsenic Biogeochemistry and Paleoredox Significance

Arsenic (As) is a redox-sensitive metalloid that is naturally present throughout Earth's surface environments and is among the most globally distributed contaminants of public health concern. Chronic exposure to inorganic arsenic via drinking water is associated with cancers of the skin, lung, and bladder, as well as cardiovascular and developmental disorders, with an estimated ~140 million people worldwide exposed to groundwater arsenic concentrations exceeding the World Health Organization guideline value of 10 μg L^{-1} (Naujokas et al., 2013; W.H.O., 2017). The U.S. Environmental Protection Agency adopted the same 10 μg L^{-1} threshold in 2001. Beyond its acute toxicological relevance, arsenic occupies a position of broader interest in Earth-system science: as a trace element whose geochemistry is tightly coupled to those of phosphorus, sulfur, iron, and manganese, it has been used as a tracer of redox conditions, chemical weathering, and biogeochemical change across both modern and ancient marine systems (Smedley and Kinniburgh, 2002; Chi Fru et al., 2015).

The modern global biogeochemical cycle of arsenic has been comprehensively re-evaluated by Schlesinger et al. (2022) (Figure 1.1). Natural mobilization of arsenic from rock weathering at the Earth's surface is similar in magnitude to the dissolved arsenic delivered to the oceans by rivers, while volcanic emissions and atmospheric circulation contribute additional natural fluxes. Human activities now dominate global arsenic mobilization: inadvertent release from mineral extraction—including non-ferrous metal smelting, coal combustion, and phosphate-rock processing—exceeds the natural weathering flux by roughly an order of magnitude. Anthropogenic emissions into the atmosphere similarly exceed natural background sources, largely as a result of the smelting of copper and other non-ferrous ores. Despite these elevated inputs, the mean residence time of dissolved arsenic in surface seawater remains long relative to mixing timescales, on the order of centuries (Schlesinger et al., 2022). These findings build on earlier surveys that documented the dual contribution of natural geochemical processes (rock weathering, volcanic emissions) and anthropogenic activities (mining, pesticide use, smelting) to global arsenic mobilization (Neff, 1997; Moriarty et al., 2014).

In aquatic environments, the speciation and mobility of arsenic are governed primarily by redox state and pH (Figure 1.2). In oxygenated waters, arsenic occurs predominantly as inorganic pentavalent arsenate (As(V), $HAsO_4^{2-}$/$H_2AsO_4^-$ at circumneutral pH), whereas under reducing conditions trivalent arsenite (As(III), $H_3AsO_3^0$) becomes increasingly important; both species can coexist over a range of natural Eh-pH conditions, and microbial processes often maintain disequilibrium between them (Smedley and Kinniburgh, 2002).

Total dissolved arsenic concentrations in the open ocean are remarkably uniform, reflecting the long oceanic residence time relative to mixing timescales (Cutter et al., 2001). In contrast, freshwater and coastal systems show much greater variability, ranging from low concentrations in

unimpacted waters to elevated levels in groundwater systems affected by reductive dissolution of arsenic-bearing iron oxyhydroxides—most notably across the Bengal Basin, where naturally elevated arsenic in shallow aquifers represents one of the largest mass exposures to a geogenic contaminant in human history (Smedley and Kinniburgh, 2002).

The fate of arsenic in marine sediments is closely tied to the cycles of iron and sulfur. Under oxic conditions, arsenate is efficiently scavenged from the water column by adsorption onto iron and manganese (oxyhydr-)oxides, and these phases deliver the bulk of authigenic arsenic to surface sediments (Tribovillard, 2021). When pore-water conditions become reducing, arsenic associated with iron oxyhydroxides may be remobilized; whether arsenic is then retained in sediments or returned to the overlying water column depends on the availability of reactive iron and dissolved sulfide. In sulfidic sediments, arsenic is incorporated into authigenic pyrite and other iron-sulfide phases, where it can be preserved over geological timescales (Gregory et al., 2015). Because the partitioning of arsenic between dissolved, oxide-bound, and sulfide-bound pools is sensitive to ambient oxygen and sulfide concentrations, bulk arsenic content of ancient sediments has been used—alongside the more widely applied U, Mo, and V proxies—as a paleoredox indicator, that is, a chemical fingerprint of the redox conditions at the time the sediment was deposited. This approach has linked sedimentary arsenic enrichment to perturbations in atmospheric oxygen across the Proterozoic (Chi Fru et al., 2015) and to organic-rich sapropelic intervals in younger marine successions (Gallego-Torres et al., 2010). The same geochemical sensitivity that makes arsenic a tracer of past redox transitions also raises the prospect that arsenic-containing biomolecules, if preserved, could record information about ancient microbial activity and biogeochemical cycling that is complementary to bulk inorganic proxies—a possibility that motivates the molecular-level investigation pursued in this dissertation.

1.3 Microbial Production of Organoarsenicals

The reactivity of arsenic with biological systems begins at the cell membrane. Because arsenate (AsO_4^{3-}) is a structural and chemical analog of the essential nutrient phosphate (PO_4^{3-}), it is inadvertently taken up by aquatic microorganisms via high-affinity phosphate transporters, particularly under phosphate-limited conditions (Wang et al., 2013). Once intracellular, arsenate inhibits ATP synthesis and other phosphate-dependent reactions, imposing a metabolic cost that has driven the evolution of dedicated detoxification pathways across all three domains of life (Bhattacharjee and Rosen, 2007).

In the canonical detoxification route, intracellular arsenate is first reduced to arsenite by a thiol-dependent arsenate reductase (ArsC), and the more mobile arsenite is then exported from the cell by a membrane efflux pump (ArsB or Acr3) as the primary detoxification response (Figure 1.3). In addition to direct efflux, many microorganisms further transform intracellular arsenic via methylation: the S-adenosylmethionine-dependent arsenite methyltransferase (ArsM) catalyses the stepwise addition of methyl groups to arsenite, generating mono-, di-, and trimethylated arsenicals through a series of redox-coupled intermediates of which the trivalent forms (MMA(III), DMA(III)) are highly reactive (Chen and Rosen, 2020). The ars gene cluster encoding these activities is widely distributed across bacterial, archaeal, and eukaryotic lineages, indicating that the capacity to take up, reduce, and methylate arsenic is an ancient and broadly conserved trait rather than the property of any single taxonomic group (Chen and Rosen, 2020). The methylated arsenic pool is widely accepted as the precursor pool from which more complex organoarsenicals are derived, but the downstream pathways that produce the structural diversity of arsenolipids are characterized to varying degrees: biosynthetic routes for arsenosugars have been outlined in eukaryotic algae through culture studies (Glabonjat et al., 2018), whereas the formation pathways

of arsenohydrocarbons (AsHCs) remain incompletely constrained and may involve both direct biosynthesis and post-cellular or diagenetic transformations (Glabonjat et al., 2019a; Heal et al., 2022).

In marine and freshwater systems, this metabolic machinery is found not only in eukaryotic algae such as *Dunaliella* and *Picocystis*—two of the most frequently used model organisms for arsenolipid biosynthesis studies in culture—but also in cyanobacteria and a range of heterotrophic bacteria (Xue et al., 2014; Heal et al., 2022). The functional consequence is that organoarsenic synthesis is a widespread metabolic capability among adapted aquatic communities, providing the biological basis for the diverse pool of organoarsenicals introduced below.

The organoarsenic compounds produced through the uptake-reduction-methylation pathway described above accumulate within aquatic food webs and are broadly divided into water-soluble species and lipid-soluble species, the latter of which are known as arsenolipids (Rahman et al., 2012). Compared with the extensively studied water-soluble forms—which include arsenobetaine, arsenocholine, and the arsenosugars—arsenolipids represent a more recently recognized and analytically challenging class. To date, over 260 arsenolipid species have been identified (Xue et al., 2022), and the structural diversity of this pool reflects the metabolic complexity of organoarsenic synthesis across the aquatic biosphere. The methodological framework developed in Chapter 2 builds on this biological and geochemical foundation to enable the detection of fossil arsenolipids in sedimentary archives.

1.4 Scope and Structure

The investigations presented in this dissertation are organized around three complementary questions that together address the analytical, distributional, and interpretive dimensions of arsenolipids as fossil molecular biomarkers.

How can fossil arsenolipids be reliably detected against the matrix background of complex sedimentary extracts? Chapter 2 develops a analytical framework for the recovery of arsenolipid signals from complex sedimentary matrices where conventional reversed-phase methods fail is proposed in Chapter 2.

How widely are arsenolipids distributed across modern aquatic environments, and how well are they preserved across geological time and across diverse sedimentary lithologies? Chapter 3 surveys fourteen samples—eight modern aquatic settings and six fossil sediments ranging from Quaternary to Cenomanian (~94–100 Ma)—and evaluates the distribution of arsenolipids in modern systems and their preservation across geological time and contrasting sedimentary lithologies.

How does arsenolipid composition respond to documented environmental transitions in a single, well-characterized sedimentary sequence? Chapter 4 examines both compound classes across thirteen samples from the Holocene Black Sea sapropel sequence (GGC18), whose well-documented limnic-to-euxinic transition provides an independently constrained framework for evaluating arsenolipid responses to environmental change.

Together, these three investigations provide an integrated framework for evaluating the occurrence, preservation, and paleoenvironmental significance of arsenolipids in sedimentary archives. Chapter 5 synthesizes the findings of these investigations, discusses their broader implications and limitations, and outlines directions for future research.

1.5 References

Bhattacharjee, H., Rosen, B.P., 2007. Arsenic metabolism in prokaryotic and eukaryotic microbes, in: Nies, D.H., Silver, S. (Eds.), Molecular Microbiology of Heavy Metals, Springer. pp. 371–406. https://doi.org/10.1007/7171_2006_086

Chen, J., Rosen, B.P., 2020. The arsenic methylation cycle: how microbial communities adapted methylarsenicals for use as weapons in the continuing war for dominance. Frontiers in Environmental Science 8, 43. https://doi.org/10.3389/fenvs.2020.00043

Chi Fru, E., Arvestål, E., Callac, N., El Albani, A., Kilias, S., Argyraki, A., Jakobsson, M., 2015. Arsenic stress after the Proterozoic glaciations. Scientific Reports 5, 17789. https://doi.org/10.1038/srep17789

Cutter, G.A., Cutter, L.S., Featherstone, A.M., Lohrenz, S.E., 2001. Antimony and arsenic biogeochemistry in the western Atlantic Ocean. Deep-Sea Research Part II: Topical Studies in Oceanography 48, 2895–2915. https://doi.org/10.1016/S0967-0645(01)00023-6

Gallego-Torres, D., Martinez-Ruiz, F., Lange, G.J., Jimenez-Espejo, F.J., Ortega-Huertas, M., 2010. Trace-elemental derived paleoceanographic and paleoclimatic conditions for Pleistocene Eastern Mediterranean sapropels. Palaeogeography, Palaeoclimatology, Palaeoecology 293, 76–89. https://doi.org/10.1016/j.palaeo.2010.05.001

Glabonjat, R.A., Duncan, E.G., Francesconi, K.A., Maher, W.A., 2019a. Transformation of arsenic lipids in decomposing *Ecklonia radiata*. Journal of Applied Phycology 31, 3979–3987. https://doi.org/10.1007/s10811-019-01845-2

Glabonjat, R.A., Ehgartner, J., Duncan, E.G., Raber, G., Jensen, K.B., Krikowa, F., Maher, W.A., Francesconi, K.A., 2018. Arsenolipid biosynthesis by the unicellular alga *Dunaliella tertiolecta* is influenced by As/P ratio in culture experiments. Metallomics 10, 145–153. https://doi.org/10.1039/c7mt00249a

Gregory, D.D., Large, R.R., Halpin, J.A., Baturina, E.L., Lyons, T.W., Wu, S., Danyushevsky, L., Sack, P.J., Chappaz, A., Maslennikov, V.V., Bull, S.W., 2015. Trace element content of sedimentary pyrite in black shales. Economic Geology 110, 1389–1410.

https://doi.org/10.2113/econgeo.110.6.1389

Heal, K.R., Maloney, A.E., Ingalls, A.E., Bundy, R.M., 2022. Diverse arsenic-containing lipids in the surface ocean. Limnology and Oceanography Letters 7, 43–51. https://doi.org/10.1002/lol2.10216

Liu, X.-L., 2023. Streamlined arsenolipid identification via direct arsenic detection using RPLC-ESI-QTOF-MS with collision-induced dissociation. Journal of the American Society for Mass Spectrometry 35, 300–306. https://doi.org/10.1021/jasms.3c00367

Moriarty, M.M., Lai, V.W.-M., Koch, I., Cui, L., Combs, C., Krupp, E.M., Feldmann, J., Cullen, W.R., Reimer, K.J., 2014. Speciation and toxicity of arsenic in mining-affected lake sediments in the Quinsam watershed, British Columbia. Science of the Total Environment 466–467, 90–99. https://doi.org/10.1016/j.scitotenv.2013.07.005

Naujokas, M.F., Anderson, B., Ahsan, H., Aposhian, H.V., Graziano, J.H., Thompson, C., Suk, W.A., 2013. The broad scope of health effects from chronic arsenic exposure: update on a worldwide public health problem. Environmental Health Perspectives 121, 295–302. https://doi.org/10.1289/ehp.1205875

Neff, J.M., 1997. Ecotoxicology of arsenic in the marine environment. Environmental Toxicology and Chemistry 16, 917–927. https://doi.org/10.1002/etc.5620160511

Rahman, M.A., Hasegawa, H., Lim, R.P., 2012. Bioaccumulation, biotransformation and trophic transfer of arsenic in the aquatic food chain. Environmental Research 116, 118–135. https://doi.org/10.1016/j.envres.2012.03.014

Schlesinger, W.H., Klein, E.M., Vengosh, A., 2022. The global biogeochemical cycle of arsenic. Global Biogeochemical Cycles 36, 2022 007515. https://doi.org/10.1029/2022GB007515

Smedley, P.L., Kinniburgh, D.G., 2002. A review of the source, behaviour and distribution of

arsenic in natural waters. Applied Geochemistry 17, 517–568. https://doi.org/10.1016/S0883-2927(02)00018-5

Tribovillard, N., 2021. Conjugated enrichments in arsenic and antimony in marine deposits used as paleoenvironmental proxies: preliminary results. BSGF - Earth Sciences Bulletin 192, 39. https://doi.org/10.1051/bsgf/2021034

Wang, N.-X., Li, Y., Deng, X.-H., Miao, A.-J., Ji, R., Yang, L.-Y., 2013. Toxicity and bioaccumulation kinetics of arsenate in two freshwater green algae under different phosphate regimes. Water Research 47, 2497–2506. https://doi.org/10.1016/j.watres.2013.02.034

W.H.O., 2017. Guidelines for drinking-water quality, 4th edition incorporating the first addendum, World Health Organization.

Xue, X.-M., Raber, G., Foster, S., Chen, S.-C., Francesconi, K.A., Zhu, Y.-G., 2014. Biosynthesis of arsenolipids by the cyanobacterium Synechocystis sp. PCC 6803. Environmental Chemistry 11, 506–513. https://doi.org/10.1071/en14069

Xue, X.-M., Xiong, C., Yoshinaga, M., Rosen, B., Zhu, Y.-G., 2022. The enigma of environmental organoarsenicals: insights and implications. Critical Reviews in Environmental Science and Technology 52, 3835–3862. https://doi.org/10.1080/10643389.2021.1947678

1.6 Figures

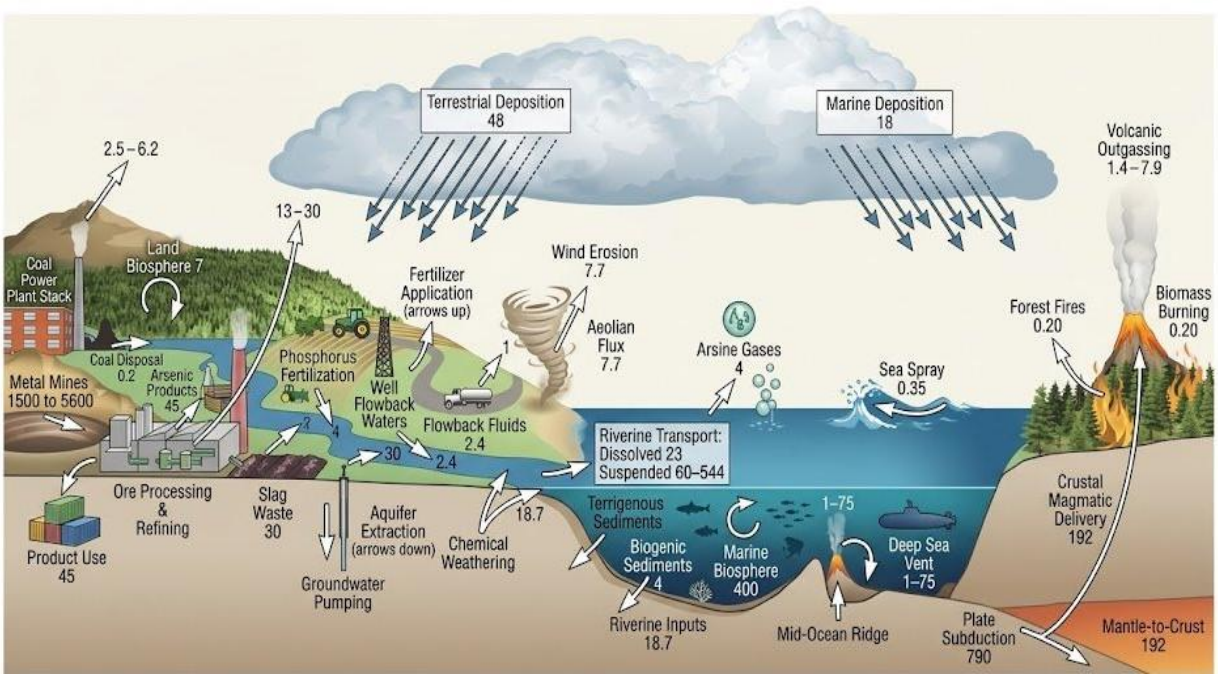

Figure 1.1. Schematic of the global biogeochemical cycle of arsenic, showing major reservoirs (atmosphere, land surface, ocean, sediments and crust) and the fluxes connecting them. Annual fluxes are reported in units of 109 g As yr−1; ranges indicate the spread of published estimates. Anthropogenic fluxes (metal mining, smelting, coal combustion, fertilizer application, groundwater extraction) are shown in the upper-left landscape; natural fluxes (volcanic outgassing, biomass burning, sea spray, hydrothermal venting, subduction) are distributed across the remaining panels. Modified after Schlesinger et al. (2022).

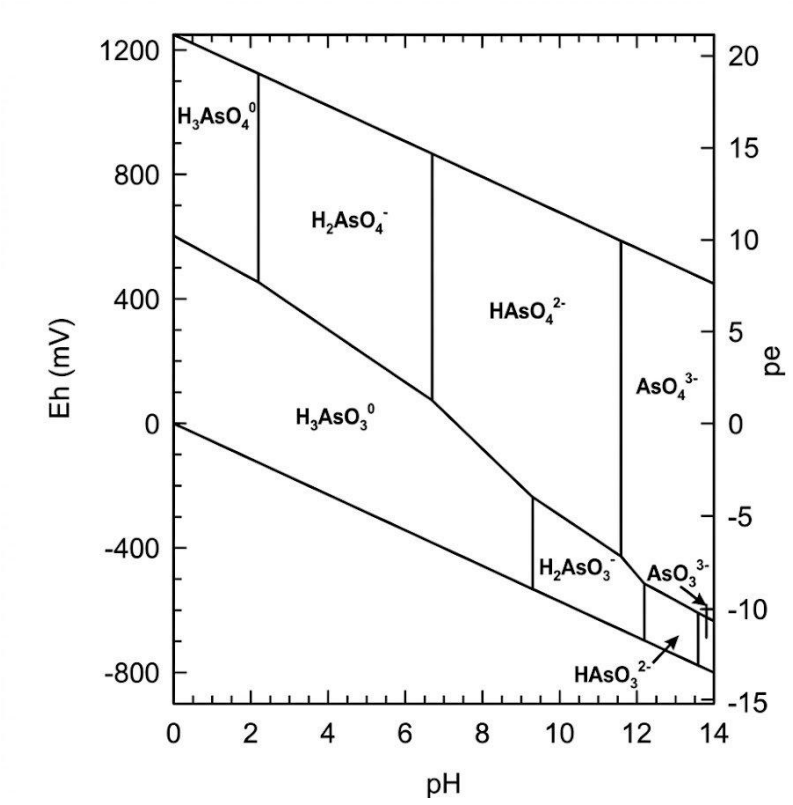

Figure 1.2 Stability diagram for aqueous arsenic species in the As–O_2–H_2O system at 25 °C and 1 bar total pressure. Field boundaries delineate the pH and Eh (or pe) ranges over which each dissolved species is thermodynamically dominant. At circumneutral pH, oxidized waters favor pentavalent arsenate species ($H_2AsO_4^-$, $HAsO_4^{2-}$), whereas reducing conditions favor trivalent arsenite (predominantly $H_3AsO_3^0$). Modified after Smedley and Kinniburgh (2002).

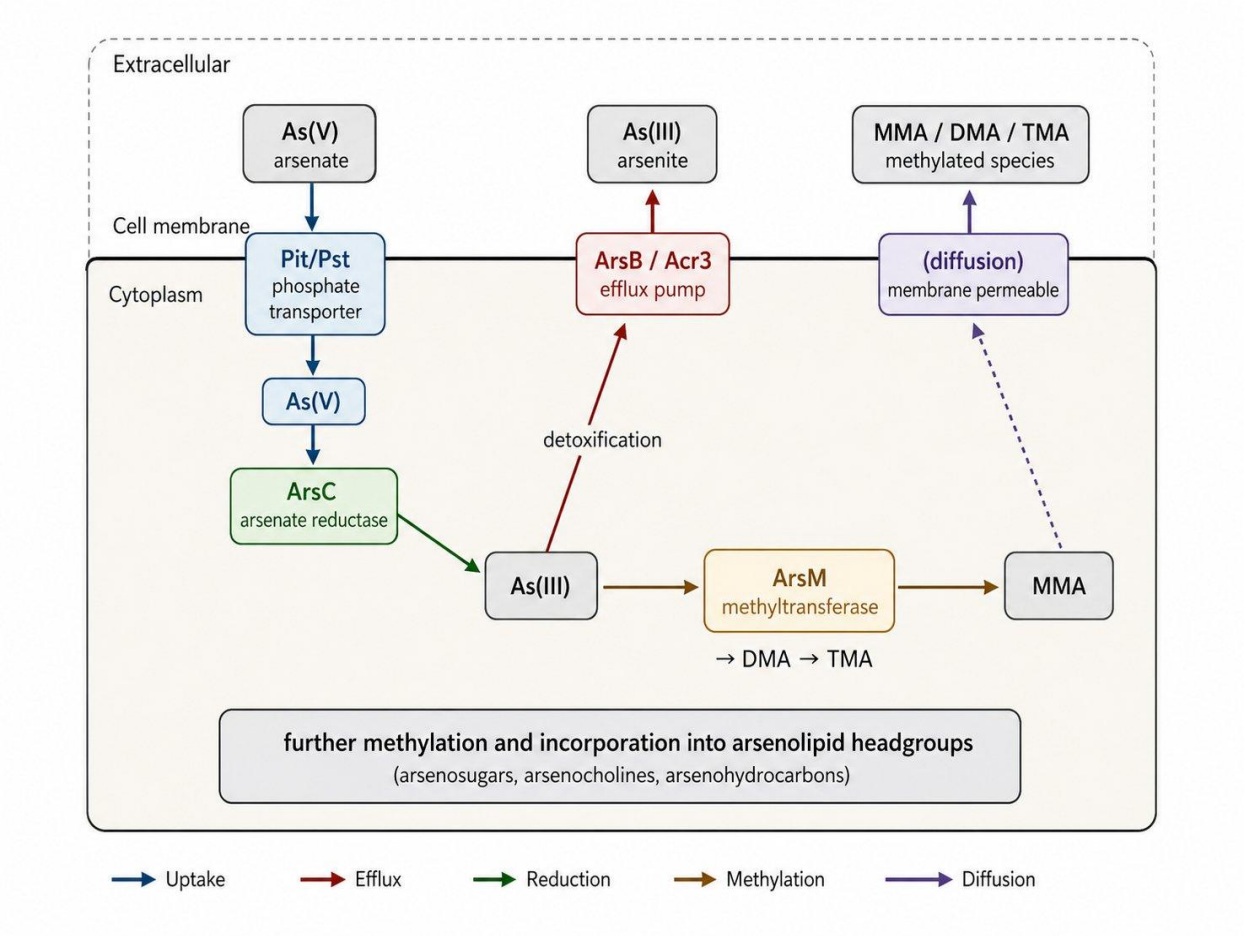

Figure 1.3 Schematic of the conserved microbial arsenic uptake-reduction-methylation pathway and downstream incorporation into arsenolipid headgroups. Arsenate (As(V)) enters the cell via high-affinity phosphate transporters (Pit/Pst) and is reduced to arsenite (As (III)) by the cytoplasmic arsenate reductase ArsC. As(III) is either expelled to the extracellular environment by efflux pumps (ArsB or Acr3) as the primary detoxification response, or methylated stepwise by the arsenite S-adenosylmethionine methyltransferase ArsM to monomethyl- (MMA), dimethyl- (DMA), and trimethylarsenic (TMA) species via a series of redox-coupled intermediates whose trivalent forms (MMA(III), DMA(III)) are highly reactive. The methylated arsenic pool is the presumed precursor for more complex organoarsenicals. Biosynthetic pathways for arsenosugars have been outlined in eukaryotic algae, whereas the formation pathways of arsenohydrocarbons

(AsHCs) remain incompletely constrained and may involve both biological synthesis and diagenetic transformation. Evidence levels (well established / partially established / hypothesized) are indicated in the figure legend.

Chapter 2 Background and Analytical Methods for Detecting Fossil Arsenolipids in Marine Sediments

2.1 Introduction

Arsenolipids are a class of organic molecules with potential as molecular fossils. The upstream metabolic pathway through which arsenate is taken up, reduced, and methylated by aquatic microorganisms was presented in Chapter 1 . The biological diversity of this pathway gives rise to a structurally diverse pool of organoarsenicals, of which more than 260 lipid-soluble species (arsenolipids) have been identified to date (Xue et al., 2022). This chapter develops the analytical framework needed to detect fossil arsenolipids in sedimentary archives, with a methodological focus on arsenohydrocarbons (AsHCs)—the class whose detection required the new chromatographic method developed here. The same workflow is also used to detect the sulfur-containing thioxoarsenolipids first reported by Liu (2023), whose sedimentary record is examined in Chapter 4. The structural diversity of arsenolipids relevant to methodological work identifies why AsHCs are the methodological focus, and describes the analytical challenges that the subsequent sections of this chapter address.

2.1.1 Structural diversity of arsenolipids: eight categories

Based on their molecular structures, these identified arsenolipids can be grouped into eight categories (Figure 2.1): (i) arsenic-containing hydrocarbons (AsHCs), characterized by a polar dimethylarsinoyl headgroup linked to a hydrophobic tail (Taleshi et al., 2008); (ii) arsenic-containing fatty acids (AsFAs), fatty acid analogs in which the terminal methyl group is replaced by a dimethylarsinoyl moiety (Rumpler et al., 2008; Amayo et al., 2013; Arroyo-Abad et al., 2013); (iii) AsFA-containing intact polar lipids, in which common phosphatidylcholine (PC), phosphatidylethanolamine (PE), phosphatidylglycerol (PG), and phosphatidylinositol (PI)

incorporate an AsFA as their fatty acyl chain (Viczek et al., 2016; Řezanka et al., 2019); (iv) arsenosugar phospholipids (AsSugPLs), acylglycerol phospholipids comprising a dimethylarsinoyl-sugar-glycerol headgroup (Morita and Shibata, 1988; Edmonds et al., 1992; García-Salgado et al., 2012; Raab et al., 2013); (v) arsenosugar phytyl esters (AsSugPhytols), ether-linked arsenosugars in which the 2-O-methyl arsenosugar is esterified to phytyl alcohol (Glabonjat et al., 2017, 2020); (vi) phosphatidylarsenocholine, a phospholipid with an arsenocholine headgroup (Edmonds et al., 1992; Fukuda et al., 2011); (vii) trimethylarsenio fatty alcohols (TMAsFOHs), fatty alcohols containing a trimethylarsenio moiety (Amayo et al., 2013; Pétursdóttir et al., 2018); and (viii) sulfur-containing analogs of oxo-arsenolipids in which an arsenic–oxygen bond is replaced by an arsenic–sulfur bond, ranging from simple thio-derivatives of AsHCs (Müller et al., 2018; Xiong et al., 2022) to the structurally more complex sedimentary thioxoarsenolipids reported by Liu (2023).

2.1.2 Arsenohydrocarbons: distribution, source organisms, and preservation potential

While the identification of these compounds highlights the structural diversity of arsenolipids, arsenohydrocarbons (AsHCs)—comprising a dimethylarsinoyl headgroup linked to a long-saturated-hydrocarbon chain—are distinguished by their simple molecular structure, a feature that subsequent degradation studies (Glabonjat et al., 2019a; discussed below) suggest may favor preservation in sediments. The arsenohydrocarbons were first isolated and structurally characterized from the oil of the plankton-feeding marine fish capelin (*Mallotus villosus*) by Taleshi et al. (2008), establishing the canonical structural framework against which subsequent reports of AsHCs across diverse biological matrices have been interpreted. In that first study, AsHC-332, AsHC-360, and AsHC-404 together constituted at least 70% of total arsenic in the fish oil. Since then, AsHCs have been identified in many additional sources. In commercial fish oils

and salmon, these homologs were identified as major arsenolipid components (Sele et al., 2014; Xiong et al., 2022). In the brown macroalga *Ectocarpus*, AsHC-360 represented 50–80% of total arsenolipids (Pétursdóttir et al., 2016), while AsHC-388, though less frequently detected, has been identified in the brown macroalga *Ecklonia radiata*, constituting 3–13% of total arsenolipids (Glabonjat et al., 2019a). Additionally, AsHCs are consistently found in suspended particles of marine surface water, comprising approximately 5–12% of the total particulate arsenolipids (Glabonjat et al., 2021; Heal et al., 2022). These findings indicate that AsHCs occur across diverse aquatic organisms and microbial source communities, including eukaryotic algae, cyanobacteria, and heterotrophic bacteria (Heal et al., 2022), and highlight their role as a molecular tool for investigating the biogeochemical cycle of arsenic.

Although degradation experiments indicate that a large fraction of algal-produced arsenolipids is rapidly remineralized under oxic conditions (Glabonjat et al., 2019a), a small but significant portion may escape degradation, become incorporated into settling particles, and ultimately be preserved following burial under anoxic or reducing conditions. Notably, AsHC-388 was reported to persist longer than the co-occurring arsenic phospholipids under long-term degradation, although the underlying mechanism remains uncertain (Glabonjat et al., 2019a); this differential persistence is consistent with the structural simplicity and saturated hydrocarbon backbone of AsHCs. Despite their detection in a number of modern environmental samples—including marine surface waters (Glabonjat et al., 2021; Heal et al., 2022) and the hypersaline sediments of the Great Salt Lake (Glabonjat et al., 2019b)—prior to the work presented in this dissertation, fossil AsHCs from ancient sedimentary records had not been reported. This absence of a fossil record currently hinders the application of AsHCs as paleoenvironmental proxies for arsenic biogeochemistry and connected processes.

2.1.3 Sulfur-containing arsenolipids in sedimentary records

Beyond the oxo-arsenolipids discussed above, a structurally distinct class of sulfur-containing arsenolipids has recently been recognized in sedimentary records. Liu (2023) reported a suite of novel thioxoarsenolipids in modern and ancient marine sediments, including a Cretaceous black shale. These thioxoarsenolipids are structurally distinct from the simple thio-derivatives of AsHCs. Their fragmentation patterns indicate that, in addition to the As=S headgroup, a second sulfur atom is directly bonded to the carbon chain, yielding a more complex molecular framework whose precise structure remains to be elucidated. Although Glabonjat et al. (2014) demonstrated that the oxo-headgroup of AsHCs can be rapidly converted to a thioxo group in the presence of H_2S, the thioxoarsenolipids reported by Liu (2023) are not simple thio-AsHC derivatives generated through this nucleophilic substitution pathway, and their formation routes remain an open question. This dissertation reports the same family of compounds within the Holocene Black Sea sedimentary record (Chapter 4), where their abundance is examined alongside that of fossil AsHCs across redox transitions.

2.2 The Analytical Challenge

The detection of fossil arsenohydrocarbons in geological samples has historically faced two distinct analytical challenges. The first concerns instrumental configuration: arsenolipid identification has long depended on the parallel coupling of two mass-spectrometric platforms. Liquid chromatography–inductively coupled plasma mass spectrometry (LC-ICP-MS) provides element-specific detection of arsenic at high sensitivity, while electrospray ionization mass spectrometry (LC-ESI-MS) supplies the molecular and structural information needed to assign chemical identity (Amayo et al., 2011; Xue et al., 2022). This dual-platform approach has been highly productive in the analysis of seafood, algae, and other biological matrices where arsenolipid

abundances are relatively high (Sele et al., 2014; Glabonjat et al., 2018, 2019a). For most geological laboratories, however, simultaneous access to both ICP-MS and high-resolution ESI-MS instruments is not routinely available, and the complexity of operating a coupled configuration further limited the application of arsenolipid analysis to sedimentary archives. This obstacle was substantially resolved by Liu (2023), who demonstrated that high-voltage collision-induced dissociation (CID at 200 eV) within a single LC-ESI-qTOF-MS platform can dissociate the covalent bonds linking arsenic to organic substrates, producing the monatomic arsenic cation As^+ (*m/z* 74.9216). This provides arsenic-selective detection without a separate ICP-MS instrument (Section 2.4.3). This advance brought arsenolipid screening within reach of standard organic geochemical laboratories.

The second challenge concerns chromatographic separation of trace-level arsenolipids in complex sedimentary matrices. Reverse-phase liquid chromatography (RPLC), which separates compounds primarily by hydrophobic chain length, is the standard method for arsenolipid analysis in biological samples and performs well when target compounds are abundant relative to the lipid background (García-Salgado et al., 2012; Raab et al., 2013). In sedimentary samples, however, AsHCs typically occur at concentrations several orders of magnitude lower than co-extracted non-arsenic lipids—including fatty acids, hopanoids, and steroidal compounds—that share similar hydrocarbon chain lengths with AsHCs and therefore co-elute in the same retention-time window on RPLC columns. The resulting matrix interference suppresses ionization efficiency, elevates background signals in the extracted ion chromatograms of AsHC molecular ions, and frequently renders AsHC peaks undetectable in low-abundance samples. Consistent with this challenge, Liu (2023), using RPLC coupled to the dual-energy CID strategy, reported a suite of novel thioxoarsenolipids in modern and ancient marine sediments while no AsHCs were observed in any

of the geological samples examined—a result that motivates the chromatographic development pursued in this dissertation.

These chromatographic limitations motivate the combined SPE–NPLC workflow developed in this dissertation. A silica-gel solid-phase extraction step is used to enrich trace-level arsenolipids and reduce bulk lipid interferences, while the NPLC method separates AsHCs according to head-group polarity rather than hydrocarbon chain length. Together with the dual-energy CID strategy of Liu (2023), these steps constitute the analytical framework employed throughout this dissertation. While neither silica-gel SPE (Glabonjat et al., 2014) nor normal-phase chromatography is itself a new technique, their combination and optimization for fossil AsHC detection in geological matrices is the principal methodological contribution of this dissertation. It enables the detection of fossil AsHCs in geological samples for the first time—compounds that remained undetectable under the RPLC-based configuration of Liu (2023), in which only thioxoarsenolipids, and no AsHCs, were observed in the geological samples examined. Their performance relative to conventional RPLC analysis is evaluated in Section 2.5.3.

2.3 Sample Preparation

Sample preparation for arsenolipid analysis in this dissertation follows a two-stage workflow. All sediment samples are first subjected to total lipid extraction; subsequent silica-gel solid-phase extraction (SPE) cleanup is applied only to low-abundance samples in which matrix interference precludes direct LC-MS analysis of the total lipid extract.

2.3.1 Sediment freeze-drying and powdering

Wet sediment samples are first freeze-dried to remove water and homogenized into fine powder using a manual mortar and pestle prior to extraction. This step ensures uniform exposure

of the sediment to the extraction solvent and minimizes between-aliquot variability when small amounts (~200 mg) of material are used per extraction.

2.3.2 Total lipid extraction

Approximately 200 mg of freeze-dried, powdered sediment is transferred into a 4 mL glass vial, and 1.5 mL of dichloromethane/methanol (DCM/MeOH, 1:1, v/v) is added. The vial is briefly vortexed and then sonicated for 20 minutes at room temperature to release lipids from the sediment matrix. After sonication, the suspension is centrifuged at 3,000 rpm for 5 minutes, and the supernatant is transferred to a clean 2 mL glass vial and dried under a gentle stream of nitrogen (N_2). This extraction–centrifugation–transfer–drying cycle is repeated two additional times on the residual sediment, yielding three combined extracts that are pooled and dried to completion under N_2 to obtain the total lipid extract (TLE). For modern reference samples, kelp seaweed (kombu) total lipid extracts prepared in Liu (2023) are also analyzed alongside sedimentary samples and serve as a positive control for AsHC identification (Section 2.6.1). Kombu was selected as a reference because its AsHC profile—dominated by AsHC-332, AsHC-360, and AsHC-388—was extensively characterized by Liu (2023), enabling direct retention-time and fragmentation-pattern matching across instruments and analytical runs in this dissertation.

The 1:1 DCM/MeOH solvent system is chosen for its broad polarity coverage—DCM efficiently dissolves non-polar lipid backbones while MeOH solubilizes polar headgroups—making it well suited to the structurally diverse arsenolipid pool described in Section 2.1.1. Triplicate extraction ensures recovery of trace-level AsHCs that may be tightly bound to the mineral matrix.

2.3.3 Silica-gel solid-phase extraction (SPE) cleanup

In modern, organic-rich samples such as Aarhus Bay surface sediments and kelp seaweed reference material, the TLE can be analyzed directly by LC-MS without further cleanup. In contrast, the detection of arsenolipids in low-abundance ancient sediments and shales requires an additional cleanup step to remove matrix interferences, as direct injection of the TLE produces extracted ion chromatograms in which AsHC peaks are obscured by matrix-derived signal.

Fractionation is performed on Bond Elut SI cartridges (Agilent Technologies, 50 mg sorbent in 1 mL tube), , adapted from the silica cleanup of Glabonjat et al. (2014) and scaled to the cartridge format. Cartridges are preconditioned with 1 mL of MeOH/acetone (1:1, v/v) containing 1% formic acid. The dried TLE is reconstituted in 100 µL of the same MeOH/acetone (1:1, v/v) containing 1% formic acid solvent and loaded onto the conditioned cartridge. The cartridge is then washed sequentially with 2 mL of MeOH/acetone (1:1, v/v) containing 1% formic acid followed by 2 mL of MeOH to remove matrix lipids (Fraction 1, discarded). The arsenolipid-enriched fraction is subsequently eluted with 4 mL of MeOH containing 1% ammonia (NH_4OH) (Fraction 2, retained). Fraction 2 is dried under N_2 and reconstituted in the appropriate injection solvent for LC-MS analysis (MeOH for RPLC, DCM for NPLC; see Section 2.5).

The fractionation gradient employed here follows the validated protocol of Glabonjat et al. (2014), in which arsenolipids were demonstrated to elute quantitatively in the ammonia-containing methanol fraction; additional independent recovery validation specific to the sediment matrices analyzed in this dissertation was not performed.

2.4 Mass Spectrometry: Dual-Energy CID Strategy

The mass spectrometric strategy employed throughout this dissertation centers on a single LC-ESI-qTOF-MS platform operated under two different collision-induced dissociation (CID) energies within the same data acquisition cycle. The mass spectrometric strategy of this chapter is adopted directly from Liu (2023) and is not itself a contribution of this dissertation; it is summarized here to define the detection platform on which the chromatographic developments of Section 2.5 build. This dual-energy approach generates complementary fragment information that simultaneously delivers element-specific arsenic detection and molecular structural characterization, eliminating the need for a separate ICP-MS instrument.

2.4.1 Instrumentation and ionization parameters

The LC-ESI-qTOF-MS analyses were performed using an Agilent 1290 series UPLC system coupled to an Agilent 6530 quadrupole time-of-flight (qTOF) mass spectrometer through an Agilent jet stream dual electrospray ionization (AJS-ESI) interface. The ESI source was operated in positive ion mode with the following parameters: drying gas (N_2) temperature at 325 °C, drying gas flow rate at 8 L min^{-1}, nebulizer gas (N_2) pressure at 35 psi, and capillary voltage at 3.5 kV. The qTOF parameters were set to a fragmentor voltage of 175 V, skimmer voltage of 65 V, and octupole voltage of 750 V. Mass spectra were acquired in auto MS/MS scanning mode over an MS scan range of *m/z* 50–2000 and an MS/MS scan range of *m/z* 20–2000. Nitrogen served as the collision gas for CID. Detailed data acquisition parameters follow the configuration established by Liu (2023).

2.4.2 Low-energy CID (20 eV): molecular structural information

At a collision energy of 20 eV—the standard setting for general lipid analysis—CID produces no major molecular fragments of AsHCs due to their fully saturated, straight-chain carbon skeleton. Nevertheless, two characteristic head-group ions are consistently observed: $[AsC_2H_6]^+$ at *m/z* 104.9668 and $[AsC_2H_8O]^+$ at *m/z* 122.9768, both corresponding to the dimethylarsinoyl moiety (Liu, 2023) (Figure 2.2). These fragments, together with the protonated molecular ion $[M + H]^+$, allow assignment of the head-group identity. For arsenolipids with more complex polar head groups—such as AsSugPLs and AsSugPhytols—low-energy CID also produces large head-group fragments that retain sugar or phytyl moieties, providing additional structural information beyond that available from accurate mass alone.

2.4.3 High-energy CID (200 eV): element-specific arsenic detection

At a collision energy of 200 eV, the substantially elevated kinetic energy drives extensive fragmentation of arsenolipid precursors and cleaves the strong covalent bonds linking arsenic to neighboring carbon, oxygen, or sulfur atoms. Under these conditions, the covalently bound arsenic atom is dissociated from its organic substrate and detected as the monatomic singly charged cation As^+ at *m/z* 74.9216 (Liu, 2023). An additional small arsenic-containing fragment, $AsHO^+$ at *m/z* 91.9243, also appears in the 200 eV MS/MS spectrum and confirms the presence of the dimethylarsinoyl head group (Figure 2.2).

Because arsenic is monoisotopic (^{75}As is the only naturally occurring stable isotope), the As^+ ion appears at a single, unambiguous *m/z* value (74.9216) with mass accuracy below 5 ppm under qTOF conditions. Contributions from carbon-, hydrogen-, oxygen-, or nitrogen-only fragments at this nominal mass are excluded by accurate-mass filtering.

The diagnostic value of As^+ lies in its origin: because the monatomic cation can be generated only from arsenic-bearing precursor ions, the extracted ion chromatogram (EIC) of *m/z* 74.9216 in the product-ion channel functions as an element-specific filter for arsenic-containing molecules. This approach is conceptually analogous to the arsenic channel of LC-ICP-MS, but is achieved within the same instrument that simultaneously delivers high-resolution accurate-mass and tandem MS structural information. For arsenolipid screening in complex sedimentary matrices, the As^+ EIC effectively suppresses background signal from non-arsenic lipids and reveals AsHC peaks that would otherwise be obscured in the total ion chromatogram.

2.4.4 Diagnostic ions for sulfur-containing arsenolipids

For arsenolipids in which the dimethylarsinoyl head group is replaced by a sulfur-containing analog, an additional diagnostic ion appears in the 200 eV CID spectrum: AsS^+ at *m/z* 106.89, indicating direct As=S bonding (Liu, 2023). The presence of AsS^+ alongside As^+ identifies a compound as a thio-derivative.

A further set of carbon–sulfur fragments—CHS^+ (*m/z* 44.98), $C_2H_3S^+$ (*m/z* 58.99), and $C_3H_3S^+$ (*m/z* 70.99)—appears in the 200 eV CID spectra of certain sedimentary thioxoarsenolipids (Liu, 2023), indicating that one or more sulfur atoms are directly bonded to the carbon chain in addition to the head-group As=S. This carbon–sulfur fragmentation pattern is the principal criterion that distinguishes the structurally simple thio-AsHCs (in which the only sulfur is at the head group) from the more complex thioxoarsenolipids reported by Liu (2023). The application of these diagnostic criteria to compound identification in this dissertation is described in Section 2.6.2.

2.4.5 Dual-energy switching as a diagnostic workflow

In practice, each selected precursor is fragmented at both 20 eV and 200 eV within the same acquisition cycle. Candidate arsenolipids are first located using the 200 eV As^+ EIC, and the corresponding 20 eV MS/MS spectra are then used to evaluate head-group fragments, precursor accurate mass, and structural assignment. This two-step workflow is used for all arsenolipid identifications in subsequent chapters.

2.5 Chromatographic Separation: From RPLC to NPLC

The chromatographic stage of the analytical workflow is where the principal original development of this dissertation departs most clearly from the configuration of Liu (2023): a normal-phase (NPLC) separation that, to our knowledge, is the first optimized for AsHC detection in geological samples. This section first describes the reverse-phase liquid chromatography (RPLC) method that has been the standard for arsenolipid analysis, then introduces the normal-phase liquid chromatography (NPLC) method developed here, and finally compares the two on a common set of samples to demonstrate the gain in AsHC detectability that motivates the methodological switch.

2.5.1 RPLC method

The RPLC analyses follow the configuration established by Liu (2023). Samples are dissolved in methanol prior to injection. Separation is performed on an ACE UltraCore Super Phenyl-Hexyl column (5 μm, 2.1 × 250 mm; ACE, Aberdeen, UK) maintained at 45 °C, with a flow rate of 0.2 mL min^{-1} throughout the analytical gradient. The mobile phase consists of three eluents: eluent A, methanol/H_2O/formic acid/14.8 M NH_3(aq) (95:5:0.04:0.3, v/v/v/v); eluent B, H_2O/formic acid/14.8 M NH_3(aq) (100:0.04:0.3, v/v/v); and eluent C, hexane/2-propanol/formic

acid/14.8 M NH_3(aq) (50:50:0.04:0.3, v/v/v/v). The gradient program begins at 80% A and 20% B, ramping to 100% A over 5 min; followed by a gradient transition to 60% A and 40% C at 20 min; then to 30% A and 70% C at 25 min. After the analytical gradient, the column is re-equilibrated to 80% A and 20% B at a flow rate of 0.4 mL min^{-1} for 5 min before the next injection. Under this RPLC method, AsHCs elute in order of increasing hydrophobic chain length: AsHC-332 (C15) elutes first, followed by AsHC-360 (C17), and AsHC-388 (C19) last.

2.5.2 NPLC method

The method described here represents, to our knowledge, the first normal-phase LC (NPLC) method optimized for AsHC separation in geological samples; the chromatographic conditions build on standard hexane/isopropanol-based normal-phase configurations widely used in polar lipid analysis but not previously applied to arsenolipids in sedimentary archives. The method employs the same LC-ESI-qTOF-MS instrumental platform and dual-energy CID strategy described in Section 2.4, but replaces the reverse-phase column with a hydrophilic interaction (HILIC) column. Samples are dissolved in dichloromethane (DCM) prior to injection. Separation is performed on an InfinityLab Poroshell 120 HILIC column (1.9 µm, 2.1 × 150 mm; Agilent Technologies) maintained at 35 °C, with a flow rate of 0.2 mL min^{-1} throughout the analytical gradient. The mobile phase consists of two eluents: eluent A, hexane/2-propanol/formic acid/14.8 M NH_3(aq) (70:30:0.04:0.10, v/v/v/v); and eluent B, methanol/H_2O/formic acid/14.8 M NH_3(aq) (95:5:0.04:0.10, v/v/v/v). The gradient program begins by holding 98% A and 2% B for 2 min, followed by a linear gradient to 40% A and 60% B over 15 min, then to 100% B at 20 min. After the analytical gradient, the column is re-equilibrated to 98% A and 2% B at a flow rate of 0.4 mL min^{-1} for 5 min before the next injection. Under this NPLC method, AsHCs elute in the reverse order from RPLC: AsHC-388 (C19) elutes first, followed by AsHC-360 (C17), and AsHC-332

(C15) last. Column temperature, gradient slope, and flow rate were optimized empirically for AsHC peak shape and resolution; the values reported here represent the conditions selected for the comparative analyses of Section 2.5.3.

The reversed elution order under NPLC reflects the fundamentally different separation mechanism. On the reverse-phase Phenyl-Hexyl column, retention is dominated by hydrophobic interactions between the AsHC hydrocarbon chain and the stationary phase, so longer, more hydrophobic chains are retained more strongly. On the HILIC column, retention is governed by polarity rather than hydrophobicity, so the more polar AsHCs are retained more strongly. Because all AsHCs share the same dimethylarsinoyl head group, their relative polarities scale inversely with hydrocarbon chain length: AsHC-332 (C15), with the shortest chain, has the highest overall polarity and elutes last; AsHC-388 (C19), with the longest chain, has the lowest overall polarity and elutes first.

2.5.3 RPLC versus NPLC: comparative performance on geological samples

The two chromatographic methods were compared by analyzing matched aliquots from the same total lipid extract (same starting material per injection) of three samples spanning a range of arsenolipid abundances and matrix complexities (a more comprehensive cross-sample comparison is presented in Chapter 3): kelp seaweed (kombu) reference material, fresh marine sediment from Aarhus Bay, and a late Turonian organic-rich black shale (ODP 207, Site 1259C, Core 15R; ~90 Ma). Under RPLC, AsHCs were well resolved in the kelp seaweed reference, but signals weakened substantially in the sedimentary samples. Only minor peaks of AsHC-332 and AsHC-360 were observed in the TLE of Aarhus Bay sediment, and no distinct AsHC peaks were detected in the arsenolipid fraction of the Cretaceous shale (Figure 2.3). Elevated background signals across the

AsHC-relevant retention window further indicate substantial co-eluting matrix interference in both sedimentary samples.

Under NPLC, the same three samples produced markedly improved results. Three AsHC homologs (AsHC-332, AsHC-360, and AsHC-388) were detected in the Aarhus Bay TLE; two homologs (AsHC-332 and AsHC-360) were detected in the SPE-cleaned arsenolipid fraction of the Cretaceous shale. The NPLC chromatograms exhibit lower background and clearer peak shape compared to their RPLC counterparts, and AsHCs that were submerged within the matrix background under RPLC become well-resolved under NPLC. Although a formal quantitative signal-to-noise comparison was not performed, the contrast between methods is qualitative in nature: AsHC homologs that produced no distinguishable peaks above background in the As^+ EIC under RPLC analysis of the Cretaceous shale extract were clearly resolved under NPLC analysis of the same extract (Figure 2.3). This categorical difference—from undetectable to detectable—is the central observation that motivated the development of the NPLC method, and is consistent with the matrix-interference mechanism discussed in Section 2.5.4.

2.5.4 Why NPLC succeeds where RPLC fails in low-abundance sedimentary samples

The differential performance between the two methods reflects what each co-elutes with AsHCs. As described in Section 2.2, RPLC retains AsHCs together with co-eluting matrix lipids of comparable hydrophobicity, whose ion suppression and elevated background submerge the AsHC peaks in low-abundance samples.

The NPLC resolves this co-elution problem at the level of the separation mechanism. By transferring the dominant retention factor from hydrophobicity to polarity, the HILIC column places AsHCs in retention-time windows that are largely separated from those occupied by the bulk of the polar matrix lipids. The matrix components that dominated the RPLC AsHC retention

window now elute in different regions of the NPLC chromatogram, where they no longer interfere with AsHC ionization. The combination of NPLC separation with the upstream SPE cleanup described in Section 2.3 thus addresses the second analytical challenge identified in Section 2.2 and enables the detection of fossil AsHCs in geological samples for the first time. The application of this combined workflow to a broader sample set is presented in Chapter 3, and to a Holocene sedimentary sequence in Chapter 4.

2.6 Identification Criteria for Fossil Arsenolipids

Arsenolipid identifications throughout this dissertation rest on accurate mass measurements, MS/MS fragmentation patterns at both 20 eV and 200 eV CID, and comparison with published data (Liu, 2023). The diagnostic ions employed at each CID energy are described in Section 2.4. This section consolidates the application of those diagnostic ions to compound assignment, and addresses one additional case—sulfur-containing arsenolipids—where extra criteria are required to distinguish structurally similar compound classes. Compound identifications reported in this dissertation are described using the confidence-level framework of Schymanski et al. (2014), which has been widely adopted in environmental high-resolution mass spectrometry. Within this framework, AsHC identifications in the present work correspond to Level 2a ("probable structure—library/literature spectrum match"), in which the candidate AsHC's accurate mass, head-group fragmentation pattern, and retention behavior are matched against the AsHC suite characterized in the kombu reference material by Liu (2023). Because no authentic, isolated AsHC standard was available, a Level 1 ("confirmed structure") assignment is not claimed. The thioxoarsenolipid identifications correspond to Level 2b ("probable structure by diagnostic evidence"), based on accurate mass, the AsS^+ diagnostic ion, and the carbon-sulfur

fragmentation pattern documented by Liu (2023), in the absence of an isotope-labeled synthetic standard.

2.6.1 Identification of AsHCs

For AsHCs, identification is based on three complementary lines of evidence (Liu, 2023): (1) accurate mass measurement of the $[M + H]^+$ precursor ion; (2) detection of the dimethylarsinoyl head-group fragments $[AsC_2H_6]^+$ and $[AsC_2H_8O]^+$ in the 20 eV MS/MS spectrum; and (3) detection of the monatomic As^+ ion at *m/z* 74.9216 in the 200 eV MS/MS spectrum. Identifications are further supported by comparison with the kombu reference material run alongside sedimentary samples (Section 2.3.2).

2.6.2 Identification of sulfur-containing arsenolipids

Sulfur-containing arsenolipids are identified following the diagnostic criteria established by Liu (2023). Two lines of evidence are applied in the 200 eV CID spectrum. First, the AsS^+ ion (*m/z* 106.89) indicates the presence of an As=S bond and identifies a compound as a thioxoarsenolipid. Second, the carbon–sulfur fragments CHS^+, $C_2H_3S^+$, and $C_3H_3S^+$ (defined in Section 2.4.4), together with accurate mass, indicate that a second sulfur atom is directly bound to the carbon chain—the structural feature characterizing the sedimentary thioxoarsenolipids reported by Liu (2023). Using these same criteria, the sulfur-containing arsenolipids detected in this dissertation are assigned to that class of sedimentary thioxoarsenolipids.

2.6.3 Method validation: limitations and detection considerations

Several method-validation steps that are routinely reported for established analytical methods could not be completed within the scope of this dissertation. (1) Method detection limits (MDLs) for individual AsHC homologs were not determined by formal serial dilution; the practical

detectability threshold in this work is operationally defined as a recognizable peak in the As^+ EIC at *m/z* 74.9216 with mass accuracy below 5 ppm in the corresponding 20 eV MS/MS spectrum. Establishing formal LODs across the relevant matrix-complexity range remains an outstanding task and is recommended for future revisions of the method. (2) No isotope-labeled internal standards specific to AsHCs or thioxoarsenolipids are commercially available, so absolute concentrations cannot be determined. Abundances are therefore semi-quantitative. In the qualitative survey of Chapter 3, no internal standard was used and results are reported as occurrence patterns only. In the Black Sea time series of Chapter 4, a fixed amount of the general-purpose internal standard C_{46}-GTGT was added to every sample prior to extraction, permitting TOC-normalized, semi-quantitative comparison of relative abundances through the sequence (Section 4.3). (3) Process blanks, replicate-extraction RSD values, and independent SPE recovery experiments specific to these sediment matrices were not performed (see Section 2.3.3). These limitations are explicitly acknowledged here and constrain the interpretive scope of subsequent chapters. R esults in Chapter 3 are presented as qualitative occurrence patterns, and those in Chapter 4 as semi-quantitative, internal-standard-normalized relative abundances rather than as absolute concentration data.

2.7 Summary

This chapter established the analytical framework used throughout the dissertation for detecting fossil arsenolipids in marine sediments. The workflow combines the dual-energy CID strategy of Liu (2023), which provides both molecular structural information and element-specific arsenic detection within a single LC-ESI-qTOF-MS platform, with sample cleanup and chromatographic developments optimized for low-abundance sedimentary matrices.

To extend this framework from biological samples to low-abundance ancient sediments, two methodological additions are introduced in this dissertation. A silica-gel solid-phase extraction step, adapted from Glabonjat et al. (2014), enriches trace-level arsenolipids and removes bulk lipid interferences in samples where direct injection of the total lipid extract does not yield resolvable AsHC signals. A normal-phase liquid chromatography (NPLC) method, developed using a HILIC column, separates AsHCs by head-group polarity rather than hydrocarbon chain length, resolving AsHCs from co-eluting polar matrix components that obscure them under conventional reverse-phase chromatography. The combination of SPE cleanup, NPLC separation, and dual-energy CID enables the detection of fossil AsHCs in sedimentary samples in which they were previously inaccessible.

The identification criteria established in Section 2.6 are applied throughout the remainder of this dissertation. Chapter 3 documents the occurrence of fossil arsenolipids across fourteen samples spanning eight modern aquatic samples and six fossil sedimentary samples, from Quaternary Peru-margin OMZ deposits to a mid- to late Cenomanian (~94–100 Ma) black shale within the OAE2 interval; AsHCs and thioxoarsenolipids show distinct preservation ranges, with thioxoarsenolipids extending to the oldest (OAE2) interval where AsHCs are no longer detected. Chapter 4 examines arsenolipid records in the Holocene Black Sea, where the same family of thioxoarsenolipids reported by Liu (2023) is detected alongside AsHCs across the sedimentary sequence, and their distributions are discussed in relation to environmental factors that may influence arsenolipid preservation.

2.8 References

Amayo, K.O., Pétursdóttir, A., Newcombe, C., Gunnlaugsdóttir, H., Raab, A., Krupp, E.M., Feldmann, J., 2011. Identification and quantification of arsenolipids using reversed-phase HPLC coupled simultaneously to high-resolution ICPMS and high-resolution electrospray MS without species-specific standards. Analytical Chemistry 83, 3589–3595. https://doi.org/10.1021/ac102187u

Amayo, K.O., Raab, A., Krupp, E.M., Gunnlaugsdóttir, H., Feldmann, J., 2013. Novel identification of arsenolipids using chemical derivatizations in conjunction with RP-HPLC-ICPMS/ESMS. Analytical Chemistry 85, 9321–9327. https://doi.org/10.1021/ac4020935

Arroyo-Abad, U., Lischka, S., Piechotta, C., Mattusch, J., Reemtsma, T., 2013. Determination and identification of hydrophilic and hydrophobic arsenic species in methanol extract of fresh cod liver by RP-HPLC with simultaneous ICP-MS and ESI-Q-TOF-MS detection. Food Chemistry 141, 3093–3102. https://doi.org/10.1016/j.foodchem.2013.05.152

Edmonds, J.S., Shibata, Y., Francesconi, K.A., Yoshinaga, J., Morita, M., 1992. Arsenic lipids in the digestive gland of the western rock lobster *Panulirus cygnus*: an investigation by HPLC ICP-MS. Science of the Total Environment 122, 321–335. https://doi.org/10.1016/0048-9697(92)90050-3

Fukuda, S., Terasawa, M., Shiomi, K., 2011. Phosphatidylarsenocholine, one of the major arsenolipids in marine organisms: synthesis and metabolism in mice. Food and Chemical Toxicology 49, 1598–1603. https://doi.org/10.1016/j.fct.2011.03.053

García-Salgado, S., Raber, G., Raml, R., Magnes, C., Francesconi, K.A., 2012. Arsenosugar phospholipids and arsenic hydrocarbons in two species of brown macroalgae. Environmental Chemistry 9, 63–66. https://doi.org/10.1071/EN11164

Glabonjat, R.A., Blum, J.S., Miller, L.G., Webb, S.M., Stolz, J.F., Francesconi, K.A., Oremland, R.S., 2020. Arsenolipids in cultured Picocystis strain ML and their occurrence in biota and sediment from Mono Lake, California. Life 10, 93. https://doi.org/10.3390/life10060093

Glabonjat, R.A., Duncan, E.G., Francesconi, K.A., Maher, W.A., 2019a. Transformation of arsenic lipids in decomposing *Ecklonia radiata*. Journal of Applied Phycology 31, 3979–3987. https://doi.org/10.1007/s10811-019-01845-2

Glabonjat, R.A., Ehgartner, J., Duncan, E.G., Raber, G., Jensen, K.B., Krikowa, F., Maher, W.A., Francesconi, K.A., 2018. Arsenolipid biosynthesis by the unicellular alga *Dunaliella tertiolecta* is influenced by As/P ratio in culture experiments. Metallomics 10, 145–153. https://doi.org/10.1039/c7mt00249a

Glabonjat, R.A., Raber, G., Holm, H.C., Mooy, B.A.S., Francesconi, K.A., 2021. Arsenolipids in plankton from high- and low-nutrient oceanic waters along a transect in the North Atlantic. Environmental Science & Technology 55, 5515–5524. https://doi.org/10.1021/acs.est.0c06901

Glabonjat, R.A., Raber, G., Jensen, K.B., Ehgartner, J., Francesconi, K.A., 2014. Quantification of arsenolipids in the certified reference material NMIJ 7405-a (Hijiki) using HPLC/mass spectrometry after chemical derivatization. Analytical Chemistry 86, 10282–10287. https://doi.org/10.1021/ac502488f

Glabonjat, R.A., Raber, G., Jensen, K.B., Guttenberger, N., Zangger, K., Francesconi, K.A., 2017. A 2-O-methylriboside unknown outside the RNA world contains arsenic. Angewandte Chemie International Edition 56, 11963–11965. https://doi.org/10.1002/anie.201706310

Glabonjat, R.A., Raber, G., Jensen, K.B., Schubotz, F., Boyd, E.S., Francesconi, K.A., 2019b. Origin of arsenolipids in sediments from Great Salt Lake. Environmental Chemistry 16, 303–311. https://doi.org/10.1071/EN19135

Heal, K.R., Maloney, A.E., Ingalls, A.E., Bundy, R.M., 2022. Diverse arsenic-containing lipids in the surface ocean. Limnology and Oceanography Letters 7, 43–51. https://doi.org/10.1002/lol2.10216

Liu, X.-L., 2023. Streamlined arsenolipid identification via direct arsenic detection using RPLC-ESI-QTOF-MS with collision-induced dissociation. Journal of the American Society for Mass Spectrometry. https://doi.org/10.1021/jasms.3c00367

Morita, M., Shibata, Y., 1988. Isolation and identification of arseno-lipid from a brown alga, *Undaria pinnatifida* (Wakame. Chemosphere 17, 1147–1152. https://doi.org/10.1016/0045-6535(88)90180-4

Müller, S.M., Finke, H., Ebert, F., Kopp, J.F., Schumacher, F., Kleuser, B., Francesconi, K.A., Raber, G., Schwerdtle, T., 2018. Arsenic-containing hydrocarbons: effects on gene expression, epigenetics, and biotransformation in HepG2 cells. Archives of Toxicology 92, 1751–1765. https://doi.org/10.1007/s00204-018-2196-x

Pétursdóttir Á.H., Fletcher K., Gunnlaugsdóttir H., Krupp E., Küpper F.C., Feldmann J., 2016. Environmental effects on arsenosugars and arsenolipids in *Ecklonia radiata* (Phaeophyta. Environmental Chemistry 13, 21–33. https://doi.org/10.1071/EN14229

Pétursdóttir, Á.H., Jesus, J., Gunnlaugsdóttir, H., Feldmann, J., 2018. Quantification of labile and stable non-polar arsenolipids in commercial fish meals and edible seaweed samples. Journal of Analytical Atomic Spectrometry 33, 102–110. https://doi.org/10.1039/c7ja00333a

Raab, A., Newcombe, C., Pitton, D., Ebel, R., Feldmann, J., 2013. Comprehensive analysis of lipophilic arsenic species in a brown alga (*Saccharina latissima*. Analytical Chemistry 85, 2817–2824. https://doi.org/10.1021/ac303340t

Řezanka, T., Nedbalová, L., Barcyte, D., Vítová, M., Sigler, K., 2019. Arsenolipids in the green alga Coccomyxa (Trebouxiophyceae, Chlorophyta. Phytochemistry 164, 243–251. https://doi.org/10.1016/j.phytochem.2019.05.002

Rumpler, A., Edmonds, J.S., Katsu, M., Jensen, K.B., Goessler, W., Raber, G., Gunnlaugsdóttir, H., Francesconi, K.A., 2008. Arsenic-containing long-chain fatty acids in cod-liver oil: a result of biosynthetic infidelity? Angewandte Chemie International Edition 47, 2665–2667. https://doi.org/10.1002/ange.200705405

Schymanski, E.L., Jeon, J., Gulde, R., Fenner, K., Ruff, M., Singer, H.P., Hollender, J., 2014. Identifying small molecules via high resolution mass spectrometry: communicating confidence. Environmental Science & Technology 48, 2097–2098. https://doi.org/10.1021/es5002105

Sele, V., Sloth, J.J., Holmelid, B., Valdersnes, S., Skov, K., Amlund, H., 2014. Arsenic-containing fatty acids and hydrocarbons in marine oils – determination using reversed-phase HPLC-ICP-MS and HPLC-qTOF-MS. Talanta 121, 89–96. https://doi.org/10.1016/j.talanta.2013.12.049

Taleshi, M.S., Jensen, K.B., Raber, G., Edmonds, J.S., Gunnlaugsdóttir, H., Francesconi, K.A., 2008. Arsenic-containing hydrocarbons: natural compounds in oil from the fish capelin, *Mallotus villosus*. Chemical Communications 39, 4706–4707. https://doi.org/10.1039/B808049F

Viczek, S.A., Jensen, K.B., Francesconi, K.A., 2016. Arsenic-containing phosphatidylcholines: a new group of arsenolipids discovered in herring caviar. Angewandte Chemie International Edition 55, 5259–5262. https://doi.org/10.1002/anie.201512031

Xiong, C., Glabonjat, R.A., Al Amin, M.H., Stiboller, M., Yoshinaga, J., Francesconi, K.A., 2022. Arsenolipids in salmon are partly converted to thioxo analogs during cooking. Journal of Trace Elements in Medicine and Biology 69, 126892. https://doi.org/10.1016/j.jtemb.2021.126892

Xue, X.-M., Xiong, C., Yoshinaga, M., Rosen, B., Zhu, Y.-G., 2022. The enigma of environmental organoarsenicals: insights and implications. Critical Reviews in Environmental Science and Technology 52, 3835–3862. https://doi.org/10.1080/10643389.2021.1947678

2.9 Figures

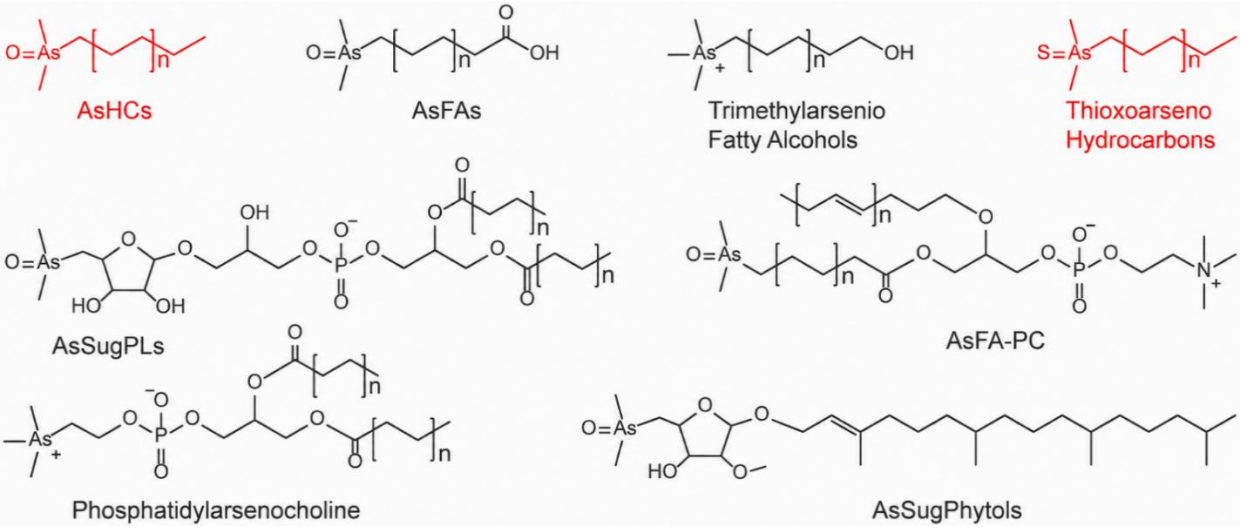

Figure 2.1 Molecular structures of representative arsenolipid classes. Eight structural categories are shown: arsenohydrocarbons (AsHCs, highlighted in red as the principal target class of this dissertation), arsenic-containing fatty acids (AsFAs), trimethylarsenio fatty alcohols, thioxoarsenohydrocarbons, arsenosugar phospholipids (AsSugPLs), arsenic-containing fatty-acid phosphatidylcholines (AsFA-PC), phosphatidylarsenocholines, and arsenosugar phytols (AsSugPhytols). The dimethylarsinoyl head group ($O{=}As(CH_3)_2^{-}$) is shared across most classes; structural diversity arises from the carbon framework attached to arsenic. Modified after Liu (2023).

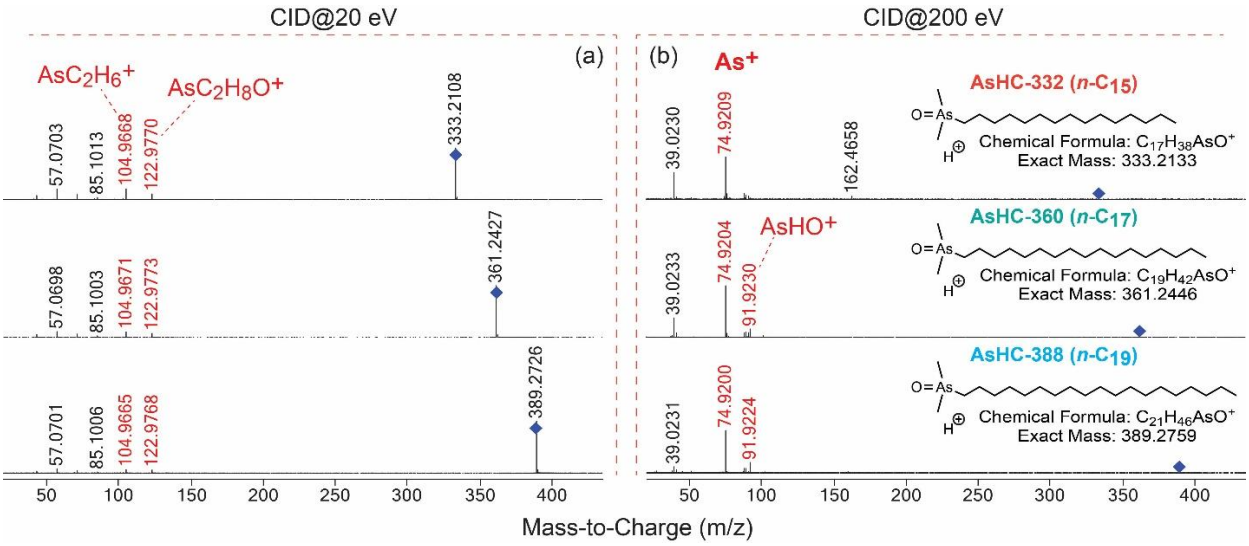

Figure 2.2 Identification of AsHC-332, -360 and -388 based on diagnostic MS/MS fragmentations with CID at 20 (a) and 200 eV (b).

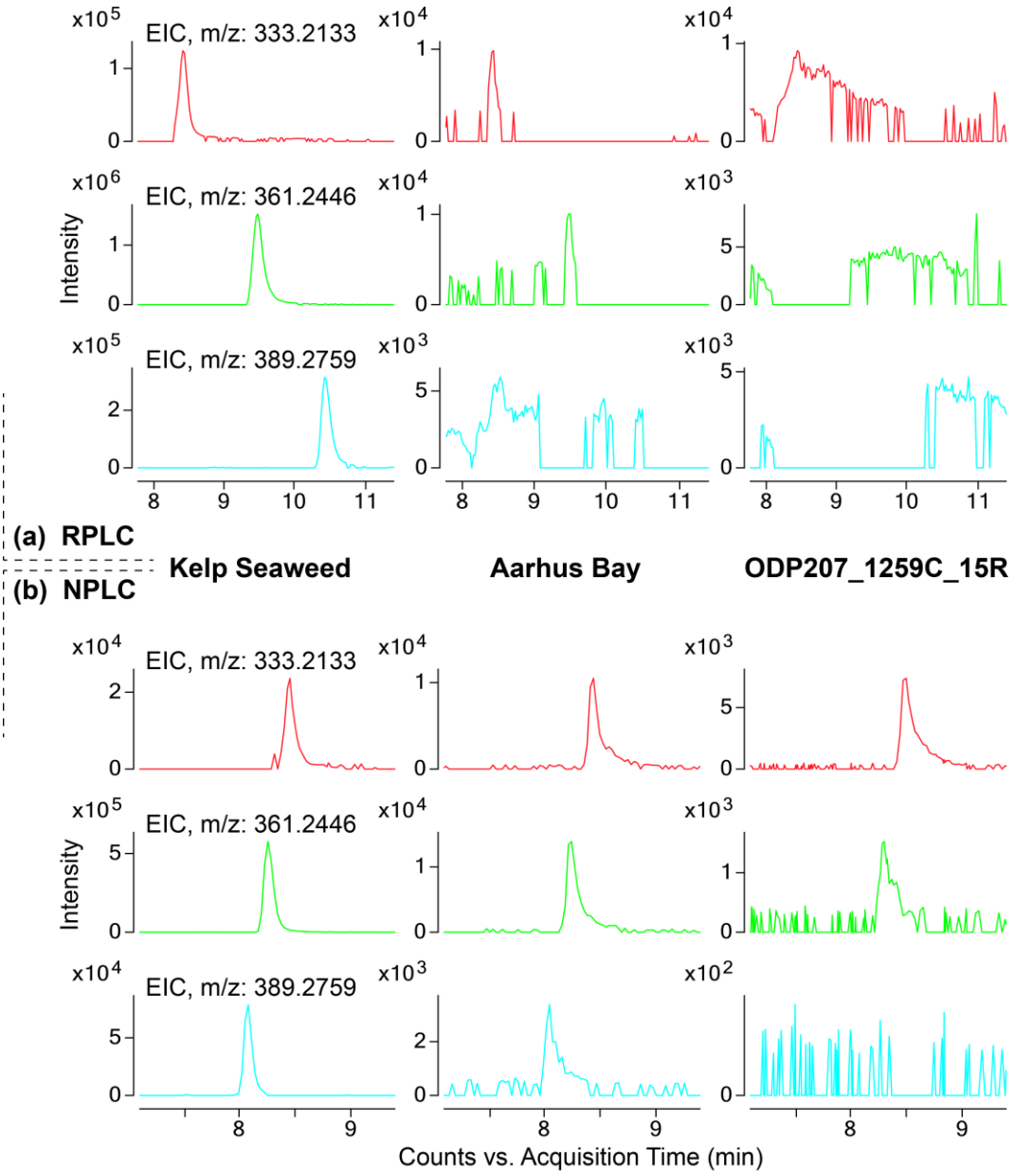

Figure 2.3 RPLC-ESI-QTOF-MS and NPLC-ESI-QTOF-MS of AsHCs detected in TLEs of Kelp Seaweed and fresh marine sediment (Aarhus Bay), and the arsenolipid fraction of Cretaceous Shale extract (ODP207_1259C_15R).

Chapter 3 Widespread Occurrence of Arsenolipids in Modern and Ancient Sediments

3.1 Introduction

The methodological framework developed in Chapter 2—combining silica-gel solid-phase extraction (SPE), normal-phase liquid chromatography (NPLC), and dual-energy collision-induced dissociation (CID)—was demonstrated on two sedimentary samples: a modern coastal sediment from Aarhus Bay and a Cretaceous black shale from ODP Site 1259C, Core 15R. These two samples established that fossil AsHCs are detectable in geological matrices, but a two-sample dataset is not sufficient to establish AsHCs as a general class of molecular fossil. Their broader applicability—across diverse modern aquatic environments, across a range of sedimentary lithologies, and across geological timescales—remains to be tested.

Building on the methodological framework of Chapter 2, this chapter addresses the two questions identified in Chapter 1 regarding the modern distribution and geological preservation of AsHCs. With respect to modern distribution, AsHCs have been documented in fish oils (Taleshi et al., 2008; Sele et al., 2014), marine algae (see Section 2.1.2), and surface-water particulates (Glabonjat et al., 2021; Heal et al., 2022), but most published reports are concentrated in a relatively narrow range of biological matrices, and AsHC occurrence in modern sediments has been examined in only a few sites. With respect to geological preservation, fossil AsHCs from ancient sedimentary records had not been reported prior to the work presented in this dissertation, and consequently the upper age limit and depositional-environment range over which AsHCs can be preserved were unknown.

This chapter addresses both questions through a survey of fourteen samples spanning modern aquatic environments and ancient sedimentary archives. The sample set comprises eight modern aquatic samples—a brown macroalga and seven freshwater, brackish, and coastal marine

settings of contrasting redox character—together with six fossil sedimentary samples ranging in age from Quaternary to mid-Cretaceous. Two compound classes are screened in parallel: AsHCs (the principal arsenolipid class historically reported in modern biological samples) and thioxoarsenolipids (a sulfur-containing class recently described by Liu, 2023). The detection of both classes across this diverse sample set provides the basis for evaluating their distribution in modern aquatic systems and their preservation potential in the geological record, and for motivating the focused time-series investigation of a single sedimentary sequence presented in Chapter 4.

3.2 Sample Set

The sample set analyzed in this chapter comprises fourteen samples organized into two complementary groups: eight modern aquatic settings and six fossil sedimentary samples. The set spans three independent gradients that together address the dual aims of this chapter. The temporal gradient (modern → Quaternary → ~48 Ma → ~52–53 Ma → ~90 Ma → ~94–100 Ma) tests whether AsHCs and thioxoarsenolipids persist across geological timescales. The environmental gradient (eutrophic reservoir → small urban pond → lacustrine meromictic → coastal seasonally meromictic → coastal hypoxic → modern OMZ → pelagic open-marine → anoxic basinal) tests whether occurrence depends on a particular depositional setting or extends across diverse aquatic environments. The lithological gradient (diatomaceous shelf sediment → organic-rich oil shale → organic-rich black shale → carbonate-rich pelagic chalk) tests the role of bulk organic matter content and matrix mineralogy in compound retention. Detailed site characteristics, coordinates, and depositional environments are summarized in Table 3.1.

3.2.1 Modern reference samples

Eight modern aquatic samples were selected to provide independent reference points along the production–deposition continuum of arsenolipids in modern aquatic systems, ranging from a brown-macroalga end-member to small urban ponds, deep tropical anoxic lakes, and coastal hypoxic basins.

Kelp seaweed (*Laminaria* sp.) was obtained from a commercial source as a biological reference for AsHC biosynthesis in brown macroalgae, a group in which AsHC distributions have been characterized in detail (Section 2.1.2). Kelp total lipid extract serves as a positive control for AsHC identification at the level of an extant primary producer, providing an algal end-member against which AsHC distributions in sedimentary samples can be compared. The same sample was also analyzed by Liu (2023) and is used here for cross-method retention-time and fragmentation-pattern verification (Section 2.6.1).

Aarhus Bay surface sediment was collected from a semi-enclosed coastal basin in Denmark (56°N, 10°E; 14–18 m water depth) characterized by seasonal hypoxia, active Fe-Mn redox cycling, and sulfate reduction in pore waters (Thamdrup et al., 1994). Surface sediments at Aarhus Bay are organic-rich (TOC ~2–4 wt% across multiple long-term monitoring stations; Chen et al., 2017). As a transitional redox environment between fully oxic open-marine settings and persistently anoxic basins, Aarhus Bay tests AsHC stability under conditions where redox boundaries fluctuate over seasonal-to-annual timescales. This sample also provides direct continuity with the methodological work of Chapter 2, where Aarhus Bay sediment was one of the two samples used to demonstrate the SPE-NPLC workflow.

Salt Pond is a small (~5 m deep) coastal seasonally meromictic pond in Falmouth, Massachusetts (41.55°N, 70.62°W), that develops a sulfidic hypolimnion below a well-defined

oxic–anoxic interface during summer stratification. Sediment from the sulfidic basin provides a coastal marine-influenced reference for arsenolipid occurrence in seasonally euxinic conditions.

Lower Mystic Lake is a permanently meromictic urban lake in the Boston area (42.43°N, 71.13°W) with brackish bottom water and a well-developed black-water anoxic chemocline at ~15–16 m depth. The varved sediment record from this lake provides a mid-latitude meromictic reference at high temporal resolution.

Fayetteville Green Lake (43.05°N, 75.96°W) is a glacial-plunge-pool meromictic marl lake in central New York with a persistently sulfidic monimolimnion below a chemocline at ~18–20 m. The sediment sample analyzed here was collected from ~53 m depth at the lake bottom, where carbonate-laminated organic sediments accumulate under continuous euxinic conditions. This sample provides a classic euxinic-lake reference of the type frequently invoked as a modern analog for ancient stratified water columns.

Lake Tanganyika (~6°S, 29–30°E) is a tropical freshwater rift lake in East Africa with a maximum depth of 1470 m and permanently anoxic deep waters below ~100–150 m, hosting the largest single body of anoxic freshwater on Earth's surface. The sediment sample analyzed here extends the modern arsenolipid survey to a deep tropical anoxic freshwater system distinct in both physical and limnological regime from the temperate meromictic lakes.

Lake Thunderbird (35.22°N, 97.23°W) is a small reservoir near Norman, Oklahoma, constructed in 1965 with a mean depth of approximately 5 m and a maximum depth of 18 m. The reservoir experiences chronic algal blooms associated with elevated nutrient loading, providing a reference for arsenolipid occurrence in an anthropogenically eutrophied freshwater system.

Duck Pond (35.21°N, 97.44°W) is a small recreational pond on the campus of the University of Oklahoma in Norman. The pond serves as a small-volume urban-pond end-member, providing the smallest aquatic system in the modern sample set.

3.2.2 Fossil sedimentary samples

Six fossil sedimentary samples were selected to test arsenolipid preservation across geological time and across contrasting depositional environments, spanning Quaternary high-productivity margin sediments, the middle Eocene Messel Shale, and three depths of the Cretaceous Demerara Rise sequence.

The ODP 1227-3H5 is a Quaternary diatomaceous-rich silty sediment from lithostratigraphic Subunit IIB of ODP Site 1227, recovered from ~24–25 mbsf on the Peru continental shelf (8.99°S, 79.96°W; 427 m water depth) within the Trujillo Basin (Shipboard Scientific Party, 2003). The Trujillo Basin lies beneath the Peru high-productivity upwelling system and accumulates organic-rich sediments (TOC 1.2–10.6 wt% across Site 1227) under suboxic-to-anoxic mid-water conditions associated with the modern Peruvian oxygen minimum zone (Paulmier and Ruiz-Pino, 2009). This sample tests arsenolipid occurrence in modern margin sediments deposited beneath an active OMZ.

The ODP 1227-5H3 is a Quaternary diatom-bearing clayey silt with dolomite-bearing layers from lithostratigraphic Unit III of the same site, recovered from ~36–37 mbsf. As a deeper interval from the same hole, this sample serves as a stratigraphic companion to ODP 1227-3H5 and tests within-core consistency of arsenolipid detection across an organic-rich margin sequence.

Messel Shale is a finely laminated lacustrine oil shale from the middle Eocene Messel Formation, Hesse, Germany (~48 Ma; 49°55'N, 8°45'E). The shale was deposited in a meromictic crater lake characterized by persistently anoxic bottom waters (Lenz et al., 2010) and is

exceptionally organic-rich, with bulk TOC averaging ~27 wt% across the 150-m-thick oil shale sequence (Bauersachs et al., 2014). It is renowned for its exceptional preservation of fossil organisms and biomolecules (Grice et al., 2019). As a non-marine sample, Messel provides a lacustrine counterpart to the marine fossil samples described below and tests AsHC preservation under stratified, anoxic lacustrine conditions.

The ODP 1259C-4R is a foraminifer-nannofossil pelagic chalk from lithostratigraphic Subunit IIC of ODP Site 1259 on the Demerara Rise (9°N, 54°W; modern water depth ~2354 mbsl), early Eocene in age (~52–53 Ma; estimated from the C24n base nannofossil datum at 329.79 mbsf, 52.66 Ma, and the local linear sedimentation rate of ~12 m/m.y.; Erbacher et al., 2004). The chalk is carbonate-rich ($CaCO_3$ ~62–69 wt%) with very low total organic carbon (TOC ~0.0–0.01 wt% in adjacent samples; Erbacher et al., 2004, Table T16) and was deposited under open-marine pelagic conditions with oxic-to-suboxic bottom waters and pervasive bioturbation, following the recovery of marine biota from the Cretaceous-Paleogene boundary (D'Hondt, 2005). This sample tests whether AsHC preservation requires the elevated organic-carbon content associated with anoxic basinal deposits, or whether AsHCs can also be recovered from carbonate-dominated, low-TOC pelagic settings.

The ODP 1259C-15R is an organic-rich, submillimeter-scale laminated calcareous claystone from lithostratigraphic Unit IV of the same site, Late Cretaceous (late Turonian) in age (~90 Ma; the analyzed interval at 516.05 mbsf lies 5.74 m below the Cenomanian/Turonian boundary at 510.31 mbsf and is bracketed by core catchers assigned to calcareous nannofossil Zone CC12 and to Turonian planktonic foraminifer assemblages; Erbacher et al., 2004). The sample has TOC = 11.4 wt% and $CaCO_3$ = 55.1 wt%, and Rock-Eval pyrolysis indicates well-preserved Type II marine kerogen (Tmax = 404 °C, hydrogen index = 763 mg HC/g TOC;

Erbacher et al., 2004, Tables T16 and T17). It was deposited under restricted, fully marine conditions with high productivity and bottom-water anoxia within the broader Cretaceous Demerara Rise black shale sequence (Schlanger and Jenkyns, 1976; Jenkyns, 2010; Jones et al., 2018), several million years after the OAE2 horizon at the Cenomanian/Turonian boundary. As with Aarhus Bay, this sample provides direct continuity with Chapter 2, where it was used as the test case for evaluating SPE-NPLC performance on low-TOC Cretaceous shales.

The ODP 1259C-18R is a laminated black shale from the same Demerara Rise site, recovered from a deeper interval of the Cretaceous black-shale sequence than 1259C-15R. Calcareous nannofossils in Section 1259C-18R-5—including the single specimen of *Lithraphidites acutus* identified during shipboard analysis—indicate a mid- to late Cenomanian age (Erbacher et al., 2004), placing this sample within the OAE2 black-shale interval that straddles the Cenomanian/Turonian boundary. As the oldest material analyzed in this dissertation (~94–100 Ma), this sample tests the upper age limit at which arsenolipids remain detectable in the geological record.

3.3 Detection Results

At least one class of arsenolipid was detected in every one of the fourteen samples, but the two classes were not co-extensive. The AsHCs were detected in twelve of the fourteen samples and thioxoarsenolipids in thirteen. The kelp algal end-member yielded AsHCs but no thioxoarsenolipid, whereas the two fossil samples—the Messel Shale and ODP 1259C-18R—yielded thioxoarsenolipids but no detectable AsHC. This complementary distribution, examined in Section 3.5, indicates that the two compound classes differ systematically in their occurrence from the freshest biological source to the most deeply buried sediments. Throughout this chapter, detection counts include both full (✓) and trace (tr) detections, classified by signal-to-noise ratio:

S/N ≥ 10 (✓), 3 ≤ S/N < 10 (tr), and S/N < 3 (not detected, —). Both ✓ and tr peaks satisfy the same identification criteria (Section 2.6).

The principal AsHC homologs detected are AsHC-332 (C_{15}), AsHC-360 (C_{17}), and AsHC-388 (C_{19}), corresponding to saturated alkyl chains of 15, 17, and 19 carbon atoms, respectively. Each compound was identified following the criteria established in Section 2.6 (Liu, 2023): accurate mass measurement of the $[M+H]^+$ precursor ion, detection of the dimethylarsinoyl head-group fragments $[AsC_2H_6]^+$ and $[AsC_2H_8O]^+$ (*m/z* 122.9768) under 20 eV CID, and detection of the monatomic As^+ ion (*m/z* 74.9216) under 200 eV CID. Detection categories for each sample are summarized in Table 3.2.

3.3.1 AsHC homolog distribution

The AsHC-360 (*m/z* 361) was detected in twelve of the fourteen samples (Table 3.2) and is the most consistently detected AsHC across the sample set, spanning algal biomass, freshwater and brackish lake sediments, coastal and continental margin sediments, and open-marine fossil samples. It was absent only from the Messel Shale and ODP 1259C-18R, the two fossil samples in which no AsHC homologue was detected.

The AsHC-332 (*m/z* 333) was detected in eight of the fourteen samples: kelp, Aarhus Bay, Salt Pond, Lower Mystic Lake, and four fossil samples (ODP 1227-3H5, 1227-5H3, 1259C-4R, and 1259C-15R). The C_{15} homolog is, therefore, recovered less consistently than AsHC-360.

The AsHC-388 (*m/z* 389) was detected in only three of the fourteen samples: the kelp algal end-member, Aarhus Bay surface sediment (trace), and Lake Tanganyika. It was not detected in any other sample, including all six fossil samples. AsHC-388 is thus the least frequently recovered of the three homologues.

3.3.2 Thioxoarsenolipid distribution

Thioxoarsenolipids were detected in thirteen of the fourteen samples; the kelp algal end-member was the only sample in which no thioxoarsenolipid channel was detected. The three channels were detected in nine (*m/z* 547), eight (*m/z* 549), and ten (*m/z* 565) of the fourteen samples respectively (Table 3.2). Detection spanned freshwater lakes, brackish and coastal basins, and all six fossil sediments, including the two samples (Messel Shale and ODP 1259C-18R) in which no AsHC was detected.

Among the fossil samples, thioxoarsenolipid detection was most complete. The ODP 1227-5H3, ODP 1259C-4R, and ODP 1259C-15R had all three channels (*m/z* 547 as a trace in 15R), and ODP 1227-3H5 had *m/z* 547 and 549. Even ODP 1259C-18R, the oldest sample and one of the two lacking any AsHC, returned thioxoarsenolipid detection (*m/z* 547 trace and *m/z* 565). The most consistent and complete thioxoarsenolipid signals, therefore, come from the fossil marine sediments rather than from the modern reference samples.

Among modern samples, the thioxoarsenolipid signals are variable in both the number and combination of channels detected. The kelp end-member returned no thioxoarsenolipid in any detection channel, in contrast to its strong AsHC signal. Among the remaining modern samples, several exhibited two of the three solutrionsx (Salt Pond and Lake Thunderbird in *m/z* 547 and 565; Lower Mystic Lake and Duck Pond in *m/z* 549 and 565), while others had only one (Aarhus Bay in *m/z* 549; Lake Tanganyika in *m/z* 547; Fayetteville Green Lake in *m/z* 565). These distributions are reported as detection categories rather than diagnostic ratios, since the absence of a neighboring channel in a sample otherwise showing characteristic thioxoarsenolipid mass responses warrants confirmation through the As^{+} co-elution test described in Section 2.6 (Liu, 2023) before structural inferences are drawn.

3.3.3 Sample-specific observations

The kelp (*Laminaria* sp.) total lipid extract had detection of all three AsHC homologues but none of the thioxoarsenolipid ions (Table 3.2). Its strong, well-characterised AsHC signal serves as the positive control for AsHC identification within this batch, and the accurate masses, retention times, and dual-energy CID fragmentation patterns observed in the kelp extract were used as the within-batch reference for AsHC identification in the sedimentary samples. The absence of thioxoarsenolipids in the living macroalga is consistent with earlier reports, in which thioxoarsenolipids were characterised in modern and ancient marine sediments rather than in fresh algal biomass (Liu, 2023), and is discussed further in Section 3.4.

Among the modern aquatic samples, the eight settings differ substantially in detection patterns despite all returning at least one detection. Aarhus Bay yielded all three AsHC homologues (AsHC-388 as a trace) following direct injection of the total lipid extract, consistent with the result reported in Section 2.5.3, but only one thioxoarsenolipid ion (*m/z* 549). Lower Mystic Lake had AsHC-332 and AsHC-360 with two thioxoarsenolipid ions, whereas Fayetteville Green Lake had only AsHC-360 (trace) among the AsHCs. Lake Tanganyika had AsHC-360 and AsHC-388 but lacked AsHC-332, with a single thioxoarsenolipid ion. The kelp end-member, by contrast, hadall three AsHC homologues but no thioxoarsenolipid. This variability likely reflects the combined influence of producer-community composition and depositional matrix at each site.

Direct injection of the total lipid extract was sufficient for compound detection in all eight modern aquatic samples, both ODP 1227 samples, and the Messel Shale; SPE fractionation prior to LC-MS analysis was required for the three Demerara Rise samples (ODP 1259C-4R, 15R, 18R), where compounds were recovered in the polar Fraction 2 of the SPE eluate (Section 2.3.3). The TLE-versus-SPE distinction reflects the combined effect of decreasing absolute abundance with

increasing sediment age and increasing complexity of the co-extracted lipid matrix in carbonate-rich and organic-poor pelagic settings, consistent with the methodological framework presented in Chapter 2.

3.3.4 Detection patterns across the sample set

Beyond the per-channel occurrence reported above, the detection data in Table 3.2 show two patterns across the full sample set; these are based on sample detection categories, not sample abundance (Section 2.6.3).

The three AsHC homologues differ markedly in detection frequency: AsHC-360 (C_{17}) was detected in twelve of the fourteen samples, AsHC-332 (C_{15}) in eight, and AsHC-388 (C_{19}) in only three (kelp, Aarhus Bay, Lake Tanganyika). Detection frequency thus follows $C_{17} > C_{15} \gg C_{19}$. No AsHC homologue was detected in the Messel Shale or ODP 1259C-18R, the two fossil samples that yielded only thioxoarsenolipids.

The thioxoarsenolipid channels were more completely detected in the fossil sediments than in the modern samples: ODP 1227-5H3, 1259C-4R, and 1259C-15R had all three ions, and every fossil sample had at least two, whereas the modern aquatic samples returned one or two ions in variable combinations (Table 3.2).

3.4 Discussion: Widespread Occurrence in Aquatic Environments

The detection of at least one arsenolipid class in every one of the fourteen samples addresses the first question raised in Section 3.1: how widely are arsenolipids distributed across modern aquatic environments? The results presented in Section 3.3 indicate that both compound classes occur across a broader range of modern aquatic settings than the seafood and algal sources that have dominated earlier reports.

3.4.1 Extension of the modern arsenolipid distribution

Previous reports of AsHCs in modern environments have concentrated on three settings: fish oils and seafood (Taleshi et al., 2008; Sele et al., 2014; Xiong et al., 2022), brown macroalgae (Section 2.1.2), and surface-water particulates from open-ocean transects (Glabonjat et al., 2021; Heal et al., 2022). The seven non-algal aquatic samples analyzed alongside the kelp end-member in this chapter (Section 3.2.1) add multiple settings to this list. The AsHC homologues were recovered from each, indicating that arsenolipid production and accumulation extend well beyond fully oxic algal biomass and surface-water particulates into stratified anoxic lakes, brackish meromictic basins, hypoxic coastal sediments, and small urban freshwater systems.

Liu (2023) first reported the thioxoarsenolipid series at *m/z* 547, 549, and 565 in modern and ancient marine sediments—including Aarhus Bay sediment and a Cretaceous shale—establishing this compound class as a recognizable component of the sedimentary arsenolipid pool. The samples analyzed in this chapter reproduce the same thioxoarsenolipid signals in additional matrices, with detection across modern aquatic settings ranging from coastal hypoxic basins to tropical anoxic rift lakes, eutrophic reservoirs and small urban ponds, and the Quaternary Peru continental margin (Table 3.2). With the exception of the kelp end-member—in which AsHCs occur without thioxoarsenolipids—the two classes co-occur across most of the sample set, indicating that thioxoarsenolipids, rather than only the AsHCs that have historically attracted analytical attention, are a recurring component of the arsenolipid pool in modern aquatic environments.

3.4.2 Source diversity beyond eukaryotic algae

The chemical and ecological diversity of the settings in which arsenolipids are detected—from a single macroalgal genus in the kelp reference to mixed microbial communities in tropical

anoxic lake sediments and seasonally hypoxic coastal basins—suggests that arsenolipid source organisms are correspondingly diverse. Eukaryotic algae such as *Dunaliella* and *Picocystis* are confirmed AsHC producers based on culture experiments (Glabonjat et al., 2018, 2020), and brown macroalgae have been characterized in detail as natural sources (Section 2.1.2). However, recent lipidomic studies challenge an exclusively algal view of arsenolipid biosynthesis. Heal et al. (2022) reported a diverse suite of arsenolipids in surface-ocean suspended particles from the Eastern Tropical North Pacific, including previously undescribed ether-bound arsenosugar phospholipids whose head-group architecture is more consistent with a bacterial than a eukaryotic origin. This finding, taken together with the recovery of AsHC homologs from freshwater and brackish lake settings dominated by mixed microbial communities, is consistent with a producer pool more diverse than the eukaryotic-algal sources documented in culture, and with the wide distribution of the *ars* gene cluster across bacterial, archaeal, and eukaryotic lineages discussed in Section 2.1.2 (Zhu et al., 2017).

The data presented here cannot identify the specific producers responsible for arsenolipids in any individual sample. Direct testing through culture experiments on bacterial isolates, or compound-specific isotope analysis on environmental samples, would be required to attribute the AsHC and thioxoarsenolipid signals observed in mixed-community settings—such as the anoxic sediments of Lake Tanganyika, the hypoxic Aarhus Bay sediments, or the Peru-margin Quaternary sediments—to specific lineages. The absence of AsHC-388 from several fresh or well-preserved modern samples that nonetheless yielded the shorter homologues (Section 3.5.7) is consistent with this source-side variability, suggesting that synthesis of the C_{19} homologue is not universal among arsenolipid producers.

3.4.3 A shared metabolic logic underlies arsenolipid production across diverse producers

Although the source organisms of arsenolipid production span multiple domains and ecological niches, the underlying biosynthetic logic is shared. As described in Section 2.1.2, organoarsenic synthesis in aquatic microorganisms proceeds through phosphate-transporter-mediated arsenate uptake, ArsC-catalysed reduction, and ArsM-catalysed methylation (Zhu et al., 2017), with subsequent elaboration into the structurally diverse arsenolipid pool. The formation pathway(s) of the thioxoarsenolipids remain incompletely characterized and are addressed further in Chapter 4 (Section 4.5.3); the present chapter establishes only that this compound class occurs alongside AsHCs across most of the diverse modern and ancient settings examined here. The widespread occurrence of arsenolipids documented in this chapter therefore reflects not the convergent evolution of arsenolipid-specific biosynthesis in unrelated lineages, but the broad distribution of a single conserved metabolic pathway whose final products include the AsHC class, with the thioxoarsenolipid class likely arising through additional, as-yet-uncharacterized formation steps. The distribution of the two classes across the present sample set is consistent with this distinction. The kelp end-member—the only living, freshly sampled primary producer examined—yielded all three AsHC homologues but no thioxoarsenolipid, whereas thioxoarsenolipids occurred in the great majority of the sediment samples, including settings where AsHCs were absent. This contrast supports the view that AsHCs are primary biosynthetic products present in living biomass, whereas thioxoarsenolipids are not a major constituent of fresh algal tissue and are instead generated or enriched after deposition, during early diagenesis in the sediment. The same pattern was reported by Liu (2023), who detected thioxoarsenolipids in modern and ancient sediments but not in fresh algal material. Independent evidence that thioxoarsenolipids can arise through post-synthetic transformation of pre-existing arsenolipids comes from Xiong et al. (2022), who

observed partial conversion of oxo-arsenolipids to their thioxo analogues during the cooking of salmon; an analogous sulfurisation of arsenolipids under the sulfidic conditions of organic-rich sediments would be consistent with the sediment-associated occurrence of thioxoarsenolipids observed here. This formation chemistry is examined mechanistically in the Black Sea record in Chapter 4 (Section 4.5.3).

3.5 Discussion: Preservation Across Geological Time and Lithologies

The detection of arsenolipids in six fossil sedimentary samples ranging from Quaternary to mid-Cretaceous in age addresses the second question raised in Section 3.1: can arsenolipids persist in sedimentary archives across geological time? The results presented in Section 3.3 indicate that arsenolipids are preserved across this temporal range and across sedimentary settings that differ markedly in their depositional and lithological characteristics—organic-rich anoxic shales, carbonate-rich pelagic chalks, and organic-rich diatomaceous OMZ sediments—but that the two compound classes differ in the age and conditions to which each persists, as discussed below.

3.5.1 Differential persistence of AsHCs and thioxoarsenolipids through geological time

AsHCs were detected in four of the six fossil samples, spanning the Quaternary Peru-margin sediments (ODP 1227-3H5 and 1227-5H3), the early Eocene ODP 1259C-4R chalk (~52–53 Ma), and the Late Cretaceous ODP 1259C-15R black shale (~90 Ma), extending the AsHC fossil record into the Mesozoic. No AsHC was detected in the middle Eocene Messel Shale (~48 Ma) or in the mid- to late Cenomanian ODP 1259C-18R black shale (~94–100 Ma). The recovery of intact AsHC molecular ions and diagnostic fragmentation patterns as old as ODP 1259C-15R indicates that AsHCs, once incorporated into sedimentary archives under appropriate conditions, can remain stable on geological timescales of at least ~90 Myr. The differential preservation of the

individual AsHC homologues, including the restricted occurrence of AsHC-388, is examined in Section 3.5.7.

Thioxoarsenolipids, by contrast, were detected in all six fossil samples, with at least one of the three monitored channels (*m/z* 547, 549, 565) returning detection in each (Table 3.2). ODP 1259C-4R and ODP 1259C-15R returned all three channels, and ODP 1259C-18R returned two (*m/z* 547 trace and *m/z* 565). Thioxoarsenolipids therefore persist in the oldest sample analyzed in this dissertation (~94–100 Ma), ~5–10 Myr older than the oldest AsHC detection, placing the most distal documented occurrence of arsenolipids within the OAE2 black-shale interval. That this oldest sample preserved thioxoarsenolipids but no detectable AsHC indicates that the thioxoarsenolipid class persists under conditions where AsHCs are no longer recoverable.

3.5.2 Arsenolipid retention in modern OMZ sediments: the ODP 1227 sequence

The two ODP 1227 samples had similar detection patterns at both depths analyzed: AsHC-332, AsHC-360, and at least two of the three thioxoarsenolipid mass channels. This within-core consistency between 1227-3H5 (~24–25 mbsf) and 1227-5H3 (~36–37 mbsf) is consistent with arsenolipid retention extending beyond a single horizon within the depositional sequence, although the two-sample comparison cannot constrain how arsenolipid abundances vary at finer stratigraphic resolution. Together with the modern Aarhus Bay result (Section 3.3.3), the ODP 1227 sequence establishes that arsenolipids are recoverable from organic-rich diatomaceous margin sediments deposited under active oxygen-minimum-zone conditions.

3.5.3 Class-selective preservation in lacustrine settings: the Messel Shale

The Messel Shale presents an informative case in which depositional conditions normally regarded as optimal for biomarker preservation did not yield detectable AsHCs. Direct injection of the total lipid extract returned two of the three thioxoarsenolipid mass channels (Section 3.3.3)

without the need for SPE cleanup, but no AsHC homologue was detected. This is notable given the persistently anoxic, meromictic conditions of the Messel paleolake, its exceptionally high organic-carbon content (TOC ~27 wt% on average; Bauersachs et al., 2014), and the relative simplicity of the lacustrine matrix compared with marine sediments of comparable age (Lenz et al., 2010; Grice et al., 2019). That thioxoarsenolipids were recovered while AsHCs were not, even under these favourable conditions, indicates that AsHC loss at Messel reflects the limited preservation of the AsHC class itself rather than an unfavourable matrix, and provides a lacustrine counterpart to the same AsHC–thioxoarsenolipid divergence seen in the oldest marine sample (ODP 1259C-18R; Section 3.5.4). The Messel result therefore reinforces the conclusion that thioxoarsenolipids persist under conditions where AsHCs are no longer detectable.

3.5.4 Anoxic marine preservation: the Demerara Rise black-shale sequence

The two Demerara Rise black shales analyzed in this study (ODP 1259C-15R, late Turonian, ~90 Ma; ODP 1259C-18R, mid- to late Cenomanian, ~94–100 Ma) represent the conventional expectation for fossil molecular biomarker preservation: organic-rich (TOC = 11.4 wt% in 15R; comparable values typical of the OAE2 interval in 18R), finely laminated, anoxic marine deposits with thermally immature, well-preserved organic matter (Tmax = 404 °C in 15R; Erbacher et al., 2004; Böttcher et al., 2006). The two samples nonetheless differed in which compound classes were recovered after SPE enrichment. ODP 1259C-15R returned AsHC-332 and AsHC-360 together with all three thioxoarsenolipid channels, whereas the older ODP 1259C-18R had thioxoarsenolipids only (*m/z* 547 and 565) and no detectable AsHC. The AsHC-388 was not detected in either sample.

The requirement for SPE cleanup, despite the favorable depositional and preservational conditions, indicates that high TOC content alone does not guarantee detectable arsenolipid signals

from total lipid extracts: the matrix-to-arsenolipid ratio in such organic-rich shales is high enough to obscure trace-level peaks under direct injection. The successful detection at this age nonetheless places the documented arsenolipid record within the OAE2 black-shale interval and establishes that thioxoarsenolipids persist through the deepest geological time interval examined in this dissertation. The contrast between 15R and 18R—where AsHCs are still recovered at ~90 Ma but are no longer detectable at ~94–100 Ma, while thioxoarsenolipids persist in both—indicates that the two compound classes diverge in their preservation across this ~5–10 Myr interval, with thioxoarsenolipids extending to the older horizon. Finer-scale variation within the sequence cannot be resolved from two samples.

3.5.5 Carbonate-rich pelagic preservation: ODP 1259C-4R

The detection of arsenolipids in the ODP 1259C-4R pelagic chalk is the most informative result of the fossil sample set with respect to preservation mechanisms. Unlike the organic-rich shales that have traditionally yielded fossil molecular biomarkers, ODP 1259C-4R was deposited under open-marine pelagic conditions and is characterized by a carbonate-rich, very low-TOC matrix ($CaCO_3$ ~62–69 wt%, TOC ~0.0–0.01 wt%; Section 3.2.2). The successful recovery of AsHC-332, AsHC-360, and all three thioxoarsenolipid ions from this sample, after SPE fractionation, indicates that arsenolipid preservation does not depend strictly on the high organic-carbon, anoxic depositional conditions associated with classical molecular biomarker archives.

Classical hydrocarbon biomarkers such as hopanes and steranes are most reliably recovered from organic-rich, fine-grained, anoxic to suboxic sedimentary deposits—the same depositional regime that has yielded the bulk of the Mesozoic and Cenozoic biomarker record, including the well-studied biomarker assemblages of Cretaceous OAE black shales (Kuypers et al., 2002). Carbonate-rich pelagic deposits, by contrast, typically yield lower biomarker abundances because

of their lower organic-matter input and more oxidizing diagenetic conditions (Hedges and Keil, 1995), and they are correspondingly underrepresented in the published hopane- and sterane-based literature (Peters et al., 2005; Brocks and Pearson, 2005). The 1259C-4R result indicates that arsenolipids may be recoverable from a wider sedimentary archive than these classical molecular fossils, and that pelagic carbonate sequences—which dominate much of the Mesozoic and Cenozoic deep-marine record (Zachos et al., 2001)—represent a target lithology for arsenolipid-based paleoenvironmental investigation that remains largely unexplored.

3.5.6 Implications for compound-specific paleoenvironmental reconstruction

The preservation behavior documented in this chapter, taken together with the analytical framework established in Chapter 2, expands the practical range of sedimentary archives in which arsenolipids can be incorporated into compound-specific paleoenvironmental work. In sedimentary intervals where classical hydrocarbon biomarkers are abundant, AsHCs and thioxoarsenolipids can be added as additional compound classes whose recovery does not depend on the same matrix conditions that constrain other biomarkers. In sedimentary intervals where classical biomarkers are limited—in particular, the carbonate-rich pelagic settings that dominate substantial portions of the global deep-marine record—the present results indicate that arsenolipid detection remains feasible, opening the possibility of compound-specific paleoenvironmental reconstruction in archives where it has not been routinely attempted.

3.5.7 Chain-length control on AsHC preservation

The three AsHC homologues were not preserved equally across the sample set (Section 3.3.4): AsHC-360 (12 of 14 samples) and AsHC-332 (8 of 14) were the more consistently detected, whereas AsHC-388 was detected in only three samples. We interpret this restricted occurrence as

evidence that the longest-chain homologue is the most sensitive to both biological origin and preservational history.

The three samples yielding AsHC-388—the kelp algal end-member and the modern Aarhus Bay and Lake Tanganyika sediments—are all modern and lie close to a fresh biological source. AsHC-388 was not detected in any fossil sample, including the exceptionally well-preserved Messel oil shale (TOC ~27 wt%; Section 3.2.2), nor in most modern samples. Its occurrence therefore tracks neither age nor depositional redox condition in a simple way, but is consistent with preferential loss of the C_{19} homologue with even modest burial and processing: the longest-chain homologue is retained only in fresh or very recently deposited material and is absent from all six fossil samples.

This pattern stands in apparent contrast to controlled decomposition experiments. Glabonjat et al. (2019) found AsHC-388 to be more resistant to early-stage decomposition than the co-occurring arsenic phospholipids (AsPLs), persisting as the last detectable arsenolipid after the AsPLs had degraded. That experiment, however, compared AsHC-388 against other arsenolipid classes and did not resolve differences among AsHC homologues of different chain length. The sediment record reported here reveals a second-order pattern the decomposition experiment could not capture: among the AsHC homologues themselves, the longest-chain AsHC-388 is the least frequently preserved (absent from all fossil samples), while the shorter AsHC-360 and AsHC-332 are recovered far more consistently, including in fossil sediments. The recalcitrance of AsHCs relative to other arsenolipid classes therefore does not extend uniformly across chain length in the geological record.

We suggest two non-exclusive controls. First, the operative timescales differ: the laboratory experiments tracked early biological decomposition over days to months, during which

AsHC-388 was a survivor relative to AsPLs, whereas the geological record integrates slower diagenetic and matrix-dependent processes over 10^4–10^8 years that need not preserve the same compound ranking. Second, AsHC-388 may not be synthesised by all arsenolipid producers: several fresh or well-preserved modern samples (the meromictic temperate lakes and small ponds) also lacked AsHC-388 despite yielding the shorter homologues, pointing to a source-side control by producer-community composition (Section 3.4.2) in addition to preservation. Resolving these source and sink controls is beyond the detection-level data presented here, but the pattern identifies AsHC-388 as the homologue most diagnostic of both the biological origin and the preservational history of a sample.

Among the AsHC homologues, the consistent detection of AsHC-360 (twelve of fourteen samples; Section 3.3.4) identifies the C_{17} homologue as the most reliable single target for AsHC screening in sedimentary archives, whereas AsHC-388 is recovered only under a restricted set of source and preservational conditions (Section 3.5.7).

3.6 Summary

Applying the SPE–NPLC workflow developed in Chapter 2, this chapter provides the first broad survey of arsenolipid distribution across modern aquatic environments and the geological record, establishing that arsenolipids occur widely in modern aquatic systems and persist across geological timescales in sedimentary archives spanning diverse depositional and lithological settings. In modern systems, this work detected at least one arsenolipid class in all eight aquatic samples examined—a brown macroalga, brackish and freshwater meromictic lakes, a tropical anoxic rift lake, a eutrophic reservoir, hypoxic coastal sediments, and small urban ponds—with AsHCs and thioxoarsenolipids co-occurring in all but the algal end-member, which yielded AsHCs alone. These findings substantially expand the known environmental range of arsenolipids, which

earlier reports had largely confined to seafood and algal sources, and indicate that arsenolipid production extends across a far wider diversity of aquatic settings than previously recognized. In the geological record, this work recovered arsenolipids from sedimentary rocks ranging in age from Quaternary Peru-margin OMZ sediments to the mid- to late Cenomanian (~94–100 Ma) ODP 1259C-18R black shale within the OAE2 interval, across lithologies from organic-rich anoxic shales to low-TOC carbonate-rich pelagic chalks. The AsHCs were recovered in fossil sediments as old as ~90 Ma, whereas thioxoarsenolipids persisted to the oldest (OAE2) sample at ~94–100 Ma; the two classes therefore differ in long-term preservation, with thioxoarsenolipids extending the preserved record across at least ~100 Myr. Together, these results position arsenolipids as a class of molecular fossil whose distribution in modern aquatic systems and preservation in the geological record are sufficiently broad to motivate their further development as a paleoenvironmental tool.

The sample set examined in this chapter, however, is composed of widely separated samples from contrasting environments, with each sample representing a single point in time within its respective setting. This survey design is well suited to establishing the breadth of arsenolipid distribution and preservation but cannot resolve how arsenolipid abundances and channel distributions respond to environmental change within a single depositional system. A different sampling strategy—stratigraphically resolved sampling within a single sedimentary sequence whose depositional history is well constrained—is required to test whether arsenolipid distributions track documented environmental transitions.

The Holocene sedimentary sequence of the Black Sea provides such a system. The Black Sea has undergone a series of well-documented environmental transitions over the Holocene, including the transition from a freshwater lacustrine system to a marine-connected basin (Major et

al., 2006; Soulet et al., 2011) and the development of the modern euxinic water column (Arthur and Dean, 1998), with these transitions recorded in lithologically distinct units that have been characterized by independent paleoenvironmental proxies. Chapter 4 presents a stratigraphically resolved analysis of arsenolipids through this sedimentary sequence, examining their distributions in relation to the documented environmental transitions and the multiple environmental factors that may influence arsenolipid preservation. The central question addressed in Chapter 4 is whether arsenolipid composition tracks the documented Holocene environmental transitions in this single, well-characterized archive—and, if so, what proximate and upstream environmental controls govern that response?

3.7 References

Arthur, M.A., Dean, W.E., 1998. Organic-matter production and preservation and evolution of anoxia in the Holocene Black Sea. Paleoceanography 13, 395–411. https://doi.org/10.1029/98PA01161

Bauersachs, T., Schouten, S., Schwark, L., 2014. Characterization of the sedimentary organic matter preserved in Messel oil shale by bulk geochemistry and stable isotopes. Palaeogeography, Palaeoclimatology, Palaeoecology 410, 390–400. https://doi.org/10.1016/j.palaeo.2014.06.015

Böttcher, M.E., Hetzel, A., Brumsack, H.-J., Schipper, A., 2006. Sulfur-iron-carbon geochemistry in sediments of the Demerara Rise, in: Mosher, D.C., Erbacher, J., Malone, M.J. (Eds.), Proceedings of the Ocean Drilling Program, Scientific Results. Ocean Drilling Program, College Station, TX, pp. 1–23. https://doi.org/10.2973/odp.proc.sr.207.108.2006

Brocks, J.J., Pearson, A., 2005. Building the biomarker tree of life. Reviews in Mineralogy and Geochemistry 59, 233–258. https://doi.org/10.2138/rmg.2005.59.10

Chen, X., Andersen, T.J., Morono, Y., Inagaki, F., Jørgensen, B.B., Lever, M.A., 2017. Bioturbation as a key driver behind the dominance of Bacteria over Archaea in near-surface sediment. Scientific Reports 7, 2400. https://doi.org/10.1038/s41598-017-02295-x

D'Hondt, S., 2005. Consequences of the Cretaceous/Paleogene mass extinction for marine ecosystems. Annual Review of Ecology, Evolution, and Systematics 36, 295–317. https://doi.org/10.1146/annurev.ecolsys.35.021103.105715

Erbacher, J., Mosher, D.C., Malone, M.J., 2004. Site 1259, in: Proceedings of the Ocean Drilling Program, Initial Reports. Ocean Drilling Program, College Station, TX. https://doi.org/10.2973/odp.proc.ir.207.106.2004

Glabonjat, R.A., Blum, J.S., Miller, L.G., Webb, S.M., Stolz, J.F., Francesconi, K.A., Oremland, R.S., 2020. Arsenolipids in cultured *Picocystis* strain ML and their occurrence in biota and sediment from Mono Lake, California. Life 10, 93. https://doi.org/10.3390/life10060093

Glabonjat, R.A., Duncan, E.G., Francesconi, K.A., Maher, W.A., 2019. Transformation of arsenic lipids in decomposing *Ecklonia radiata*. Journal of Applied Phycology 31, 3979–3987. https://doi.org/10.1007/s10811-019-01845-2

Glabonjat, R.A., Ehgartner, J., Duncan, E.G., Raber, G., Jensen, K.B., Krikowa, F., Maher, W.A., Francesconi, K.A., 2018. Arsenolipid biosynthesis by the unicellular alga *Dunaliella tertiolecta* is influenced by As/P ratio in culture experiments. Metallomics 10, 145–153. https://doi.org/10.1039/c7mt00249a

Glabonjat, R.A., Raber, G., Holm, H.C., Mooy, B.A.S., Francesconi, K.A., 2021. Arsenolipids in plankton from high- and low-nutrient oceanic waters along a transect in the North Atlantic. Environmental Science & Technology 55, 5515–5524. https://doi.org/10.1021/acs.est.0c06901

Grice, K., Holman, A.I., Plet, C., Tripp, M., 2019. Fossilised biomolecules and biomarkers in carbonate concretions from Konservat-Lagerstätten. Minerals 9, 158. https://doi.org/10.3390/min9030158

Heal, K.R., Maloney, A.E., Ingalls, A.E., Bundy, R.M., 2022. Diverse arsenic-containing lipids in the surface ocean. Limnology and Oceanography Letters 7, 43–51. https://doi.org/10.1002/lol2.10216

Hedges, J.I., Keil, R.G., 1995. Sedimentary organic matter preservation: an assessment and speculative synthesis. Marine Chemistry 49, 81–115. https://doi.org/10.1016/0304-4203(95)00008-F

Jenkyns, H.C., 2010. Geochemistry of oceanic anoxic events. Geochemistry, Geophysics, Geosystems 11, 03004. https://doi.org/10.1029/2009GC002788

Jones, M.M., Sageman, B.B., Meyers, S.R., 2018. Turonian sea level and paleoclimatic events in astronomically tuned records from the tropical North Atlantic and Western Interior Seaway. Paleoceanography and Paleoclimatology 33, 470–492. https://doi.org/10.1029/2017PA003158

Kuypers, M.M.M., Pancost, R.D., Nijenhuis, I.A., Sinninghe Damsté, J.S., 2002. Enhanced productivity led to increased organic carbon burial in the euxinic North Atlantic basin during the late Cenomanian oceanic anoxic event. Paleoceanography 17, 1051. https://doi.org/10.1029/2000PA000569

Lenz, O.K., Wilde, V., Riegel, W., 2010. Short-term fluctuations in vegetation and phytoplankton during the Middle Eocene greenhouse climate: a 640-kyr record from the Messel oil shale (Germany. International Journal of Earth Sciences (Geologische Rundschau 100, 1851–1874. https://doi.org/10.1007/s00531-010-0609-z

Liu, X.-L., 2023. Streamlined arsenolipid identification via direct arsenic detection using RPLC-ESI-QTOF-MS with collision-induced dissociation. Journal of the American Society for Mass Spectrometry. https://doi.org/10.1021/jasms.3c00367

Major, C.O., Goldstein, S.L., Ryan, W.B.F., Lericolais, G., Piotrowski, A.M., Hajdas, I., 2006. The co-evolution of Black Sea level and composition through the last deglaciation and its paleoclimatic significance. Quaternary Science Reviews 25, 2031–2047. https://doi.org/10.1016/j.quascirev.2006.01.032

Party, S.S., 2003. Site 1227, in: D'Hondt, S.L., Jørgensen, B.B., Miller, D.J. (Eds.), Proceedings of the Ocean Drilling Program, Initial Reports. Ocean Drilling Program, College Station, TX. https://doi.org/10.2973/odp.proc.ir.201.108.2003

Paulmier, A., Ruiz-Pino, D., 2009. Oxygen minimum zones (OMZs) in the modern ocean. Progress in Oceanography 80, 113–128. https://doi.org/10.1016/j.pocean.2008.08.001

Peters, K.E., Walters, C.C., Moldowan, J.M., 2005. The biomarker guide, 2nd ed. Cambridge University Press, Cambridge.

Schlanger, S.O., Jenkyns, H.C., 1976. Cretaceous oceanic anoxic events: causes and consequences. Geologie en Mijnbouw 55, 179–184.

Sele, V., Sloth, J.J., Holmelid, B., Valdersnes, S., Skov, K., Amlund, H., 2014. Arsenic-containing fatty acids and hydrocarbons in marine oils – determination using reversed-phase HPLC-ICP-MS and HPLC-qTOF-MS. Talanta 121, 89–96. https://doi.org/10.1016/j.talanta.2013.12.049

Soulet, G., Ménot, G., Lericolais, G., Bard, E., 2011. A revised calendar age for the last reconnection of the Black Sea to the global ocean. Quaternary Science Reviews 30, 1019–1026. https://doi.org/10.1016/j.quascirev.2011.03.001

Taleshi, M.S., Jensen, K.B., Raber, G., Edmonds, J.S., Gunnlaugsdóttir, H., Francesconi, K.A., 2008. Arsenic-containing hydrocarbons: natural compounds in oil from the fish capelin, *Mallotus villosus*. Chemical Communications 39, 4706–4707. https://doi.org/10.1039/B808049F

Thamdrup, B., Fossing, H., Jørgensen, B.B., 1994. Manganese, iron and sulfur cycling in a coastal marine sediment, Aarhus Bay, Denmark. Geochimica et Cosmochimica Acta 58, 5115–5129. https://doi.org/10.1016/0016-7037(94)90298-4

Xiong, C., Glabonjat, R.A., Al Amin, M.H., Stiboller, M., Yoshinaga, J., Francesconi, K.A., 2022. Arsenolipids in salmon are partly converted to thioxo analogs during cooking. Journal of Trace Elements in Medicine and Biology 69, 126892. https://doi.org/10.1016/j.jtemb.2021.126892

Zachos, J., Pagani, M., Sloan, L., Thomas, E., Billups, K., 2001. Trends, rhythms, and aberrations in global climate 65 Ma to present. Science 292, 686–693. https://doi.org/10.1126/science.1059412

Zhu, Y.-G., Xue, X.-M., Kappler, A., Rosen, B.P., Meharg, A.A., 2017. Linking genes to microbial biogeochemical cycling: lessons from arsenic. Environmental Science & Technology 51, 7326–7339. https://doi.org/10.1021/acs.est.7b00689

3.8 Figures

Sample	Location	Age	Depositional environment	Lithology / TOC	Selection rationale
Modern aquatic settings					
Kelp (*Laminaria* sp.)	Commercial source	Modern	Brown macroalga (extant primary producer)	—	Algal end-member; positive control for AsHC identification (Liu, 2023 reference)
Aarhus Bay surface sediment	56°N, 10°E (Denmark)	Modern (~14–18 m water depth)	Semi-enclosed coastal basin; seasonal hypoxia; active Fe–Mn redox cycling and pore-water sulfate reduction	TOC ~2–4 wt%	Coastal redox-transitional reference; methodological continuity with Chapter 2
Salt Pond	41.55°N, 70.62°W (Falmouth, MA)	Modern (~5 m depth)	Small coastal seasonally meromictic pond; well-defined oxic–anoxic interface; sulfidic hypolimnion	Sediment from sulfidic basin	Marine-influenced meromictic end-member at sub-lake scale
Lower Mystic Lake	42.43°N, 71.13°W (Boston area, MA)	Modern (varved sediment archive)	Permanently meromictic urban lake; brackish bottom water; black-water anoxic chemocline at ~15–16 m	Annually laminated (varved) sediment	Mid-latitude meromictic reference with high-resolution varve archive
Fayetteville Green Lake	43.05°N, 75.96°W (Fayetteville, NY)	Modern (53 m sediment, lake bottom)	Glacial-plunge-pool meromictic marl lake; persistently sulfidic monimolimnion below ~18–20 m chemocline; calcite-laminated sediments	Carbonate-laminated organic sediment	Classic euxinic lake; modern analog for Proterozoic ocean chemistry
Lake Tanganyika	~6°S, 29–30°E (East African Rift Valley)	Modern (sediment 14)	Tropical freshwater rift lake; max depth 1470 m; permanently anoxic below ~100–150 m; largest body of anoxic freshwater on Earth	Lacustrine organic-rich sediment	Tropical large-rift-lake reference; deep anoxic freshwater system
Lake Thunderbird	35.22°N, 97.23°W (Norman, OK)	Modern (constructed reservoir, 1965)	Eutrophic reservoir; mean depth ~5 m, max 18 m; persistent algal blooms	Fine-grained reservoir sediment	Anthropogenically eutrophied freshwater system
Duck Pond	35.21°N, 97.44°W (Norman, OK)	Modern	Small recreational pond on University of Oklahoma campus	Surface pond sediment / suspended matter	Small-volume urban-pond end-member

Fossil sedimentary samples					
ODP 1227-3H5	8.99°S, 79.96°W; ~427 m water depth (Peru margin, Trujillo Basin)	Quaternary (~24–25 mbsf)	Modern Peru OMZ upwelling system; suboxic-to-anoxic margin sediment	Diatomaceous-rich silty sediment (Subunit IIB); TOC 1.2–10.6 wt%	Peru-margin OMZ end-member; tests AsHC in modern high-productivity upwelling sediments
ODP 1227-5H3	8.99°S, 79.96°W (same site as above)	Quaternary (~36–37 mbsf)	Same Peru OMZ system; deeper and slightly older interval	Diatom-bearing clayey silt with dolomite-bearing layers (Unit III)	Stratigraphic companion to 1227-3H5; tests within-core AsHC consistency
Messel Shale	49°55'N, 8°45'E (Hesse, Germany)	~48 Ma (middle Eocene)	Lacustrine meromictic oil shale; persistently anoxic bottom waters; finely laminated	TOC ~27 wt%	Lacustrine fossil reference; renowned for exceptional biomolecule preservation
ODP 1259C-4R	9°N, 54°W; 2354 m water depth (Demerara Rise)	~52–53 Ma (early Eocene)	Open-marine pelagic; oxic-to-suboxic bottom waters; pervasive bioturbation	Foraminifer-nannofossil pelagic chalk; $CaCO_3$ ~62–69 wt%; TOC ~0.0–0.01 wt%	Tests AsHC preservation in low-TOC, carbonate-dominated pelagic settings
ODP 1259C-15R	9°N, 54°W; 2354 m water depth (Demerara Rise, ~380 km N of Suriname)	~90 Ma (Late Cretaceous, late Turonian)	Restricted marine; bottom-water anoxia; high productivity; Demerara Rise black-shale sequence	Calcareous claystone (sub-mm laminated); TOC 11.4 wt%, $CaCO_3$ 55.1 wt%; Type II marine kerogen	Methodological continuity with Chapter 2; post-OAE2 black-shale interval
ODP 1259C-18R	9°N, 54°W (same Demerara Rise site)	Mid–late Cenomanian (~94–100 Ma); spans OAE2 interval	Laminated organic-rich black shale; strongly euxinic conditions during OAE2	Laminated black shale; mid–late Cenomanian dated by *Lithraphidites acutus* nannofossil; OAE2 black-shale interval	Oldest sample analyzed; tests upper age limit of arsenolipid detectability across OAE2

Table 3.1 Characteristics of the fourteen samples analyzed in this chapter, organized by sample type (modern aquatic settings and fossil sedimentary samples). Coordinates, depositional environments, lithology, and the rationale for inclusion in the sample set are summarized for each entry.

Sample	**AsHC-332** *m/z* **333**	**AsHC-360** *m/z* **361**	**AsHC-388** *m/z* **389**	**thioxoarsenolipid** *m/z* **547**	**thioxoarsenolipid** *m/z* **549**	**thioxoarsenolipid** *m/z* **565**
Modern aquatic settings						
Kelp Seaweed (*Laminaria* sp.)	✓	✓	✓	—	—	—
Aarhus Bay surface sediment	✓	✓	tr	—	✓	—
Salt Pond	tr	✓	—	✓	—	✓
Lower Mystic Lake	✓	✓	—	—	tr	tr
Fayetteville Green Lake	—	tr	—	tr	—	✓
Lake Tanganyika	—	✓	✓	✓	—	—
Lake Thunderbird	—	✓	—	✓	—	✓
Duck Pond	—	✓	—	—	tr	tr
Fossil sedimentary samples						
ODP 1227-3H5	tr	✓	—	✓	✓	—
ODP 1227-5H3	✓	✓	—	✓	✓	✓
Messel Shale	—	—	—	—	✓	✓
ODP 1259C-4R	✓	✓	—	✓	✓	✓
ODP 1259C-15R	✓	tr	—	tr	✓	✓
ODP 1259C-18R	—	—	—	tr	—	✓

Table 3.2 Detection summary for arsenolipid target compounds across the fourteen samples. Three AsHC homologs (AsHC-332, AsHC-360, AsHC-388, detected as their [M+H]+ ions at *m/z* 333, 361, and 389) and three thioxoarsenolipid species (at *m/z* 547, 549, 565) were screened by extracted-ion chromatography. Symbols: ✓ = detected (clear peak meeting all identification criteria in Section 2.6, integrated area > 10^4); tr = trace: a low-abundance peak that is clearly distinguishable from baseline noise and meets the same identification criteria, but with integrated area ≤ 10^4; — = not detected (no peak distinguishable from baseline noise). Integrated areas are used only to classify detections within each sample and are not compared across samples or interpreted as relative abundance; relatively quantitative cross-sample comparison is reserved for Chapter 4.

Chapter 4 The Holocene Black Sea Arsenolipid Record: A Time-Resolved Case Study from GGC18

4.1 Introduction

The Holocene sedimentary archive of the Black Sea preserves a continuous record of one of the most pronounced redox and salinity transitions in the recent geological past: the transformation of a brackish-to-freshwater lacustrine basin into a marine-connected, persistently euxinic system. This transition is recorded in three lithologically distinct sapropel units (Hay et al., 1991; Major et al., 2006): Unit III (11.7–7.6 ka), spanning the late lake phase and the initial Mediterranean inflow at ~9.4 ka; Unit II (7.6–2.6 ka), recording the development and stabilization of photic-zone euxinia (PZE) following water-column stratification; and Unit I (2.6–0 ka), reflecting the late-Holocene surface-water freshening associated with increased fluvial discharge from major regional rivers. The high temporal resolution of this record, combined with the documented chronology of environmental transitions, makes the Holocene Black Sea an exceptional natural laboratory for evaluating how distinct organic-geochemical proxies respond to redox and salinity change in a single sedimentary system (Coolen et al., 2013; Arthur and Sageman, 2005).

This chapter builds on a sequence of recent investigations of the Holocene Black Sea sapropel sequence carried out on the same GGC18 sediment core (42°46.6′N, 28°40.6′E; 971 m water depth; cruise AK06; Coolen et al., 2009; Huang et al., 2021). Two parallel investigations of these thirteen samples—Alo et al. (2026) reconstructing the producer-side ecological response through coupled long-chain alkenone and chlorophyll-a derivative analyses, and Zhao et al. (2026) resolving water-column degradation pathways through chlorin-derivative class partitioning—together establish a multi-dimensional environmental baseline against which arsenolipid

distributions in the same sedimentary sequence can be interpreted. The full proxy framework derived from these two studies is described in Section 4.2.3.

Three questions guide the present chapter, building on the methodological framework of Chapter 2 and the survey results of Chapter 3. First, how do AsHC abundances and homolog distributions vary through the GGC18 sequence in relation to the documented phytoplankton-community turnover? Second, how do the thioxoarsenolipids in the same Black Sea sapropel distribute through the sequence, and do their abundances correspond to specific intervals within the established redox and water-column frameworks? Third, what is the relationship—if any—between AsHC and thioxoarsenolipid distributions through the sequence, and what does this relationship imply for the controls on arsenolipid composition in a stratified, redox-evolving depositional system? The chapter is organized as follows. Section 4.2 describes the GGC18 sample set and the stratigraphic framework derived from Alo et al. (2026) and Zhao et al. (2026). Section 4.3 presents the detection results for AsHCs and thioxoarsenolipids across the thirteen-sample sequence. Sections 4.4 and 4.5 discuss the stratigraphic records of each compound class in turn, with reference to the producer-side and degradation-pathway frameworks established in the parallel studies. Section 4.6 examines the relationship between the two compound classes across the sequence and considers the multiple environmental factors that may shape the arsenolipid record. Section 4.7 summarizes the chapter and situates the Black Sea record within the broader paleoenvironmental potential of arsenolipids developed in this dissertation.

4.2 Sample Set and Stratigraphic Framework

4.2.1 GGC18 sediment core and sample selection

The samples analyzed in this chapter come from the Giant Gravity Core GGC18, collected from the western Black Sea basin (42°46.569'N, 28°40.647'E) at 971 m water depth during cruise

AK06 of the R/V Akademik in 2006 (Coolen et al., 2009; Filipova-Marinova et al., 2013; Huang et al., 2021). The core captures a continuous Holocene sapropel sequence spanning from the late lake phase of the Black Sea through the Mediterranean inflow, the development of photic-zone euxinia, and the late-Holocene freshening transition to the present day. Thirteen sediment samples spanning approximately 11.7 to 0.6 cal. ka B.P. were selected for arsenolipid analysis (Table 4.1). This sample set is identical to the suite analyzed by Alo et al. (2026) and Zhao et al. (2026), enabling direct stratigraphic comparison of arsenolipid signals with the chlorophyll-derivative and bulk geochemical records developed in those parallel investigations. Sample preparation followed the freeze-drying and total lipid extraction protocols described in Section 2.3, with subsequent silica-gel SPE cleanup applied to enrich arsenolipids prior to LC-MS analysis.

4.2.2 Stratigraphic units of the Holocene Black Sea sapropel

The Holocene sapropel sequence is divided into three lithologically distinct units following the classification of Hay et al. (1991), each corresponding to a distinct depositional and environmental regime.

Unit III (11.7–7.6 ka) encompasses the late lake phase (11.7–9.4 ka) and the period of initial Mediterranean inflow (9.4–7.6 ka) (Soulet et al., 2011). Sediments deposited during this interval are characterized by variable total organic carbon contents and reflect a stratified-to-mixed water column under low-salinity, oxygenated-to-suboxic conditions (Alo et al., 2026). The transition from lacustrine to brackish marine conditions is recorded by the first appearance of *Emiliania huxleyi* at ~9.3 ka and by progressive changes in salinity-sensitive biomarker assemblages (Coolen et al., 2013; Alo et al., 2026).

Unit II (7.6–2.6 ka) records the development and stabilization of photic-zone euxinia (PZE) following water-column stratification driven by sustained Mediterranean inflow and rising surface

salinity. The onset of PZE is estimated at ~7.5 ka (Arthur and Dean, 1998; Arthur and Sageman, 2005), and intensified euxinia between ~5 and 3 ka B.P. has been inferred from peaks in the 31-meso-pyropheophytin-*a*/pyropheophytin-*a* ratio (Zhao et al., 2026), consistent with earlier molecular and isotopic evidence for Holocene chemocline oscillations and shoaling phases reported by Sinninghe Damsté et al. (1993) and Huang et al. (2000); the meso/pyropheophytin-a marker reflects anaerobic bacterial degradation of haptophyte chlorophyll-a under sulfate-reducing conditions (Spooner et al., 1995). Unit II sediments are organic-rich (TOC up to ~10 wt% in the western shelf location of GGC18) and finely laminated, consistent with anoxic bottom-water deposition.

Unit I (2.6–0 ka) is composed predominantly of coccolith marl reflecting a late-Holocene surface-water freshening event associated with increased fluvial discharge from the Danube, Dnieper, and Don rivers (Giosan et al., 2009, 2012). The freshening event lowered surface-water salinity and increased nutrient delivery, triggering a resurgence of *Isochrysis* algae and a sharp rise in long-chain alkenone abundances (Alo et al., 2026). Total organic carbon (TOC) declines from the Unit II maximum due to dilution by carbonate input, while the chemocline progressively deepens under the combined influence of freshwater inflow and partial water-column ventilation (Zhao et al., 2026).

4.2.3 Existing paleoenvironmental constraints from parallel studies

The chlorophyll-derivative and bulk geochemical records developed by Alo et al. (2026) and Zhao et al. (2026) on the same thirteen samples provide a multi-proxy baseline against which the arsenolipid record presented in this chapter can be interpreted. Alo et al. (2026) established that primary productivity, as recorded by total Chl-*a*-DD concentration, increases stepwise from Unit III (~280 µg/g OC average) to Unit II (~1100 µg/g OC average), and that the relative

contribution of *Isochrysis* algae versus other phytoplankton groups, tracked by the Chl-*a*-DDs/LCAs ratio, is stable in Unit III, elevated in Unit II (indicating *Isochrysis* suppression), and reduced again in Unit I (indicating *Isochrysis* resurgence). Bulk parameters from the same study—TOC, $\delta^{13}C$(org), $\delta^{15}N$(org), and perylene—document the parallel environmental shifts in organic-carbon burial, photic-zone irradiance, nitrogen-cycle perturbation, and terrestrial input across the three units.

Zhao et al. (2026) further partitioned the Chl-*a*-DD pool into reductive (ReCs), oxidative (OxCs), steryl chlorin ester (SCEs), and cyclopheophorbide (CPBs) classes, each tracking a distinct water-column or sedimentary process. Reductive derivatives (ReCs) and the meso/pPhe-*a* ratio respond to redox state and the intensity of euxinia, with the meso/pPhe-*a* peak between ~5 and 3 ka B.P. interpreted as an interval of intensified euxinia. Oxidative derivatives (OxCs), elevated in Units II and I, reflect intracellular oxidation associated with photic-zone light stress under shoaled chemocline conditions. Steryl chlorin esters (SCEs), dominant in Unit III and reduced in Units II and I, track macrozooplankton grazing-mediated organic-carbon export. Cyclopheophorbide derivatives (CPBs), elevated under euxinic conditions, reflect protist-mediated grazing combined with antioxidative response to oxidative stress.

Together, these two studies establish a multi-dimensional environmental baseline for the Holocene GGC18 sequence: Alo et al. (2026) provides the producer-side constraints—what phytoplankton groups dominated, when, and under what salinity and nutrient regimes—while Zhao et al. (2026) provides the water-column process constraints—how chlorophyll-derived organic matter was modified during transit and deposition under varying redox, light-stress, and grazing regimes. The arsenolipid distributions presented in Section 4.3 will be interpreted against

this baseline in Sections 4.4 through 4.6, enabling a stratigraphic-resolution test of how arsenolipid signals respond to the documented environmental and ecological transitions.

4.3 Detection Results

Both AsHCs and thioxoarsenolipids were detected across all thirteen GGC18 samples. Two AsHC homologs—AsHC-332 (C15) and AsHC-360 (C17)—were identified using the criteria established in Section 2.6.1, while AsHC-388 (C19) was below the detection limit in all samples, consistent with the absence of AsHC-388 from all fossil samples and most modern settings reported in Sections 3.3.1 and 3.5.7. Three thioxoarsenolipid homologs—*m/z* 547, 549, and 565, corresponding to compounds 23, 24, and 19 of Liu (2023)—were identified following the carbon–sulfur fragmentation criteria established in Section 2.6.2. Quantification followed the internal-standard protocol applied to the parallel chlorin-derivative studies on this sample set (Alo et al., 2026; Zhao et al., 2026). Prior to extraction, 500 ng of C_{46} glycerol trialkyl glycerol tetraether (C_{46}-GTGT) was added to each of the thirteen samples as an internal standard for chromatographic quantification. Because authentic standards for the individual AsHC and thioxoarsenolipid homologues were not available, compound abundances were estimated from their peak areas relative to that of the C_{46}-GTGT internal standard and are therefore considered semi-quantitative. Abundances are reported as TOC-normalized values (μg/g OC) using the bulk organic-carbon contents determined for the same samples by Alo et al. (2026), enabling comparison across the sequence. Unlike the qualitative survey of Chapter 3, in which no internal standard was used and detection was assessed only as presence or absence (Section 2.6.3), the addition of a fixed amount of internal standard to every GGC18 sample permits relative-abundance comparison through the sequence.

4.3.1 AsHC abundance and distribution

Total AsHC concentrations (sum of AsHC-332 and AsHC-360) across the thirteen samples vary by approximately a factor of seven, from 0.248 μg/g OC at 3.66 ka (Unit II) to 1.86 μg/g OC at 1.35 ka (Unit I). The unit-averaged abundances follow a non-monotonic stratigraphic pattern: Unit III samples yield an average total AsHC concentration of 0.959 μg/g OC, Unit II samples decrease to an average of 0.604 μg/g OC, and Unit I samples reach the highest unit-averaged concentration of 1.58 μg/g OC. The minimum-to-maximum range of unit averages spans approximately 2.6-fold across the Holocene sequence.

Beyond the changes in total abundance, the relative proportions of the two homologs shift systematically across the stratigraphic units. In Unit III, AsHC-360 is the more abundant homolog, with an average AsHC-332/AsHC-360 ratio of 0.628. In Unit II, the two homologs are present in approximately similar proportions, with an average ratio of 1.42. In Unit I, AsHC-332 becomes strongly dominant, with an average ratio of 3.20. The progressive increase in the AsHC-332/AsHC-360 ratio from Unit III through Unit I represents a more than five-fold change across the Holocene sequence, larger in magnitude than the variation observed in the total AsHC concentration itself.

4.3.2 Thioxoarsenolipid abundance and distribution

Total thioxoarsenolipid concentrations (sum of *m/z* 547, 549, and 565) vary by more than a factor of twenty across the thirteen samples, from 14.6 μg/g OC at 11.7 ka (Unit III) to 332 μg/g OC at 6.73 ka (Unit II). The unit-averaged abundances follow a markedly stepped stratigraphic pattern: Unit III samples yield an average total thioxoarsenolipid concentration of 28.3 μg/g OC, Unit II samples increase approximately seven-fold to an average of 194 μg/g OC, and Unit I

samples remain elevated at an average of 154 µg/g OC. The maximum value of 332 µg/g OC occurs at 6.73 ka, immediately above the Unit III/II transition.

Among the three thioxoarsenolipid homologs, *m/z* 549 is consistently the most abundant component across all units, accounting for 49–83% of the total thioxoarsenolipid pool in any given sample, with an average contribution of approximately 65%. Compound *m/z* 547 is the second most abundant homolog (13–30% of total), while *m/z* 565 contributes the smallest fraction in most samples (typically 2–18%). Variations in the *m/z* 549 concentration are strongly correlated with variations in the total thioxoarsenolipid concentration across the thirteen samples (Pearson r = +0.982, n = 13), indicating that variations in total thioxoarsenolipid concentration are largely co-incident with variations in *m/z* 549. In contrast to the systematic five-fold shift observed for the AsHC-332/AsHC-360 homolog ratio in AsHCs, the relative proportions of the three thioxoarsenolipid homologs do not show a corresponding stratigraphic trend across Unit III, II, and I.

4.3.3 Stratigraphic profiles, the AsHC-to-thioxoarsenolipid ratio, and within-unit variability

The stratigraphic distributions of AsHCs and thioxoarsenolipids across the thirteen samples are presented in Figure 4.1, alongside the chlorophyll-derivative and bulk geochemical proxies developed by Alo et al. (2026) and Zhao et al. (2026) on the same sample set.

A central feature of the combined arsenolipid record is the contrasting behavior of the two compound classes through Unit II. While total AsHC concentrations decrease in Unit II relative to Unit III, total thioxoarsenolipid concentrations increase by approximately seven-fold over the same interval. The ratio of total AsHC to total thioxoarsenolipid (AsHC/thioxoarsenolipid ratio in Figure 4.1) captures this contrast in a single quantity: the unit-averaged ratio is 0.0391 in Unit III, decreases by approximately an order of magnitude to 0.00344 in Unit II, and partially recovers to

0.0105 in Unit I. The minimum AsHC/thioxoarsenolipid ratio across the entire sequence, 0.000803, occurs at 6.73 ka, which also corresponds to the maximum absolute thioxoarsenolipid concentration. The Unit II interval is therefore characterized simultaneously by suppressed AsHC abundance, elevated thioxoarsenolipid abundance, and a strongly thioxoarsenolipid-dominated arsenolipid pool.

The stratigraphic transition between the 7.79 ka sample (Unit III) and the 6.73 ka sample (Unit II) corresponds to the largest single inter-sample change in arsenolipid abundance observed across the entire sequence: total thioxoarsenolipid concentration increases by 266 μg/g OC (a 5-fold rise across the Unit III/II boundary), while total AsHC concentration decreases by 1.36 μg/g OC over the same step. The 6.73 ka sample, which lies immediately above this boundary, exhibits coincident extremes in three independent arsenolipid metrics within a single stratigraphic horizon: the maximum total thioxoarsenolipid concentration (332 μg/g OC), the second-lowest total AsHC concentration (0.267 μg/g OC), and the minimum AsHC/thioxoarsenolipid ratio (0.000803). On this same sample, TOC reaches one of the highest values of the sequence, while the chlorophyll-derivative ratios fall within their respective Unit II ranges. The arsenolipid metrics therefore record a more abrupt step change at this stratigraphic horizon than the chlorophyll-derivative ratios on the same sample.

The dispersion of arsenolipid metrics within each stratigraphic unit, expressed as coefficients of variation (CV), reveals contrasting structural behavior across the three units. Unit II exhibits the largest within-unit variability across all four primary metrics—total AsHC concentration (CV = 64%), total thioxoarsenolipid concentration (CV = 44%), AsHC/thioxoarsenolipid ratio (CV = 62%), and AsHC-332/AsHC-360 homolog ratio (CV = 68%). Unit I, in contrast, shows the smallest within-unit variability across all four metrics (CV = 13–

23%), and Unit III is intermediate (CV = 20–77%). Within Unit III, total AsHC and total thioxoarsenolipid concentrations are strongly co-varying across the five samples (Pearson r = +0.989, n = 5), suggesting that the two compound classes track one another within this baseline interval, although the small within-unit sample size limits the strength of this inference. Within Unit II and Unit I, this strong co-variation breaks down (r = −0.169 in Unit II, n = 5; r = −0.014 in Unit I, n = 3). The arsenolipid distributions, the systematic AsHC-332/AsHC-360 homolog shift, the contrasting Unit-scale behavior of the two compound classes, and the within-unit variability structure together provide the empirical basis for the producer-side and water-column interpretations developed in the following sections.

4.4 Discussion: The AsHC Stratigraphic Record

The thirteen-sample AsHC record presented in Section 4.3 raises two interpretive questions. First, what does the non-monotonic pattern of total AsHC abundance across the stratigraphic units, combined with the systematic five-fold increase in the AsHC-332/AsHC-360 homolog ratio from Unit III through Unit I, indicate about the producer communities that contributed to AsHC biosynthesis through the Holocene Black Sea sequence? Second, how does the AsHC record relate to the phytoplankton-community dynamics documented by Alo et al. (2026) for the same samples?

4.4.1 Stratigraphic patterns in the AsHC record

Two features of the AsHC record carry interpretive weight beyond simple variation in concentration. First, the unit-averaged total AsHC abundance follows a non-monotonic stratigraphic pattern: an intermediate baseline in Unit III (0.959 µg/g OC), a depression in Unit II (0.604 µg/g OC), and the highest values of the sequence in Unit I (1.58 µg/g OC). Both Alo et al. (2026) and Zhao et al. (2026) attribute the elevated organic-carbon content of Unit II to a

combination of enhanced primary productivity and improved preservation under euxinic conditions. If improved preservation were the dominant control on the arsenolipid record, both compound classes would be expected to benefit; instead, total thioxoarsenolipid abundance rises roughly seven-fold across the Unit III/II transition while total AsHC abundance falls to its lowest values of the sequence (Section 4.3.3). The opposite behaviour of the two compound classes under the same conditions of improved bulk preservation indicates that the Unit II AsHC depression cannot be explained by preservation efficiency, and instead reflects a reduced supply of AsHCs to the sediment, a selective loss of AsHCs relative to thioxoarsenolipids, or both.

Second, the AsHC-332/AsHC-360 homolog ratio shifts systematically from a Unit III value of 0.628 (AsHC-360 dominant) through a Unit II transitional value of 1.42 to a Unit I value of 3.20 (AsHC-332 dominant), a five-fold change that exceeds the range of variation in the total AsHC concentration itself. The progressive nature of this shift across stratigraphic units, including its continuation into Unit I where total AsHC abundance recovers, suggests that the homolog ratio carries information distinct from that carried by the total abundance. The two metrics—total abundance and homolog composition—are therefore likely to reflect partially independent controls on the producer-side input of AsHCs to the sediment. The progressive, monotonic increase in the AsHC-332/AsHC-360 ratio from Unit III through Unit I (0.63 → 1.43 → 3.20) is unlikely to reflect differential diagenetic loss of the two homologues. Preferential loss of the longer-chain AsHC-360 with burial would predict the highest ratios in the oldest, most deeply buried samples; instead, the observed ratios are highest in the youngest Unit I sediments and lowest in the oldest Unit III samples, the opposite of the trend expected from burial-related degradation. The monotonic increase therefore more plausibly reflects a directional change in the chain-length distribution of the AsHCs supplied to the sediment—a producer-side compositional signal—consistent with the

strong correlation between the homolog ratio and total Chl-a-DD concentration (r = +0.881, n = 13; Section 4.4.2). The specific producer-community or physiological controls on AsHC chain length cannot be resolved from the present dataset and will require calibration against modern source organisms.

4.4.2 Co-variation with phytoplankton dynamics from Alo et al. (2026)

The total AsHC concentration record on the GGC18 samples co-varies with the phytoplankton-community indicators developed by Alo et al. (2026), with both records reaching their lowest values in Unit II and their highest values in Unit I. Alo et al. (2026) demonstrated, through paired analysis of long-chain alkenones (LCAs) and chlorophyll-a degradation derivatives (Chl-a-DDs) on these thirteen samples, that *Isochrysis* algae maintained a stable contribution to the phytoplankton community through Unit III, were strongly suppressed during the photic-zone euxinia interval of Unit II, and underwent a rapid resurgence following the Late-Holocene freshening event in Unit I (Section 4.2.3). The non-monotonic AsHC pattern—intermediate Unit III, suppressed Unit II, elevated Unit I—follows a similar Unit-by-Unit pattern to this *Isochrysis* trajectory documented by Alo et al. (2026).

This co-variation is supported quantitatively by the relationship between the AsHC-332/AsHC-360 homolog ratio and the chlorophyll-derivative records on the same samples. The homolog ratio is strongly correlated with total Chl-*a*-DD concentration across the thirteen samples (Pearson r = +0.881, n = 13; Figure 4.2a), and moderately correlated with LCA concentration (r = +0.655, n = 13). The strength of these correlations indicates that the systematic homolog-ratio shift is not independent of the phytoplankton-community dynamics documented by Alo et al. (2026) but co-varies with them at the level of compositional change in the AsHC pool. The simultaneous behavior of the two records—the recovery of both *Isochrysis* productivity and elevated AsHC

abundances in Unit I, and the strong positive correlation between the homolog ratio and the Chl-*a*-DD record—is consistent with a producer-side coupling between AsHC biosynthesis and the phytoplankton community that contributed Chl-*a*-DD-bearing biomass to the sediment.

4.4.3 Implications for AsHC source communities in the Holocene Black Sea archive

The co-variation between the AsHC record and the phytoplankton-community dynamics documented by Alo et al. (2026) is consistent with two non-exclusive interpretations regarding AsHC source organisms in this sedimentary archive. The first is that *Isochrysis* algae, or members of the broader phytoplankton assemblage that fluctuates synchronously with *Isochrysis*, contribute directly to AsHC biosynthesis under the redox and salinity conditions of the Black Sea Holocene. *Isochrysis* belongs to the haptophyte algal lineage, which had not yet been characterized as an AsHC producer in published culture work, although AsHC has been documented in brown algae and other marine organisms (García-Salgado et al., 2012; Raab et al., 2013); if confirmed by future culture studies, the present results would extend the documented producer range of AsHCs to this lineage. The second interpretation is that AsHC biosynthesis is performed by other components of the producer community whose abundance covaries with *Isochrysis* under the salinity and nutrient regimes that govern *Isochrysis* productivity. Bacterial producers, including the cyanobacterial and heterotrophic-bacterial sources discussed in Section 3.4.2, would respond to similar environmental controls and could therefore generate a similar stratigraphic signal without being themselves part of the *Isochrysis* lineage.

The thirteen-sample dataset cannot statistically deconvolve the contributions of these two interpretations on its own, both because the source organisms of AsHCs in natural environments remain incompletely characterized (Section 3.4.2) and because correlation between the AsHC record and *Isochrysis*-related proxies does not establish that *Isochrysis* itself is the AsHC source.

However, established results from culture experiments and the broader literature on marine arsenic biogeochemistry (Edmonds and Francesconi, 1987) provide one plausible interpretation of the stratigraphic patterns observed across the GGC18 sequence. The AsHC biosynthesis has been documented in culture for a phylogenetically diverse range of producer organisms, including the green algae *Dunaliella tertiolecta* (Wrench and Addison, 1981; Glabonjat et al., 2018) and *Picocystis* strain ML (Glabonjat et al., 2020), and the cyanobacterium *Synechocystis* sp. PCC 6803 (Xue et al., 2014). In these culture studies, the relative production of arsenolipids versus water-soluble arsenicals depends strongly on the As/P ratio in the growth medium (Glabonjat et al., 2018, 2020), with arsenolipid yields rising under conditions of phosphate limitation. In the Holocene Black Sea, both the phytoplankton-community composition and the surface-water nutrient regime change systematically across the Unit transitions (Alo et al., 2026), which is consistent with the observed AsHC patterns reflecting a combination of compositional shifts in the producer community and physiological responses of those producers to the changing salinity and nutrient regimes documented by Alo et al. (2026). Distinguishing the relative contributions of taxonomic turnover and physiological adjustment within the same lineages will require culture-based experiments with phytoplankton from the Holocene Black Sea or close analogs, and is beyond the scope of the present study.

The implication of the co-variation, however, is that the Holocene AsHC record is consistent with a producer-side record reflecting the stratigraphic ecology of AsHC biosynthesis in this sedimentary system, rather than being well explained by organic-matter preservation alone. The AsHC homolog composition, encoded in the AsHC-332/AsHC-360 ratio, may therefore serve as a complementary signal of producer-community change in sedimentary archives where

Isochrysis- or LCA-based proxies are unavailable, with calibration against modern source organisms providing the next step toward a quantitative interpretation.

4.5 Discussion: The Thioxoarsenolipid Stratigraphic Record

The thirteen-sample thioxoarsenolipid record presented in Section 4.3 provides the first stratigraphic profile for the arsenolipids in Black Sea sapropel sediments. Two interpretive questions follow from this record. First, what controls the seven-fold stepwise increase in total thioxoarsenolipid abundance across the Unit III/II boundary, and the persistence of elevated abundances through Unit II and into Unit I? Second, how does the thioxoarsenolipid record relate to the water-column processes documented by Zhao et al. (2026) for the same samples?

4.5.1 Stratigraphic patterns in the thioxoarsenolipid record

Three features of the thioxoarsenolipid record carry interpretive weight beyond the simple Unit-averaged trend. First, the abundance increase between Unit III and Unit II is sharp rather than gradual: total thioxoarsenolipid concentration rises from a Unit III average of 28.3 μg/g OC to a Unit II average of 194 μg/g OC, a seven-fold increase concentrated largely at the Unit III/II transition (Section 4.3.3). The maximum value of 332 μg/g OC occurs at 6.73 ka, immediately above this boundary and within the early phase of photic-zone euxinia (PZE) development (Section 4.2.2). The stepwise nature of the increase, together with its location at the redox transition, is consistent with a rapid response of thioxoarsenolipid formation or accumulation to the shift from oxic-to-suboxic to euxinic conditions, the timing of which is independently constrained by pyrite framboid size distributions in the same sedimentary sequence (Wilkin et al., 1997). The precise mechanism by which the depositional change couples to the thioxoarsenolipid record is not constrained by the present dataset.

Second, the elevated abundances persist through Unit II (mean 194 µg/g OC) and into Unit I (mean 154 µg/g OC), even as Unit I records the late-Holocene surface-water freshening event and the partial deepening of the chemocline described in Section 4.2.2. The Unit I thioxoarsenolipid abundance is therefore not consistent with an immediate decline upon weakening of euxinic conditions. Two non-exclusive interpretations are consistent with this observation. First, thioxoarsenolipids may preserve well once formed and undergo limited subsequent degradation. Particle-hosted sulfurization forms acid-resistant organic sulfur rapidly and enhances organic-carbon preservation in sediments underlying oxygen-deficient waters (Raven et al., 2021), and sulfurization is widely understood to limit the bioavailability of organic matter to microbial respiration—by removing energy-yielding functional groups, increasing molecular weight, and producing structures less susceptible to enzymatic breakdown (Raven et al., 2018; Phillips et al., 2022). The incorporation of reduced sulfur correspondingly enhances the preservation of biomarker lipids in anoxic sediments (Werne et al., 2008) and of dissolved organic matter in the modern Black Sea water column (Gomez-Saez et al., 2021). A comparable stabilization of the arsenic–sulfur bond once formed would plausibly explain why thioxoarsenolipid abundances remain elevated into Unit I even as euxinic intensity wanes. Second, thioxoarsenolipid production may continue at appreciable rates in the still-stratified water column of the late Holocene despite the partial chemocline deepening.

Third, the relative proportions of the three thioxoarsenolipid homologs (*m/z* 547, 549, and 565) remain broadly stable across the three stratigraphic units, in contrast to the systematic five-fold shift observed in the AsHC-332/AsHC-360 homolog ratio (Section 4.3.2). The dominance of *m/z* 549 across all units, which was indicated by the strong correlation between *m/z* 549 concentration and total thioxoarsenolipid concentration (Pearson r = +0.982, n = 13; Section 4.3.2),

is consistent with a relatively stable channel for *m/z* 549 across the redox and salinity transitions documented in the GGC18 sequence, although the chemical and biological details of this channel are not resolved by the present data.

4.5.2 Co-variation with redox and water-column proxies from Zhao et al. (2026)

The thioxoarsenolipid record on the GGC18 samples co-varies systematically with several of the chlorophyll-derivative proxies developed by Zhao et al. (2026) on the same thirteen samples, providing quantitative evidence for a link between thioxoarsenolipid abundance and the water-column processes those proxies track. The strongest of these relationships is between total thioxoarsenolipid concentration and the SCE/Total ratio (Pearson $r = -0.751$, $n = 13$). Zhao et al. (2026) interpreted SCE/Total as a tracker of macrozooplankton-grazing-mediated organic carbon export, building on earlier work that established phorbin steryl esters as a major chlorophyll-degradation pool in Black Sea sapropels and linked their formation to phytoplankton grazing by zooplanktonic herbivores (King and Repeta, 1991). High values reflect fecal-pellet-dominated export under non-stratified conditions and low values reflect reduced grazing under euxinia. The strong negative correlation between thioxoarsenolipid abundance and SCE/Total is therefore consistent with thioxoarsenolipid maxima coinciding with intervals in which macrozooplankton grazing was suppressed and the SCE-based export pathway was diminished, although the correlation alone does not establish whether the relationship reflects shared environmental drivers, distinct response timing, or some other coupling.

A second relationship is between total thioxoarsenolipid concentration and the OxC/Total ratio (Pearson $r = +0.621$). Zhao et al. (2026) interpreted OxC/Total as a tracker of intracellular oxidation associated with photic-zone light stress under shoaled chemocline conditions, with high values reflecting elevated reactive-oxygen-species production in primary producers. The positive

correlation between thioxoarsenolipid abundance and OxC/Total is consistent with thioxoarsenolipid maxima occurring within intervals also characterized by elevated light stress in the surface ocean. Total thioxoarsenolipid concentration is also moderately positively correlated with total Chl-*a*-DD concentration ($r = +0.553$, $n = 13$) and with $\delta^{13}C$ of organic carbon ($r = +0.533$, $n = 13$), both of which reach their highest values in Unit II.

The thioxoarsenolipid record and the meso/pyropheophytin-*a* peak reported by Zhao et al. (2026) between ~5 and 3 ka capture the same broad interval of intensified euxinia, but their respective maxima do not coincide exactly: the thioxoarsenolipid maximum at 6.73 ka precedes the meso-pPhe-*a* maximum by approximately 1–2 kyr. The two records, therefore, appear to capture related but not identical aspects of the redox-stratification dynamics in the Black Sea Holocene, with the thioxoarsenolipid record peaking early in the PZE development phase and the meso-pPhe-*a* record peaking during the most intensified euxinic phase.

4.5.3 Implications for thioxoarsenolipid formation and preservation

The co-variations described in Section 4.5.2 constrain, but do not uniquely determine, the formation pathway of the thioxoarsenolipids in this sedimentary system. Three non-exclusive pathways are consistent with the observed stratigraphic patterns. The widespread detection of thioxoarsenolipids documented in Chapter 3, including in modern aquatic settings whose surface waters are not sulfidic (Lake Thunderbird, Duck Pond), establishes that at least some fraction of the global sulfur pool must arise through a non-sulfide pathway, and this constraint frames the candidate pathways considered below. The first is direct biosynthesis of thioxoarsenolipids by microbial communities specialized to euxinic or sulfide-rich environments, with the seven-fold abundance increase across the Unit III/II boundary potentially reflecting a shift in producer-community composition associated with the development of PZE; recent work has implicated

marine bacteria as an overlooked source of arsenolipids in the broader surface ocean (Heal et al., 2022), suggesting that prokaryotic producers in the Black Sea Holocene chemocline could plausibly contribute to the thioxoarsenolipid pool. The second is post-depositional or in-water-column sulfidation of arsenic-bearing precursors, generating thioxoarsenolipids through reaction of pre-existing molecules with hydrogen sulfide or polysulfide species under euxinic conditions—a class of process that has been independently demonstrated for organic substrates in modern anoxic water columns and sinking particles (Werne et al., 2008; Gomez-Saez et al., 2021; Raven et al., 2021). The third is a combination of both pathways, with biological synthesis dominating in some intervals and abiotic sulfidation dominating in others. The present results do not distinguish among these pathways, and the structural information available for the thioxoarsenolipids reported by Liu (2023) does not yet allow a mechanistic assignment.

The thirteen-sample dataset cannot statistically deconvolve the contributions of these candidate pathways. However, established chemistry and microbiology provide one plausible interpretation of the thioxoarsenolipid response across the Unit III/II transition. Sulfide-driven thiolation of arsenic-bearing molecules, in which oxygen ligands of As(III) and As(V) species are replaced by sulfur ligands to form thioarsenites and thioarsenates, is a well-documented chemical reaction under sulfidic conditions (Helz et al., 1995; Stauder et al., 2005; Wallschläger and Stadey, 2007; Planer-Friedrich et al., 2007), and sulfide-driven thiolation has been demonstrated for both inorganic arsenic species and methylated arsenic species (Pinel-Raffaitin et al., 2007; DC.Rubin et al., 2014). Microbially mediated thioarsenate formation under sulfidic conditions has been demonstrated for sulfate-reducing bacteria from natural and laboratory settings (DCRubin et al., 2014; Wu et al., 2017), and porewater studies in lake sediments confirm that thioarsenic species form during early diagenesis under the combined influence of sulfide and arsenic (Couture et al.,

2010). The seven-fold increase in thioxoarsenolipid abundance and the corresponding approximately eleven-fold drop in the AsHC/thioxoarsenolipid ratio across the Unit III/II boundary coincide with the development of euxinic, sulfide-rich conditions in the Black Sea water column documented independently by Sinninghe Damsté et al. (1993), Huang et al. (2000), and the meso/pPhe-*a* record of Zhao et al. (2026). The combination of the established sulfide-driven thiolation chemistry, the parallel microbial thiolation literature, and the timing of the thioxoarsenolipid response across the Unit III/II boundary is consistent with sulfide-mediated chemistry being among the more plausible contributors to the observed stratigraphic patterns, although the relative balance between abiotic sulfidation and microbially mediated thiolation cannot be resolved by the present dataset.

The relationship between the thioxoarsenolipid record and the AsHC record discussed in Section 4.4 provides one further set of observations relevant to formation pathway considerations. The two compound classes vary in opposite directions across the Unit III/II transition—AsHC abundance decreases while thioxoarsenolipid abundance increases—but their behaviors within Unit III are tightly linked, with Pearson correlation r = +0.989 between total AsHC and total thioxoarsenolipid concentrations across the five Unit III samples (Section 4.3.3). This co-variation within the pre-euxinic baseline interval, followed by decoupling once euxinic conditions develop, is consistent with several non-exclusive scenarios, including the possibility that the two compound classes share input pathways under non-euxinic conditions but respond to environmental change through different mechanisms once the depositional system enters the euxinic regime, or that distinct input pathways for the two classes are differentially modulated by the development of euxinia. Whether this difference reflects substrate availability, redox-controlled formation

specificity, selective preservation of thioxoarsenolipids over AsHCs under euxinic conditions, or some combination of these factors cannot be resolved from the present dataset alone.

4.6 Discussion: The Coupled Arsenolipid Record and Multiple Environmental Controls

Sections 4.4 and 4.5 examined the AsHC and thioxoarsenolipid records separately, drawing primarily on the producer-side framework of Alo et al. (2026) and the water-column-process framework of Zhao et al. (2026), respectively. The contrasting stratigraphic behavior of the two compound classes, however—decreasing AsHC abundance and increasing thioxoarsenolipid abundance across the Unit III/II transition (Section 4.3.3)—indicates that neither compound class alone captures the full arsenolipid response to the Holocene Black Sea environmental transitions. The ratio of total AsHC concentration to total thioxoarsenolipid concentration (the AsHC/thioxoarsenolipid ratio) provides a single composite metric in which the coupled behavior of the two compound classes can be examined, and against which the influence of multiple environmental factors documented by Alo et al. (2026) and Zhao et al. (2026) can be tested simultaneously.

4.6.1 The AsHC/thioxoarsenolipid ratio as a coupled-record metric

The AsHC/thioxoarsenolipid ratio shows the largest range of variation observed in any of the arsenolipid metrics in this study, spanning approximately two orders of magnitude across the thirteen-sample sequence: the unit-averaged ratio is 0.0391 in Unit III, decreases by approximately an order of magnitude to 0.00344 in Unit II, and partially recovers to 0.0105 in Unit I (Section 4.3.3). This range exceeds the 2.6-fold range of total AsHC unit averages and is comparable to the seven-fold range of total thioxoarsenolipid unit averages, indicating that the two compound classes are responding to the Holocene transitions in opposing directions and that the ratio amplifies signals that the individual compound classes capture independently.

The use of the AsHC/thioxoarsenolipid ratio as a coupled-record metric also addresses a limitation of the individual-compound interpretations developed in Sections 4.4 and 4.5. The interpretation of total AsHC abundance is complicated by the multiple producer- and preservation-side controls discussed in Section 4.4; the interpretation of total thioxoarsenolipid abundance is complicated by the unresolved formation pathway discussed in Section 4.5. The ratio of the two abundances, by contrast, depends on the relative behavior of the two compound classes rather than on the absolute behavior of either, and is therefore less sensitive to overall variations in arsenolipid input or preservation that affect the two classes similarly. The AsHC/thioxoarsenolipid ratio is therefore best interpreted as a metric of compositional balance within the arsenolipid pool rather than as a proxy for any single environmental factor.

4.6.2 Multiple environmental factors co-vary with the AsHC/thioxoarsenolipid ratio

The AsHC/thioxoarsenolipid ratio co-varies with several of the chlorophyll-derivative and bulk geochemical proxies developed by Alo et al. (2026) and Zhao et al. (2026) on the same thirteen samples, with three relationships standing out for their strength and stratigraphic consistency.

The AsHC/thioxoarsenolipid ratio is strongly positively correlated with the SCE/Total ratio of Zhao et al. (2026) (Pearson $r = +0.824$, $n = 13$; Figure 4.2b), the strongest correlation observed between any of the arsenolipid metrics and any of the published proxy records on these samples. SCE/Total reaches its highest values in Unit III, where macrozooplankton grazing-mediated export dominated organic-carbon delivery to the sediment under non-euxinic conditions, and decreases sharply in Units II and I as grazing was suppressed under euxinia. The AsHC/thioxoarsenolipid ratio follows the same general pattern, with its Unit III maximum coinciding with the SCE/Total maximum, suggesting that the relative balance of AsHCs and thioxoarsenolipids in the

sedimentary record is influenced by, or at least co-varies with, the dominant organic-carbon export pathway operating in the water column.

The AsHC/thioxoarsenolipid ratio is also strongly negatively correlated with the OxC/Total ratio of Zhao et al. (2026) ($r = -0.760$, $n = 13$; Figure 4.2c). OxC/Total reaches elevated values in Unit II and Unit I, reflecting intracellular oxidation associated with photic-zone light stress under shoaled chemocline conditions, and is lowest in Unit III. The negative correlation indicates that the AsHC/thioxoarsenolipid ratio is depressed precisely in those intervals where light stress in the surface ocean was most pronounced. The third strong relationship is between the AsHC/thioxoarsenolipid ratio and total Chl-*a*-DD concentration ($r = -0.744$, $n = 13$), with the AsHC/thioxoarsenolipid ratio at its lowest values in Unit II where total Chl-*a*-DD reaches its highest values.

These three correlations describe partially overlapping but distinct aspects of the Holocene Black Sea environmental evolution: SCE/Total tracks grazing-pathway dominance, OxC/Total tracks light stress, and total Chl-*a*-DD tracks primary productivity. The coincident behavior of the AsHC/thioxoarsenolipid ratio with respect to all three proxies is consistent with a coupled arsenolipid response to multiple, non-exclusive environmental factors operating together in the Black Sea Holocene system, rather than to any one of these factors in isolation. The transitions across Unit boundaries—the depression of the AsHC/thioxoarsenolipid ratio in Unit II coinciding with suppressed grazing, intensified light stress, and elevated productivity, and the partial recovery in Unit I coinciding with the late-Holocene freshening event—are consistent with a multi-factor interpretation in which the redox transition, the salinity transition, the productivity changes, and the surface-water-column stress regime together shape the relative abundances of AsHCs and thioxoarsenolipids in the sedimentary record.

4.6.3 Implications for arsenolipid records as paleoenvironmental indicators

The Holocene Black Sea record presented in this chapter indicates that the AsHC/thioxoarsenolipid ratio co-varies with multiple environmental factors documented by Alo et al. (2026) and Zhao et al. (2026) on the same samples—productivity, light stress, and grazing-pathway dominance among them—rather than with any single environmental factor in isolation. This multi-factor sensitivity precludes the use of the AsHC/thioxoarsenolipid ratio, on the basis of the present dataset alone, as a quantitative proxy for any one specific environmental variable. The ratio cannot be inverted to recover, for example, a redox state or a productivity level independently of the other co-varying factors, because the correlations documented in Section 4.6.2 do not establish which of the multiple factors controls the ratio under any given depositional regime, or how their relative contributions might shift between regimes.

The thirteen-sample dataset cannot statistically deconvolve the contributions of these co-varying environmental factors. However, established chemistry provides one plausible interpretation of the AsHC/thioxoarsenolipid ratio response across the Unit III/II transition. The sulfide-driven thiolation chemistry that has been demonstrated for inorganic, methylated, and microbially mediated arsenic species (Section 4.5.3) provides a mechanistic basis on which to interpret the seven-fold increase in thioxoarsenolipid abundance and the corresponding approximately eleven-fold drop in the AsHC/thioxoarsenolipid ratio across the Unit III/II boundary. These changes coincide with the development of euxinic, sulfide-rich conditions in the Black Sea water column documented independently by Sinninghe Damsté et al. (1993), Huang et al. (2000), and the meso/pPhe-*a* record of Zhao et al. (2026). The combination of the established sulfide-driven thiolation chemistry and the timing of the AsHC/thioxoarsenolipid response is consistent with the redox transition—and specifically the development of sulfidic conditions—

being one of the more plausible drivers among the co-varying environmental factors documented across the Unit III/II boundary.

The producer-side controls discussed in Section 4.4 and the sulfide-mediated chemistry discussed in Section 4.5 are not independent of one another in this sedimentary system. Both the producer-community shifts that accompanied PZE development—suppression of *Isochrysis* productivity, reorganization of the surface phytoplankton assemblage under high-salinity, low-light conditions—and the sulfide-driven thiolation chemistry that operates under euxinic conditions are linked through their shared dependence on the redox transition that established water-column stratification and PZE in the Black Sea Holocene. Within this framework, the differing proximate controls identified for the two compound classes—producer-community-mediated supply for AsHCs (Section 4.4) and sulfide-mediated formation chemistry for thioxoarsenolipids (Section 4.5)—reflect different points along a connected sequence of environmental and biogeochemical changes initiated by the redox transition. The AsHC/thioxoarsenolipid ratio, which integrates the responses of both compound classes into a single composite metric, therefore captures the cascade of effects propagating from this upstream environmental driver more comprehensively than either compound class examined alone.

This interpretation does not exclude the simultaneous influence of producer-community changes, grazing-pathway shifts, light-stress effects, or productivity changes documented by Alo et al. (2026) and Zhao et al. (2026) over the same interval, all of which co-vary with the redox transition and may contribute additively to the observed signal. The strong negative correlations between the AsHC/thioxoarsenolipid ratio and the OxC/Total, SCE/Total, and total Chl-*a*-DD records may reflect, at least in part, that these processes are themselves co-incident with the redox transition rather than each independently controlling arsenolipid composition. Disentangling the

relative contributions of sulfide-driven thiolation chemistry, producer-community shifts, and other co-varying processes will require culture-based and laboratory-based experiments that systematically vary these factors independently, beyond the scope of the sedimentary record analyzed here.

A more limited application of the AsHC/thioxoarsenolipid ratio is, however, supported by the present results. The AsHC/thioxoarsenolipid ratio undergoes a stratigraphic change of approximately eleven-fold across the Unit III/II transition, a range that exceeds the variation observed in any of the individual arsenolipid metrics on the same samples (a 2.6-fold range in AsHC unit averages and a seven-fold range in thioxoarsenolipid unit averages; Section 4.3.3). The ratio therefore amplifies the signal of major depositional transitions in the GGC18 sequence, with its minimum value at 6.73 ka coinciding with the most pronounced single-step change in arsenolipid abundance observed across the entire record (Section 4.3.3). This sensitivity is consistent with a use of the AsHC/thioxoarsenolipid ratio as an indicator of major regime transitions in sedimentary archives—events in which multiple environmental factors change concurrently, such as the redox–salinity–productivity transition recorded across the Unit III/II boundary—rather than as a quantitative proxy for any individual environmental variable. Application of the ratio in this more limited mode does not require the multiple co-varying factors to be deconvolved, and is supported by the strong amplitude of the ratio's response across the documented Holocene transitions in this archive.

The development of arsenolipid metrics into quantitative paleoenvironmental proxies, in contrast, will require constraints that are not available from the present dataset. By contrast, trace-metal-based paleoredox and paleoproductivity proxies (e.g., Mo, U, V, Ni, Cu) have been developed and calibrated through extensive multi-basin syntheses (Tribovillard et al., 2006; Algeo

and Rowe, 2012), and provide a useful methodological reference for the steps that arsenolipid proxies would need to follow. The thirteen-sample sequence represents a single sedimentary archive in a single basin, and the strength of the cross-proxy correlations reported here, while striking, is computed from a sample size that limits statistical generalization (n = 13). The source organisms of arsenolipids in the Black Sea Holocene remain incompletely characterized, as discussed in Section 3.4.2, and the formation pathways of the thioxoarsenolipids reported by Liu (2023) are not yet mechanistically resolved (Section 4.5.3). Calibration of arsenolipid responses against controlled environmental variables in modern systems, application to other sedimentary archives with independently constrained environmental gradients, and culture-based identification of AsHC and thioxoarsenolipid producers will collectively be required to evaluate whether the patterns documented in the GGC18 sequence reflect general features of the arsenolipid response to environmental change or features specific to the Black Sea Holocene system, and to determine whether arsenolipid metrics can be developed beyond the regime-transition application described here.

4.7 Summary

This chapter has examined the stratigraphic distribution of two arsenolipid compound classes—AsHCs and the thioxoarsenolipids—through thirteen sediment samples from the Holocene Black Sea sapropel sequence of GGC18. Three findings emerge. First, the two compound classes follow contrasting stratigraphic patterns across the Unit III/II transition: total AsHC concentration decreases by approximately 37% while total thioxoarsenolipid concentration increases by approximately seven-fold, yielding an approximately eleven-fold drop in the AsHC/thioxoarsenolipid ratio across the transition from a non-stratified to a euxinic depositional system. Second, the proximate controls on the two classes differ: the AsHC record co-varies with

phytoplankton-community dynamics and is consistent with producer-side controls, while the thioxoarsenolipid record co-varies with redox and water-column proxies and is consistent with sulfide-mediated formation chemistry. Third, both controls trace to the same upstream transition—the development of photic-zone euxinia following Mediterranean inflow—so that the AsHC/thioxoarsenolipid ratio integrates the responses of both classes into a single metric recording the propagation of this transition through the coupled water-column–sediment system more comprehensively than either class alone.

4.8 References

Algeo, T.J., Rowe, H., 2012. Paleoceanographic applications of trace-metal concentration data. Chem. Geol 324–325, 6–18. https://doi.org/10.1016/j.chemgeo.2011.09.002.

Alo, O.O., Fu, J., Zhao, W., Zhang, Y.G., Huang, Y., Liu, X.-L., 2026. Simultaneous analysis of long-chain alkenones and chlorophyll derivatives offers new insights into the ecology of *Isochrysis* algae in the Holocene Black Sea. Marine Chemistry 279, 104634. https://doi.org/10.1016/j.marchem.2026.104634.

Arthur, M.A., Dean, W.E., 1998. Organic-matter production and preservation and evolution of anoxia in the Holocene Black Sea. Paleoceanography 13, 395–411. https://doi.org/10.1029/98PA01161.

Arthur, M.A., Sageman, B.B., 2005. Sea-level control on source-rock development: perspectives from the Holocene Black Sea, the mid-Cretaceous Western Interior Basin of North America, and the Late Devonian Appalachian Basin. SEPM Special Publication 82, 35–59. https://doi.org/10.2110/pec.05.82.0035.

Coolen, M.J.L., Orsi, W.D., Balkema, C., 2013. Evolution of the plankton paleome in the Black Sea from the Deglacial to Anthropocene. PNAS 110, 8609–8614. https://doi.org/10.1073/pnas.1219283110.

Coolen, M.J.L., Saenz, J.P., Giosan, L., 2009. DNA and lipid molecular stratigraphic records of haptophyte succession in the Black Sea during the Holocene. Earth Planet. Sci. Lett 284, 610–621. https://doi.org/10.1016/j.epsl.2009.05.029.

Couture, R.M., Gobeil, C., Tessier, A., 2010. Arsenic, iron and sulfur co-diagenesis in lake sediments. Geochim. Cosmochim. Acta 74, 1238–1255. https://doi.org/10.1016/j.gca.2009.11.028.

DCRubin, S.S., Alava, P., Zekker, I., Laing, G., Wiele, T., 2014. Arsenic thiolation and the role of sulfate-reducing bacteria from the human intestinal tract. Environ. Health Perspect 122, 817–822. https://doi.org/10.1289/ehp.1307759.

Edmonds, J.S., Francesconi, K.A., 1987. Transformations of arsenic in the marine environment. Experientia 43, 553–557. https://doi.org/10.1007/BF02143584.

Filipova-Marinova, M.V., Giosan, L., Angelova, H., 2013. Palaeoecological and geochemical evidence for late Pleistocene-early Holocene Black Sea environmental change. Palaeogeogr. Palaeoclimatol. Palaeoecol 387, 49–60. https://doi.org/10.1016/j.quaint.2012.05.002.

García-Salgado, S., Raber, G., Raml, R., Magnes, C., Francesconi, K.A., 2012. Arsenosugar phospholipids and arsenic hydrocarbons in two species of brown macroalgae. Environ. Chem 9, 63–66. https://doi.org/10.1071/EN11164.

Giosan, L., Coolen, M.J.L., Kaplan, J.O., 2012. Early anthropogenic transformation of the Danube-Black Sea system. Sci. Rep 2, 582. https://doi.org/10.1038/srep00582.

Giosan, L., Filip, F., Constantinescu, S., 2009. Was the Black Sea catastrophically flooded in the early Holocene? Quat. Sci. Rev 28, 1–6. https://doi.org/10.1016/j.quascirev.2008.10.012.

Glabonjat, R.A., Blum, J.S., Miller, L.G., 2020. Arsenolipids in cultured *Picocystis* strain ML and their occurrence in biota and sediment from Mono Lake, California. Life 10, 93. https://doi.org/10.3390/life10060093.

Glabonjat, R.A., Ehgartner, J., Duncan, E.G., 2018. Arsenolipid biosynthesis by the unicellular alga *Dunaliella tertiolecta* is influenced by As/P ratio in culture experiments. Metallomics 10, 145–153. https://doi.org/10.1039/c7mt00249a.

Gomez-Saez, G.V., Dittmar, T., Holtappels, M., Pohlabeln, A.M., Lichtschlag, A., Schnetger, B., Boetius, A., Niggemann, J., 2021. Sulfurization of dissolved organic matter in the anoxic water column of the Black Sea. Sci. Adv 7, 6199. https://doi.org/10.1126/sciadv.abf6199.

Hay, B.J., Arthur, M.A., Dean, W.E., Neff, E.D., Honjo, S., 1991. Sediment deposition in the Late Holocene abyssal Black Sea with climatic and chronological implications. Deep-Sea Res 38, 1211–1235. https://doi.org/10.1016/S0198-0149(10)80031-7.

Heal, K.R., Maloney, A.E., Ingalls, A.E., Bundy, R.M., 2022. Diverse arsenic-containing lipids in the surface ocean. Limnol. Oceanogr. Lett 7, 43–51. https://doi.org/10.1002/lol2.10216.

Helz, G.R., Tossell, J.A., Charnock, J.M., Pattrick, R.A.D., Vaughan, D.J., Garner, C.D., 1995. Oligomerization in As(III) sulfide solutions: theoretical constraints and spectroscopic evidence. Geochim. Cosmochim. Acta 59, 4591–4604. https://doi.org/10.1016/0016-7037(95)00330-4.

Huang, Y., Freeman, K.H., Wilkin, R.T., Arthur, M.A., Jones, A.D., 2000. Black Sea chemocline oscillations during the Holocene: molecular and isotopic studies of marginal sediments. Org. Geochem 31, 1525–1531. https://doi.org/10.1016/S0146-6380(00)00090-5.

Huang, Y., Zheng, Y., Heng, P., Giosan, L., Coolen, M.J.L., 2021. Black Sea paleosalinity evolution since the last deglaciation reconstructed from alkenone-inferred Isochrysidales diversity. Earth Planet. Sci. Lett 564, 116881. https://doi.org/10.1016/j.epsl.2021.116881.

King, L.L., Repeta, D.J., 1991. Novel pyrophaeophorbide steryl esters in Black Sea sediments. Geochim. Cosmochim. Acta 55, 2067–2074. https://doi.org/10.1016/0016-7037(91)90044-6.

Liu, X.-L., 2023. Streamlined arsenolipid identification via direct arsenic detection using RPLC-ESI-QTOF-MS with collision-induced dissociation. J. Am. Soc. Mass Spectrom 35, 300–306. https://doi.org/10.1021/jasms.3c00367.

Major, C.O., Goldstein, S.L., Ryan, W.B.F., Lericolais, G., Piotrowski, A.M., Hajdas, I., 2006. The co-evolution of Black Sea level and composition through the last deglaciation and its paleoclimatic significance. Quat. Sci. Rev 25. https://doi.org/10.1016/j.quascirev.2006.01.032.

Phillips, A.A., White, M.E., Seidel, M., Wu, F., Pavia, F.F., Kemeny, P.C., Sessions, A.L., 2022. Novel sulfur isotope analyses constrain sulfurized porewater fluxes as a minor component of marine dissolved organic matter. Proceedings of the National Academy of Sciences 119, 2209152119. https://doi.org/10.1073/pnas.2209152119

Pinel-Raffaitin, P., Le Hecho, I., Amouroux, D., Potin-Gautier, M., 2007. Distribution and fate of inorganic and organic arsenic species in landfill leachates and biogases. Environ. Sci. Technol 41, 4536–4541. https://doi.org/10.1021/es0628506.

Planer-Friedrich, B., London, J., McCleskey, R.B., Nordstrom, D.K., Wallschläger, D., 2007. Thioarsenates in geothermal waters of Yellowstone National Park: determination, preservation, and geochemical importance. Environ. Sci. Technol 41, 5245–5251. https://doi.org/10.1021/es070273v.

Raab, A., Newcombe, C., Pitton, D., Ebel, R., Feldmann, J., 2013. Comprehensive analysis of lipophilic arsenic species in a brown alga (Saccharina latissima. Anal. Chem 85, 2817–2824. https://doi.org/10.1021/ac303340t.

Raven, M.R., Fike, D.A., Gomes, M.L., Webb, S.M., Bradley, A.S., McClelland, H.L.O., 2018. Organic carbon burial during OAE2 driven by changes in the locus of organic matter sulfurization. Nat. Commun 9, 3409. https://doi.org/10.1038/s41467-018-05943-6

Raven, M.R., Keil, R.G., Webb, S.M., 2021. Microbial sulfate reduction and organic sulfur formation in sinking marine particles. Science 371, 178–181. https://doi.org/10.1126/science.abc6035.

References, n.d.

Sinninghe Damsté, J.S., Wakeham, S.G., Kohnen, M.E.L., Hayes, J.M., Leeuw, J.W., 1993. A 6,000-year sedimentary molecular record of chemocline excursions in the Black Sea. Nature 362, 827–829. https://doi.org/10.1038/362827a0.

Soulet, G., Ménot, G., Lericolais, G., Bard, E., 2011. A revised calendar age for the last reconnection of the Black Sea to the global ocean. Quat. Sci. Rev 30, 1019–1026. https://doi.org/10.1016/j.quascirev.2011.03.001.

Spooner, N., Getliff, J.M., Teece, M.A., Parkes, R.J., Leftley, J.W., Harris, P.G., Maxwell, J.R., 1995. Formation of mesopyrophaeophorbide a during anaerobic bacterial degradation of the marine prymnesiophyte *Emiliania huxleyi*. Org. Geochem 22, 225–229. https://doi.org/10.1016/0146-6380(95)90019-5.

Stauder, S., Raue, B., Sacher, F., 2005. Thioarsenates in sulfidic waters. Environ. Sci. Technol 39, 5933–5939. https://doi.org/10.1021/es048034k.

Tribovillard, N., Algeo, T.J., Lyons, T.W., Riboulleau, A., 2006. Trace metals as paleoredox and paleoproductivity proxies: an update. Chem. Geol 232, 12–32. https://doi.org/10.1016/j.chemgeo.2006.02.012.

Wallschläger, D., Stadey, C.J., 2007. Determination of (oxy)thioarsenates in sulfidic waters. Anal. Chem 79, 3873–3880. https://doi.org/10.1021/ac070061g.

Werne, J.P., Lyons, T.W., Hollander, D.J., Schouten, S., Hopmans, E.C., Sinninghe Damsté, J.S., 2008. Investigating pathways of diagenetic organic matter sulfurization using compound-specific sulfur isotope analysis. Geochim. Cosmochim. Acta 72, 3489–3502. https://doi.org/10.1016/j.gca.2008.04.033.

Wilkin, R.T., Arthur, M.A., Dean, W.E., 1997. History of water-column anoxia in the Black Sea indicated by pyrite framboid size distributions. Earth Planet. Sci. Lett 148, 517–525. https://doi.org/10.1016/S0012-821X(97)00053-8.

Wrench, J.J., Addison, R.F., 1981. Reduction, methylation, and incorporation of arsenic into lipids by the marine phytoplankton *Dunaliella tertiolecta*. Can. J. Fish. Aquat. Sci 38, 518–523. https://doi.org/10.1139/f81-073.

Wu, G., Huang, L., Jiang, H., 2017. Thioarsenate formation coupled with anaerobic arsenite oxidation by a sulfate-reducing bacterium isolated from a hot spring. Front. Microbiol 8, 1336. https://doi.org/10.3389/fmicb.2017.01336.

Xue, X.M., Raber, G., Foster, S., Chen, S.C., Francesconi, K.A., Zhu, Y.G., 2014. Biosynthesis of arsenolipids by the cyanobacterium *Synechocystis* sp. PCC 6803. Environ. Chem 11, 506–513. https://doi.org/10.1071/EN14069.

Zhao, W., Fu, J., Alo, O.O., Liu, X.-L., 2026. The distribution of chlorophyll-a degradation derivatives in the Holocene Black Sea and their marine ecological significance. Marine Chemistry 278, 104606. https://doi.org/10.1016/j.marchem.2026.104606.

4.9 Figures

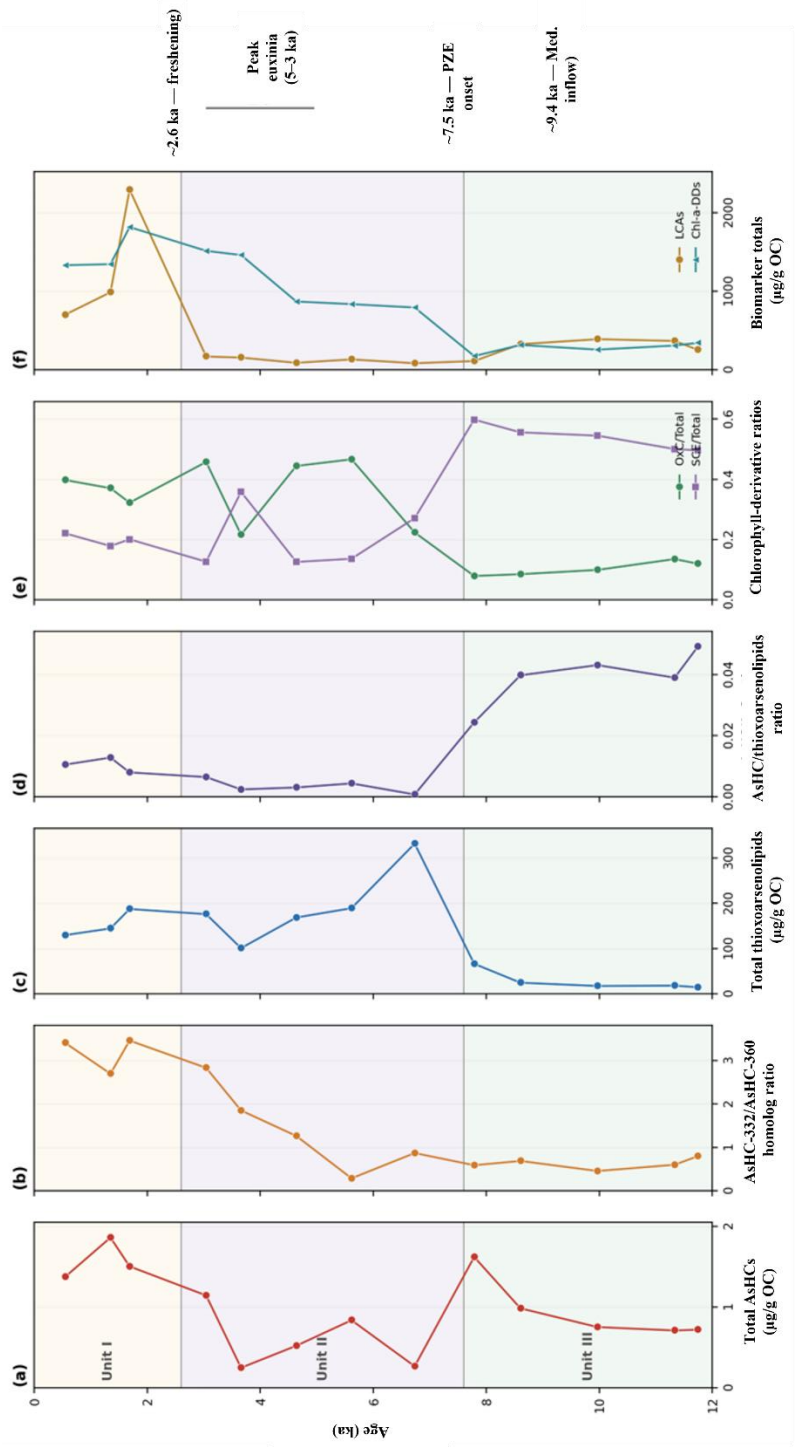

Figure 4.1 Stratigraphic profiles of arsenolipid biomarkers in GGC18 across the Holocene Black Sea sequence (11.7–0.6 ka). Panels show, from left to right: (a) total AsHC concentration

(sum of AsHC-332 and AsHC-360, µg/g OC); (b) AsHC-332/AsHC-360 homolog ratio; (c) total thioxoarsenolipid concentration (sum of *m/z* 547, 549, and 565 species, µg/g OC); (d) AsHC/thioxoarsenolipid ratio (total AsHC ÷ total thioxoarsenolipid); (e) selected chlorophyll-derivative proxies from Zhao et al. (2026), including OxC/Total Chl-*a*-DD and SCE/Total Chl-*a*-DD ratios; and (f) selected biomarker proxies from Alo et al. (2026), including LCAs and Chl-*a*-DD totals (µg/g OC). Lithological Units I–III are indicated by background shading and labels in panel (a). Key environmental transitions are marked to the right of panel (f): the onset of Mediterranean inflow (~9.4 ka), the development of photic-zone euxinia (~7.5 ka), peak intensified euxinia (5–3 ka), and late-Holocene surface-water freshening (~2.6 ka onwards). SCE/Total data from Zhao et al. (2026); LCAs data from Alo et al. (2026).

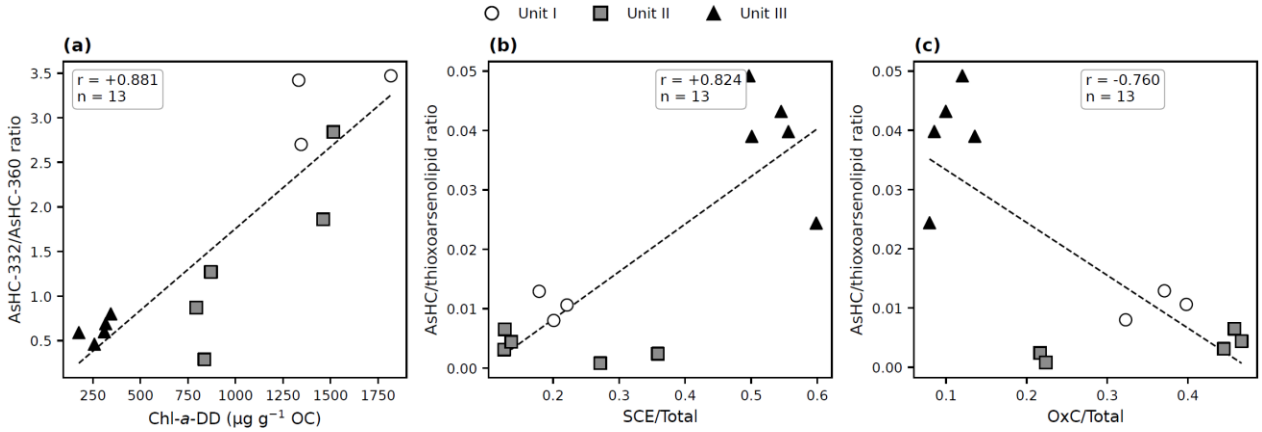

Figure 4.2 Cross-plots of arsenolipid metrics against chlorophyll-derived proxies for the thirteen GGC18 samples, coded by stratigraphic unit (Unit I, open circles; Unit II, grey squares; Unit III, filled triangles). (a) AsHC-332/AsHC-360 homolog ratio versus total Chl-a-DD concentration; (b) AsHC/thioxoarsenolipid ratio versus SCE/Total; (c) AsHC/thioxoarsenolipid ratio versus OxC/Total. Dashed lines are ordinary least-squares regressions; Pearson correlation coefficients are shown in each panel (n = 13). Chl-a-DD, OxC/Total, and SCE/Total data from Zhao et al. (2026). See Tables 4.1 and 4.2 for underlying data.

Age (ka)	Unit	TOC (wt%)	AsHC-332 (µg/g OC)	AsHC-360 (µg/g OC)	AsHC total (µg/g OC)	332/360 ratio	thioxoarsenolipid total (µg/g OC)	AsHC/thioxoarsenolipid ratio
0.55	Unit I	0.80	1.06	0.31	1.37	3.4170	130.00	0.0106
1.35	Unit I	0.99	1.36	0.50	1.86	2.7033	144.75	0.0129
1.69	Unit I	0.75	1.17	0.34	1.51	3.4675	187.79	0.0080
3.04	Unit II	0.58	0.85	0.30	1.15	2.8390	176.41	0.0065
3.66	Unit II	0.76	0.16	0.09	0.25	1.8552	101.23	0.0024
4.64	Unit II	5.25	0.29	0.23	0.52	1.2675	168.96	0.0031
5.62	Unit II	8.28	0.19	0.65	0.84	0.2883	189.59	0.0044
6.73	Unit II	9.78	0.12	0.14	0.27	0.8724	332.42	0.0008
7.79	Unit III	6.25	0.60	1.02	1.62	0.5910	66.50	0.0244
8.61	Unit III	7.01	0.40	0.58	0.99	0.6894	24.74	0.0398
9.97	Unit III	1.50	0.24	0.52	0.75	0.4575	17.45	0.0432
11.34	Unit III	2.93	0.27	0.44	0.71	0.6020	18.21	0.0390
11.75	Unit III	3.32	0.32	0.40	0.72	0.7994	14.65	0.0492

Table 4.1. Stratigraphic, lithological, and arsenolipid data for the thirteen GGC18 samples analyzed in this chapter. Sample ages are calibrated radiocarbon years before present (cal yr B.P.) from Alo et al. (2026) and Zhao et al. (2026), based on the combined age model of Coolen et al. (2009) for Units I–II and Huang et al. (2021) for Unit III. TOC (total organic carbon) values are from Alo et al. (2026). All arsenolipid concentrations are normalized to total organic carbon (µg/g OC). AsHC total = AsHC-332 (C15) + AsHC-360 (C17). Thioxoarsenolipid total = the sum of thioxoarsenolipids with *m/z* 547, 549, and 565. The 332/360 ratio is the AsHC-332/AsHC-360 homolog ratio; the AsHC/thioxoarsenolipid ratio is total AsHC concentration divided by total thioxoarsenolipid concentration. Ratios were calculated from unrounded values.

Age (ka)	Unit	TOC	Chl-a-DD (µg/g OC)	OxC/Total	LCAs (µg/g OC)	SCE/Total
0.55	Unit I	0.80	1332.81	0.40	702.28	0.22
1.35	Unit I	0.99	1345.72	0.37	988.03	0.18
1.69	Unit I	0.75	1817.84	0.32	2294.54	0.20
3.04	Unit II	0.58	1515.29	0.46	170.59	0.13
3.66	Unit II	0.76	1461.79	0.22	156.63	0.36
4.64	Unit II	5.25	870.78	0.44	90.34	0.13
5.62	Unit II	8.28	837.04	0.47	133.68	0.14
6.73	Unit II	9.78	793.95	0.22	84.80	0.27
7.79	Unit III	6.25	176.27	0.08	112.74	0.60
8.61	Unit III	7.01	317.46	0.09	327.21	0.56
9.97	Unit III	1.50	258.00	0.10	391.03	0.55
11.34	Unit III	2.93	310.39	0.14	368.84	0.50
11.75	Unit III	3.32	344.25	0.12	255.41	0.50

Table 4.2. Chlorophyll-derived and alkenone proxy data for the Black Sea core GGC18 samples, used in the correlation analyses of Sections 4.4–4.6. Chl-a-DD, chlorophyll-a degradation derivatives; OxC/Total, fraction of oxidized chlorins; SCE/Total, fraction of steryl chlorin esters; LCAs, long-chain alkenones. Chl-a-DD, OxC/Total, and SCE/Total data from Zhao et al. (2026); LCAs data from Alo et al. (2026). Ages are reported on the same scale as Table 4.1.

Chapter 5 General Conclusions

5.1 Synthesis of Findings

The three investigations presented in this dissertation, taken together, characterize fossil arsenolipids along three complementary dimensions: analytical detection, distribution across modern and ancient sedimentary archives, and stratigraphic response to documented environmental transitions.

The analytical framework developed in Chapter 2 establishes that fossil arsenolipids can be reliably detected in sedimentary matrices through the combination of SPE-based matrix simplification, NPLC-based chromatographic resolution, and dual-energy CID-based identification. This framework recovers arsenolipid signals from samples ranging from modern algal biomass to mid- to late Cenomanian (~94–100 Ma) anoxic marine shale, and resolves trace-level arsenolipids in carbonate-rich pelagic chalk where conventional reversed-phase approaches yield no detection. The methodological infrastructure provides a foundation for the broader application of arsenolipid biomarkers in paleoenvironmental work.

The survey of Chapter 3 establishes that AsHCs and thioxoarsenolipids occur across a broader range of modern aquatic environments than previously documented and persist in geological sedimentary archives spanning Quaternary Peru-margin OMZ deposits to a mid- to late Cenomanian black shale within the OAE2 interval; AsHCs were recovered to ~90 Ma and thioxoarsenolipids to the OAE2 interval (~94–100 Ma), together extending the preserved record across at least ~100 Myr. The detection of arsenolipids in the ODP 1259C-4R pelagic chalk extends the lithological range over which arsenolipids can be sought into carbonate-rich, low-TOC depositional settings, which constitute a substantial fraction of the global Mesozoic and Cenozoic deep-marine record but have been underrepresented in the classical biomarker literature. The

survey establishes both that arsenolipid production is a widespread among modern aquatic primary producers and that arsenolipid preservation extends across the depositional regimes most relevant to long-term paleoenvironmental reconstruction.

The case study of Chapter 4 establishes that arsenolipid composition in a single, well-constrained sedimentary sequence responds systematically to documented environmental transitions. Two arsenolipid compound classes—AsHCs and thioxoarsenolipids—follow contrasting stratigraphic patterns across the Holocene Black Sea Unit III/II transition, with the AsHC record co-varying with phytoplankton-community dynamics documented by Alo et al. (2026) and the thioxoarsenolipid record co-varying with redox and water-column proxies documented by Zhao et al. (2026). The proximate controls on the two compound classes appear to differ—producer-side controls for AsHCs and sulfide-mediated formation chemistry for thioxoarsenolipids—but both trace to the same upstream environmental transition (the development of photic-zone euxinia following Mediterranean inflow). The AsHC/thioxoarsenolipid ratio integrates the responses of both compound classes into a composite metric that records the cascade of redox, salinity, and productivity changes at the resolution of a single sedimentary core, with an approximately eleven-fold response across the Unit III/II boundary that exceeds the response of either compound class examined alone.

5.2 Limitations

The investigations presented here are subject to limitations that constrain the immediate generalization of the results and define the directions for future work. The source organisms of arsenolipids in natural environments remain incompletely characterized, and the present results cannot establish unique producer assignments for the AsHC homologs recovered from sedimentary archives. The formation pathways of the thioxoarsenolipids reported by Liu (2023) are not yet

mechanistically resolved; the present results are consistent with sulfide-mediated chemistry but do not distinguish abiotic sulfidation from microbially mediated thiolation. The case study of Chapter 4 examines a single sedimentary archive in a single basin, with thirteen samples whose statistical correlations, while striking, are computed from a sample size that limits broader generalization. Application of the framework developed here to other archives, calibration against modern source organisms, and mechanistic characterization of arsenolipid formation under controlled conditions will be required to extend the regime-transition application demonstrated here into a more general paleoenvironmental tool.

5.3 Future Directions

Three principal directions for future work emerge from the investigations presented here. First, modern calibration: culture-based experiments with phytoplankton from the Holocene Black Sea (or close analogs) and from contrasting modern depositional regimes will be needed to constrain the producer-side dependencies of arsenolipid composition under controlled conditions. The As/P ratio dependencies documented by Glabonjat et al. (2018, 2020) for *Dunaliella* and *Picocystis* provide a starting framework, and extension to haptophyte producers including *Isochrysis* would directly test the producer-side interpretation developed in Section 4.4.3. Second, mechanistic characterization of thioxoarsenolipid formation: laboratory experiments that systematically vary sulfide concentration, microbial community composition, and arsenic substrate availability will be needed to distinguish abiotic sulfidation from microbially mediated thiolation as candidate formation pathways. Third, application to additional sedimentary archives: the analytical framework of Chapter 2 and the regime-transition application of Chapter 4 are most readily tested by application to other Holocene-Pleistocene records of redox transition, including

Cariaco Basin, Saanich Inlet, and the Baltic Sea Holocene, and to additional deep-time archives spanning major paleoclimate transitions.

These three directions are interdependent: modern calibration constrains source assignments needed for paleoenvironmental interpretation; mechanistic characterization clarifies the chemistry underlying compound-class behavior; cross-archive application tests the generality of the regime-transition response. Together, they define a research program through which arsenolipids may be developed from the methodological and observational foundation laid by this dissertation into a quantitative paleoenvironmental tool that extends compound-specific arsenic biomarker analysis into broader paleoenvironmental applications.

5.4 References

Alo, O.O., Fu, J., Zhao, W., Zhang, Y.G., Huang, Y., Liu, X.-L., 2026. Simultaneous analysis of long-chain alkenones and chlorophyll derivatives offers new insights into the ecology of *Isochrysis* algae in the Holocene Black Sea. Marine Chemistry 279, 104634. https://doi.org/10.1016/j.marchem.2026.104634.

Glabonjat, R.A., Blum, J.S., Miller, L.G., Webb, S.M., Stolz, J.F., Francesconi, K.A., Oremland, R.S., 2020. Arsenolipids in cultured *Picocystis* strain ML and their occurrence in biota and sediment from Mono Lake, California. Life 10, 93. https://doi.org/10.3390/life10060093.

Glabonjat, R.A., Ehgartner, J., Duncan, E.G., Raber, G., Jensen, K.B., Krikowa, F., Maher, W.A., Francesconi, K.A., 2018. Arsenolipid biosynthesis by the unicellular alga *Dunaliella tertiolecta* is influenced by As/P ratio in culture experiments. Metallomics 10, 145–153. https://doi.org/10.1039/c7mt00249a.

Liu, X.-L., 2023. Streamlined arsenolipid identification via direct arsenic detection using RPLC-ESI-QTOF-MS with collision-induced dissociation. J. Am. Soc. Mass Spectrom 35, 300–306. https://doi.org/10.1021/jasms.3c00367.

Zhao, W., Fu, J., Alo, O.O., Liu, X.-L., 2026. The distribution of chlorophyll-a degradation derivatives in the Holocene Black Sea and their marine ecological significance. Marine Chemistry 278, 104606. https://doi.org/10.1016/j.marchem.2026.104606.

REFERENCES

Algeo, T.J., Rowe, H., 2012. Paleoceanographic applications of trace-metal concentration data. Chem. Geol 324–325, 6–18. https://doi.org/10.1016/j.chemgeo.2011.09.002.

Alo, O.O., Fu, J., Zhao, W., Zhang, Y.G., Huang, Y., Liu, X.-L., 2026. Simultaneous analysis of long-chain alkenones and chlorophyll derivatives offers new insights into the ecology of *Isochrysis* algae in the Holocene Black Sea. Marine Chemistry 279, 104634. https://doi.org/10.1016/j.marchem.2026.104634.

Amayo, K.O., Pétursdóttir, A., Newcombe, C., Gunnlaugsdóttir, H., Raab, A., Krupp, E.M., Feldmann, J., 2011. Identification and quantification of arsenolipids using reversed-phase HPLC coupled simultaneously to high-resolution ICPMS and high-resolution electrospray MS without species-specific standards. Analytical Chemistry 83, 3589–3595. https://doi.org/10.1021/ac102187u.

Amayo, K.O., Raab, A., Krupp, E.M., Gunnlaugsdóttir, H., Feldmann, J., 2013. Novel identification of arsenolipids using chemical derivatizations in conjunction with RP-HPLC-ICPMS/ESMS. Analytical Chemistry 85, 9321–9327. https://doi.org/10.1021/ac4020935.

Arroyo-Abad, U., Lischka, S., Piechotta, C., Mattusch, J., Reemtsma, T., 2013. Determination and identification of hydrophilic and hydrophobic arsenic species in methanol extract of fresh cod liver by RP-HPLC with simultaneous ICP-MS and ESI-Q-TOF-MS detection. Food Chemistry 141, 3093–3102. https://doi.org/10.1016/j.foodchem.2013.05.152.

Arthur, M.A., Dean, W.E., 1998. Organic-matter production and preservation and evolution of anoxia in the Holocene Black Sea. Paleoceanography 13, 395–411. https://doi.org/10.1029/98PA01161.

Arthur, M.A., Sageman, B.B., 2005. Sea-level control on source-rock development: perspectives from the Holocene Black Sea, the mid-Cretaceous Western Interior Basin of North America, and the Late Devonian Appalachian Basin. SEPM Special Publication 82, 35–59. https://doi.org/10.2110/pec.05.82.0035.

Bauersachs, T., Schouten, S., Schwark, L., 2014. Characterization of the sedimentary organic matter preserved in Messel oil shale by bulk geochemistry and stable isotopes. Palaeogeography, Palaeoclimatology, Palaeoecology 410, 390–400. https://doi.org/10.1016/j.palaeo.2014.06.015.

Bhattacharjee, H., Rosen, B.P., 2007. Arsenic metabolism in prokaryotic and eukaryotic microbes, in: Nies, D.H., Silver, S. (Eds.), Molecular Microbiology of Heavy Metals, Springer. pp. 371–406. https://doi.org/10.1007/7171_2006_086.

Böttcher, M.E., Hetzel, A., Brumsack, H.-J., Schipper, A., 2006. Sulfur-iron-carbon geochemistry in sediments of the Demerara Rise, in: Mosher, D.C., Erbacher, J., Malone, M.J. (Eds.), Proceedings of the Ocean Drilling Program, Scientific Results. Ocean Drilling Program, College Station, TX, pp. 1–23. https://doi.org/10.2973/odp.proc.sr.207.108.2006.

Brocks, J.J., Pearson, A., 2005. Building the biomarker tree of life. Reviews in Mineralogy and Geochemistry 59, 233–258. https://doi.org/10.2138/rmg.2005.59.10.

Chen, J., Rosen, B.P., 2020. The arsenic methylation cycle: how microbial communities adapted methylarsenicals for use as weapons in the continuing war for dominance. Frontiers in Environmental Science 8, 43. https://doi.org/10.3389/fenvs.2020.00043.

Chen, X., Andersen, T.J., Morono, Y., Inagaki, F., Jørgensen, B.B., Lever, M.A., 2017. Bioturbation as a key driver behind the dominance of Bacteria over Archaea in near-surface sediment. Scientific Reports 7, 2400. https://doi.org/10.1038/s41598-017-02295-x.

Chi Fru, E., Arvestål, E., Callac, N., El Albani, A., Kilias, S., Argyraki, A., Jakobsson, M., 2015. Arsenic stress after the Proterozoic glaciations. Scientific Reports 5, 17789. https://doi.org/10.1038/srep17789.

Coolen, M.J.L., Orsi, W.D., Balkema, C., 2013. Evolution of the plankton paleome in the Black Sea from the Deglacial to Anthropocene. PNAS 110, 8609–8614. https://doi.org/10.1073/pnas.1219283110.

Coolen, M.J.L., Saenz, J.P., Giosan, L., 2009. DNA and lipid molecular stratigraphic records of haptophyte succession in the Black Sea during the Holocene. Earth Planet. Sci. Lett 284, 610–621. https://doi.org/10.1016/j.epsl.2009.05.029.

Couture, R.M., Gobeil, C., Tessier, A., 2010. Arsenic, iron and sulfur co-diagenesis in lake sediments. Geochim. Cosmochim. Acta 74, 1238–1255. https://doi.org/10.1016/j.gca.2009.11.028.

Cutter, G.A., Cutter, L.S., Featherstone, A.M., Lohrenz, S.E., 2001. Antimony and arsenic biogeochemistry in the western Atlantic Ocean. Deep-Sea Research Part II: Topical Studies in Oceanography 48, 2895–2915. https://doi.org/10.1016/S0967-0645(01)00023-6.

DC.Rubin, S.S., Alava, P., Zekker, I., Laing, G., Wiele, T., 2014. Arsenic thiolation and the role of sulfate-reducing bacteria from the human intestinal tract. Environ. Health Perspect 122, 817–822. https://doi.org/10.1289/ehp.1307759.

D'Hondt, S., 2005. Consequences of the Cretaceous/Paleogene mass extinction for marine ecosystems. Annual Review of Ecology, Evolution, and Systematics 36, 295–317. https://doi.org/10.1146/annurev.ecolsys.35.021103.105715.

Edmonds, J.S., Francesconi, K.A., 1987. Transformations of arsenic in the marine environment. Experientia 43, 553–557. https://doi.org/10.1007/BF02143584.

Edmonds, J.S., Shibata, Y., Francesconi, K.A., Yoshinaga, J., Morita, M., 1992. Arsenic lipids in the digestive gland of the western rock lobster *Panulirus cygnus*: an investigation by HPLC ICP-MS. Science of the Total Environment 122, 321–335. https://doi.org/10.1016/0048-9697(92)90050-3.

Erbacher, J., Mosher, D.C., Malone, M.J., 2004. Site 1259, in: Proceedings of the Ocean Drilling Program, Initial Reports. Ocean Drilling Program, College Station, TX. https://doi.org/10.2973/odp.proc.ir.207.106.2004.

Filipova-Marinova, M.V., Giosan, L., Angelova, H., 2013. Palaeoecological and geochemical evidence for late Pleistocene-early Holocene Black Sea environmental change. Palaeogeogr. Palaeoclimatol. Palaeoecol 387, 49–60. https://doi.org/10.1016/j.quaint.2012.05.002.

Fukuda, S., Terasawa, M., Shiomi, K., 2011. Phosphatidylarsenocholine, one of the major arsenolipids in marine organisms: synthesis and metabolism in mice. Food and Chemical Toxicology 49, 1598–1603. https://doi.org/10.1016/j.fct.2011.03.053.

Gallego-Torres, D., Martinez-Ruiz, F., Lange, G.J., Jimenez-Espejo, F.J., Ortega-Huertas, M., 2010. Trace-elemental derived paleoceanographic and paleoclimatic conditions for Pleistocene Eastern Mediterranean sapropels. Palaeogeography, Palaeoclimatology, Palaeoecology 293, 76–89. https://doi.org/10.1016/j.palaeo.2010.05.001.

García-Salgado, S., Raber, G., Raml, R., Magnes, C., Francesconi, K.A., 2012. Arsenosugar phospholipids and arsenic hydrocarbons in two species of brown macroalgae. Environmental Chemistry 9, 63–66. https://doi.org/10.1071/EN11164.

Giosan, L., Coolen, M.J.L., Kaplan, J.O., 2012. Early anthropogenic transformation of the Danube-Black Sea system. Sci. Rep 2, 582. https://doi.org/10.1038/srep00582.

Giosan, L., Filip, F., Constantinescu, S., 2009. Was the Black Sea catastrophically flooded in the early Holocene? Quat. Sci. Rev 28, 1–6. https://doi.org/10.1016/j.quascirev.2008.10.012.

Glabonjat, R.A., Blum, J.S., Miller, L.G., Webb, S.M., Stolz, J.F., Francesconi, K.A., Oremland, R.S., 2020. Arsenolipids in cultured *Picocystis* strain ML and their occurrence in biota and sediment from Mono Lake, California. Life 10, 93. https://doi.org/10.3390/life10060093.

Glabonjat, R.A., Duncan, E.G., Francesconi, K.A., Maher, W.A., 2019a. Transformation of arsenic lipids in decomposing *Ecklonia radiata*. Journal of Applied Phycology 31, 3979–3987. https://doi.org/10.1007/s10811-019-01845-2.

Glabonjat, R.A., Ehgartner, J., Duncan, E.G., Raber, G., Jensen, K.B., Krikowa, F., Maher, W.A., Francesconi, K.A., 2018. Arsenolipid biosynthesis by the unicellular alga *Dunaliella tertiolecta* is influenced by As/P ratio in culture experiments. Metallomics 10, 145–153. https://doi.org/10.1039/c7mt00249a.

Glabonjat, R.A., Raber, G., Holm, H.C., Mooy, B.A.S., Francesconi, K.A., 2021. Arsenolipids in plankton from high- and low-nutrient oceanic waters along a transect in the North Atlantic. Environmental Science & Technology 55, 5515–5524. https://doi.org/10.1021/acs.est.0c06901.

Glabonjat, R.A., Raber, G., Jensen, K.B., Ehgartner, J., Francesconi, K.A., 2014. Quantification of arsenolipids in the certified reference material NMIJ 7405-a (Hijiki) using HPLC/mass spectrometry after chemical derivatization. Analytical Chemistry 86, 10282–10287. https://doi.org/10.1021/ac502488f.

Glabonjat, R.A., Raber, G., Jensen, K.B., Guttenberger, N., Zangger, K., Francesconi, K.A., 2017. A 2-O-methylriboside unknown outside the RNA world contains arsenic. Angewandte Chemie International Edition 56, 11963–11965. https://doi.org/10.1002/anie.201706310.

Glabonjat, R.A., Raber, G., Jensen, K.B., Schubotz, F., Boyd, E.S., Francesconi, K.A., 2019b. Origin of arsenolipids in sediments from Great Salt Lake. Environmental Chemistry 16, 303–311. https://doi.org/10.1071/EN19135.

Gomez-Saez, G.V., Dittmar, T., Holtappels, M., Pohlabeln, A.M., Lichtschlag, A., Schnetger, B., Boetius, A., Niggemann, J., 2021. Sulfurization of dissolved organic matter in the anoxic water column of the Black Sea. Sci. Adv 7, 6199. https://doi.org/10.1126/sciadv.abf6199.

Gregory, D.D., Large, R.R., Halpin, J.A., Baturina, E.L., Lyons, T.W., Wu, S., Danyushevsky, L., Sack, P.J., Chappaz, A., Maslennikov, V.V., Bull, S.W., 2015. Trace element content of sedimentary pyrite in black shales. Economic Geology 110, 1389–1410. https://doi.org/10.2113/econgeo.110.6.1389.

Grice, K., Holman, A.I., Plet, C., Tripp, M., 2019. Fossilised biomolecules and biomarkers in carbonate concretions from Konservat-Lagerstätten. Minerals 9, 158. https://doi.org/10.3390/min9030158.

Hay, B.J., Arthur, M.A., Dean, W.E., Neff, E.D., Honjo, S., 1991. Sediment deposition in the Late Holocene abyssal Black Sea with climatic and chronological implications. Deep-Sea Res 38, 1211–1235. https://doi.org/10.1016/S0198-0149(10)80031-7.

Heal, K.R., Maloney, A.E., Ingalls, A.E., Bundy, R.M., 2022. Diverse arsenic-containing lipids in the surface ocean. Limnology and Oceanography Letters 7, 43–51. https://doi.org/10.1002/lol2.10216.

Hedges, J.I., Keil, R.G., 1995. Sedimentary organic matter preservation: an assessment and speculative synthesis. Marine Chemistry 49, 81–115. https://doi.org/10.1016/0304-4203(95)00008-F.

Helz, G.R., Tossell, J.A., Charnock, J.M., Pattrick, R.A.D., Vaughan, D.J., Garner, C.D., 1995. Oligomerization in As(III) sulfide solutions: theoretical constraints and spectroscopic evidence. Geochim. Cosmochim. Acta 59, 4591–4604. https://doi.org/10.1016/0016-7037(95)00330-4.

Huang, Y., Freeman, K.H., Wilkin, R.T., Arthur, M.A., Jones, A.D., 2000. Black Sea chemocline oscillations during the Holocene: molecular and isotopic studies of marginal sediments. Org. Geochem 31, 1525–1531. https://doi.org/10.1016/S0146-6380(00)00090-5.

Huang, Y., Zheng, Y., Heng, P., Giosan, L., Coolen, M.J.L., 2021. Black Sea paleosalinity evolution since the last deglaciation reconstructed from alkenone-inferred Isochrysidales diversity. Earth Planet. Sci. Lett 564, 116881. https://doi.org/10.1016/j.epsl.2021.116881.

Jenkyns, H.C., 2010. Geochemistry of oceanic anoxic events. Geochemistry, Geophysics, Geosystems 11, 03004. https://doi.org/10.1029/2009GC002788.

Jones, M.M., Sageman, B.B., Meyers, S.R., 2018. Turonian sea level and paleoclimatic events in astronomically tuned records from the tropical North Atlantic and Western Interior Seaway. Paleoceanography and Paleoclimatology 33, 470–492. https://doi.org/10.1029/2017PA003158.

King, L.L., Repeta, D.J., 1991. Novel pyrophaeophorbide steryl esters in Black Sea sediments. Geochim. Cosmochim. Acta 55, 2067–2074. https://doi.org/10.1016/0016-7037(91)90044-6.

Kuypers, M.M.M., Pancost, R.D., Nijenhuis, I.A., Sinninghe Damsté, J.S., 2002. Enhanced productivity led to increased organic carbon burial in the euxinic North Atlantic basin during the late Cenomanian oceanic anoxic event. Paleoceanography 17, 1051. https://doi.org/10.1029/2000PA000569.

Lenz, O.K., Wilde, V., Riegel, W., 2010. Short-term fluctuations in vegetation and phytoplankton during the Middle Eocene greenhouse climate: a 640-kyr record from the Messel oil shale (Germany. International Journal of Earth Sciences (Geologische Rundschau 100, 1851–1874. https://doi.org/10.1007/s00531-010-0609-z.

Liu, X.-L., 2023. Streamlined arsenolipid identification via direct arsenic detection using RPLC-ESI-QTOF-MS with collision-induced dissociation. Journal of the American Society for Mass Spectrometry 35, 300–306. https://doi.org/10.1021/jasms.3c00367.

Major, C.O., Goldstein, S.L., Ryan, W.B.F., Lericolais, G., Piotrowski, A.M., Hajdas, I., 2006. The co-evolution of Black Sea level and composition through the last deglaciation and its paleoclimatic significance. Quaternary Science Reviews 25, 2031–2047. https://doi.org/10.1016/j.quascirev.2006.01.032.

Moriarty, M.M., Lai, V.W.-M., Koch, I., Cui, L., Combs, C., Krupp, E.M., Feldmann, J., Cullen, W.R., Reimer, K.J., 2014. Speciation and toxicity of arsenic in mining-affected lake sediments in the Quinsam watershed, British Columbia. Science of the Total Environment 466–467, 90–99. https://doi.org/10.1016/j.scitotenv.2013.07.005.

Morita, M., Shibata, Y., 1988. Isolation and identification of arseno-lipid from a brown alga, *Undaria pinnatifida* (Wakame. Chemosphere 17, 1147–1152. https://doi.org/10.1016/0045-6535(88)90180-4.

Müller, S.M., Finke, H., Ebert, F., Kopp, J.F., Schumacher, F., Kleuser, B., Francesconi, K.A., Raber, G., Schwerdtle, T., 2018. Arsenic-containing hydrocarbons: effects on gene expression, epigenetics, and biotransformation in HepG2 cells. Archives of Toxicology 92, 1751–1765. https://doi.org/10.1007/s00204-018-2196-x.

Naujokas, M.F., Anderson, B., Ahsan, H., Aposhian, H.V., Graziano, J.H., Thompson, C., Suk, W.A., 2013. The broad scope of health effects from chronic arsenic exposure: update on a worldwide public health problem. Environmental Health Perspectives 121, 295–302. https://doi.org/10.1289/ehp.1205875.

Neff, J.M., 1997. Ecotoxicology of arsenic in the marine environment. Environmental Toxicology and Chemistry 16, 917–927. https://doi.org/10.1002/etc.5620160511.

Party, S.S., 2003. Site 1227, in: D'Hondt, S.L., Jørgensen, B.B., Miller, D.J. (Eds.), Proceedings of the Ocean Drilling Program, Initial Reports. Ocean Drilling Program, College Station, TX. https://doi.org/10.2973/odp.proc.ir.201.108.2003.

Paulmier, A., Ruiz-Pino, D., 2009. Oxygen minimum zones (OMZs) in the modern ocean. Progress in Oceanography 80, 113–128. https://doi.org/10.1016/j.pocean.2008.08.001.

Peters, K.E., Walters, C.C., Moldowan, J.M., 2005. The biomarker guide, 2nd ed. Cambridge University Press, Cambridge.

Pétursdóttir Á.H., Fletcher K., Gunnlaugsdóttir H., Krupp E., Küpper F.C., Feldmann J., 2016. Environmental effects on arsenosugars and arsenolipids in *Ectocarpus* (Phaeophyta. Environmental Chemistry 13, 21–33. https://doi.org/10.1071/EN14229.

Pétursdóttir, Á.H., Jesus, J., Gunnlaugsdóttir, H., Feldmann, J., 2018. Quantification of labile and stable non-polar arsenolipids in commercial fish meals and edible seaweed samples. Journal of Analytical Atomic Spectrometry 33, 102–110. https://doi.org/10.1039/c7ja00333a.

Phillips, A.A., White, M.E., Seidel, M., Wu, F., Pavia, F.F., Kemeny, P.C., Sessions, A.L., 2022. Novel sulfur isotope analyses constrain sulfurized porewater fluxes as a minor component

of marine dissolved organic matter. Proceedings of the National Academy of Sciences 119, 2209152119. https://doi.org/10.1073/pnas.2209152119.

Pinel-Raffaitin, P., Le Hecho, I., Amouroux, D., Potin-Gautier, M., 2007. Distribution and fate of inorganic and organic arsenic species in landfill leachates and biogases. Environ. Sci. Technol 41, 4536–4541. https://doi.org/10.1021/es0628506.

Planer-Friedrich, B., London, J., McCleskey, R.B., Nordstrom, D.K., Wallschläger, D., 2007. Thioarsenates in geothermal waters of Yellowstone National Park: determination, preservation, and geochemical importance. Environ. Sci. Technol 41, 5245–5251. https://doi.org/10.1021/es070273v.

Raab, A., Newcombe, C., Pitton, D., Ebel, R., Feldmann, J., 2013. Comprehensive analysis of lipophilic arsenic species in a brown alga (Saccharina latissima. Analytical Chemistry 85, 2817–2824. https://doi.org/10.1021/ac303340t.

Rahman, M.A., Hasegawa, H., Lim, R.P., 2012. Bioaccumulation, biotransformation and trophic transfer of arsenic in the aquatic food chain. Environmental Research 116, 118–135. https://doi.org/10.1016/j.envres.2012.03.014.

Raven, M.R., Fike, D.A., Gomes, M.L., Webb, S.M., Bradley, A.S., McClelland, H.L.O., 2018. Organic carbon burial during OAE2 driven by changes in the locus of organic matter sulfurization. Nat. Commun 9, 3409. https://doi.org/10.1038/s41467-018-05943-6.

Raven, M.R., Keil, R.G., Webb, S.M., 2021. Microbial sulfate reduction and organic sulfur formation in sinking marine particles. Science 371, 178–181. https://doi.org/10.1126/science.abc6035.

Řezanka, T., Nedbalová, L., Barcyte, D., Vítová, M., Sigler, K., 2019. Arsenolipids in the green alga Coccomyxa (Trebouxiophyceae, Chlorophyta. Phytochemistry 164, 243–251. https://doi.org/10.1016/j.phytochem.2019.05.002.

Rumpler, A., Edmonds, J.S., Katsu, M., Jensen, K.B., Goessler, W., Raber, G., Gunnlaugsdóttir, H., Francesconi, K.A., 2008. Arsenic-containing long-chain fatty acids in cod-liver oil: a result of biosynthetic infidelity? Angewandte Chemie International Edition 47, 2665–2667. https://doi.org/10.1002/ange.200705405.

Schlanger, S.O., Jenkyns, H.C., 1976. Cretaceous oceanic anoxic events: causes and consequences. Geologie en Mijnbouw 55, 179–184.

Schlesinger, W.H., Klein, E.M., Vengosh, A., 2022. The global biogeochemical cycle of arsenic. Global Biogeochemical Cycles 36, 2022 007515. https://doi.org/10.1029/2022GB007515.

Schymanski, E.L., Jeon, J., Gulde, R., Fenner, K., Ruff, M., Singer, H.P., Hollender, J., 2014. Identifying small molecules via high resolution mass spectrometry: communicating confidence. Environmental Science & Technology 48, 2097–2098. https://doi.org/10.1021/es5002105.

Sele, V., Sloth, J.J., Holmelid, B., Valdersnes, S., Skov, K., Amlund, H., 2014. Arsenic-containing fatty acids and hydrocarbons in marine oils – determination using reversed-phase HPLC-ICP-MS and HPLC-qTOF-MS. Talanta 121, 89–96. https://doi.org/10.1016/j.talanta.2013.12.049.

Sinninghe Damsté, J.S., Wakeham, S.G., Kohnen, M.E.L., Hayes, J.M., Leeuw, J.W., 1993. A 6,000-year sedimentary molecular record of chemocline excursions in the Black Sea. Nature 362, 827–829. https://doi.org/10.1038/362827a0.

Smedley, P.L., Kinniburgh, D.G., 2002. A review of the source, behaviour and distribution of arsenic in natural waters. Applied Geochemistry 17, 517–568. https://doi.org/10.1016/S0883-2927(02)00018-5.

Soulet, G., Ménot, G., Lericolais, G., Bard, E., 2011. A revised calendar age for the last reconnection of the Black Sea to the global ocean. Quaternary Science Reviews 30, 1019–1026. https://doi.org/10.1016/j.quascirev.2011.03.001.

Spooner, N., Getliff, J.M., Teece, M.A., Parkes, R.J., Leftley, J.W., Harris, P.G., Maxwell, J.R., 1995. Formation of mesopyrophaeophorbide a during anaerobic bacterial degradation of the marine prymnesiophyte *Emiliania huxleyi*. Org. Geochem 22, 225–229. https://doi.org/10.1016/0146-6380(95)90019-5.

Stauder, S., Raue, B., Sacher, F., 2005. Thioarsenates in sulfidic waters. Environ. Sci. Technol 39, 5933–5939. https://doi.org/10.1021/es048034k.

Taleshi, M.S., Jensen, K.B., Raber, G., Edmonds, J.S., Gunnlaugsdóttir, H., Francesconi, K.A., 2008. Arsenic-containing hydrocarbons: natural compounds in oil from the fish capelin, *Mallotus villosus*. Chemical Communications 39, 4706–4707. https://doi.org/10.1039/B808049F.

Thamdrup, B., Fossing, H., Jørgensen, B.B., 1994. Manganese, iron and sulfur cycling in a coastal marine sediment, Aarhus Bay, Denmark. Geochimica et Cosmochimica Acta 58, 5115–5129. https://doi.org/10.1016/0016-7037(94)90298-4.

Tribovillard, N., 2021. Conjugated enrichments in arsenic and antimony in marine deposits used as paleoenvironmental proxies: preliminary results. BSGF - Earth Sciences Bulletin 192, 39. https://doi.org/10.1051/bsgf/2021034.

Tribovillard, N., Algeo, T.J., Lyons, T.W., Riboulleau, A., 2006. Trace metals as paleoredox and paleoproductivity proxies: an update. Chem. Geol 232, 12–32. https://doi.org/10.1016/j.chemgeo.2006.02.012.

Viczek, S.A., Jensen, K.B., Francesconi, K.A., 2016. Arsenic-containing phosphatidylcholines: a new group of arsenolipids discovered in herring caviar. Angewandte Chemie International Edition 55, 5259–5262. https://doi.org/10.1002/anie.201512031.

W.H.O., 2017. Guidelines for drinking-water quality, 4th edition incorporating the first addendum, World Health Organization.

Wallschläger, D., Stadey, C.J., 2007. Determination of (oxy)thioarsenates in sulfidic waters. Anal. Chem 79, 3873–3880. https://doi.org/10.1021/ac070061g.

Wang, N.-X., Li, Y., Deng, X.-H., Miao, A.-J., Ji, R., Yang, L.-Y., 2013. Toxicity and bioaccumulation kinetics of arsenate in two freshwater green algae under different phosphate regimes. Water Research 47, 2497–2506. https://doi.org/10.1016/j.watres.2013.02.034.

Werne, J.P., Lyons, T.W., Hollander, D.J., Schouten, S., Hopmans, E.C., Sinninghe Damsté, J.S., 2008. Investigating pathways of diagenetic organic matter sulfurization using compound-specific sulfur isotope analysis. Geochim. Cosmochim. Acta 72, 3489–3502. https://doi.org/10.1016/j.gca.2008.04.033.

Wilkin, R.T., Arthur, M.A., Dean, W.E., 1997. History of water-column anoxia in the Black Sea indicated by pyrite framboid size distributions. Earth Planet. Sci. Lett 148, 517–525. https://doi.org/10.1016/S0012-821X(97)00053-8.

Wrench, J.J., Addison, R.F., 1981. Reduction, methylation, and incorporation of arsenic into lipids by the marine phytoplankton *Dunaliella tertiolecta*. Can. J. Fish. Aquat. Sci 38, 518–523. https://doi.org/10.1139/f81-073.

Wu, G., Huang, L., Jiang, H., 2017. Thioarsenate formation coupled with anaerobic arsenite oxidation by a sulfate-reducing bacterium isolated from a hot spring. Front. Microbiol 8, 1336. https://doi.org/10.3389/fmicb.2017.01336.

Xiong, C., Glabonjat, R.A., Al Amin, M.H., Stiboller, M., Yoshinaga, J., Francesconi, K.A., 2022. Arsenolipids in salmon are partly converted to thioxo analogs during cooking. Journal of Trace Elements in Medicine and Biology 69, 126892. https://doi.org/10.1016/j.jtemb.2021.126892.

Xue, X.-M., Raber, G., Foster, S., Chen, S.-C., Francesconi, K.A., Zhu, Y.-G., 2014. Biosynthesis of arsenolipids by the cyanobacterium *Synechocystis* sp. PCC 6803. Environmental Chemistry 11, 506–513. https://doi.org/10.1071/en14069.

Xue, X.-M., Xiong, C., Yoshinaga, M., Rosen, B., Zhu, Y.-G., 2022. The enigma of environmental organoarsenicals: insights and implications. Critical Reviews in Environmental Science and Technology 52, 3835–3862. https://doi.org/10.1080/10643389.2021.1947678.

Zachos, J., Pagani, M., Sloan, L., Thomas, E., Billups, K., 2001. Trends, rhythms, and aberrations in global climate 65 Ma to present. Science 292, 686–693. https://doi.org/10.1126/science.1059412.

Zhao, W., Fu, J., Alo, O.O., Liu, X.-L., 2026. The distribution of chlorophyll-a degradation derivatives in the Holocene Black Sea and their marine ecological significance. Marine Chemistry 278, 104606. https://doi.org/10.1016/j.marchem.2026.104606.

Zhu, Y.-G., Xue, X.-M., Kappler, A., Rosen, B.P., Meharg, A.A., 2017. Linking genes to microbial biogeochemical cycling: lessons from arsenic. Environmental Science & Technology 51, 7326–7339. https://doi.org/10.1021/acs.est.7b00689.